Ceramics International

Fabrication of Sustainable Magnesium Phosphate Cement Micromortar using Design of Experiments Statistical Modelling: Valorization of Ceramic-Stone-Porcelain containing waste as filler

--Manuscript Draft--

Manuscript Number:	CERI-D-20-10985R1
Article Type:	Full length article
Keywords:	B. Microstructure-final; C. Mechanical properties; D. MgO; E. Structural applications; Design of experiments
Corresponding Author:	Joan Formosa, PhD Universitat de Barcelona Barcelona, SPAIN
First Author:	Sergio Huete-Hernández
Order of Authors:	Sergio Huete-Hernández
	Alex Maldonado-Alameda
	Jessica Giro-Paloma, PhD
	Josep M Chimenos, PhD
	Joan Formosa, PhD
Abstract:	Magnesium phosphate cement (MPC) is a potential sustainable alternative to Portland cement. It is possible to lower the total CO 2 emissions related to MPC manufacturing by using by-products and wastes as raw materials. When by-products are used to develop MPC, the resultant binder can be referred to as sustainable magnesium phosphate cement (sust-MPC). This research incorporates ceramic, stone, and porcelain waste (CSP) as a filler in sust-MPC to obtain a micromortar. Sust-MPC is formulated with KH 2 PO 4 and low-grade MgO (LG-MgO), a by-product composed of 40–60 wt.% MgO. CSP is the non-recyclable glass fraction generated by the glass recycling industry. The effect of water and CSP addition on the mechanical properties of sust-MPC was analyzed using design of experiments (DoE). A statistical model was obtained and validated by testing ideally formulated samples achieved through optimization of the DoE. The optimal formulation (15 wt.% of CSP and a water to cement ratio of 0.34) was realized by maximizing the compressive strength at 7 and 28 days of curing, resulting in values of 18 and 25 MPa respectively. After one year of curing, the micromortar was physico-chemically characterized in-depth using backscattered scanning electron microscopy (BSEM-EDS) and Fourier transform infrared-attenuated total reflectance spectroscopy (FTIR-ATR). The optimal formulation showed good integration of CSP particles in the ceramic matrix. Thus, a potential reaction between silica and the K-struvite matrix may have occurred after one year of curing.

UNIVERSITAT DE BARCELONA

Tenured-track 2 Lecturer Joan Formosa

Chemistry Faculty
Martí i Franquès, 1
Office708B
08028 Barcelona
Tel. +34 934 021 316
joanformosa@ub.edu
www.ub.edu

Ceramics International,
Editor

Barcelona, September 18th 2020

Dear Editor,

I enclose you the manuscript entitled "**Preparation of Sustainable Magnesium Phosphate cement mortars by recycling Ceramic - Stone - Porcelain containing wastes"**. The publication of the present paper is crucial because of the benefit of using a **waste from glass cullet industry (CSP) as filler** for obtaining Sustainable Magnesium Phosphate Cement mortars could suppose a low-cost possibility for these building materials of increasing interest in the research community. Nowadays **CSP glass waste is landfilled in our country** because of its melting point is greater than pure soda-lime glass and inhibits melting process, complicating glass recovery procedure.

Moreover, we use an industrial by-product (LG-MgO) as raw material for obtaining the **ceramic k-struvite cementitious matrix or Magnesium Phosphate Cement (MPC)**. This industrial by-product is obtained during the calcination process of magnesite for producing MgO for the refractory industry. LG-MgO is mainly compound by MgO. As you may already know MPC is included in Chemically Bonded Phosphate Ceramic (CBPC) group. This kind of ceramic materials have attracted the attention of the scientific community as an alternative to Portland Cement. Our research is focused on the **improvement of the ceramic final product by recycling a ceramic waste and an industrial by-product (LG-MgO)**. The LG-MgO reduces the cost of the final product and therefore provides a competitive alternative, reinforcing the criteria of sustainability and recyclability. Consequently, we named the Magnesium Phosphate Cement obtained with this by-product as sustainable-MPC (sust-MPC). In this regard, we published several articles in your journal.

The present research is related with preliminary studies published in your journal. We aim to promote the use of sust-MPC by following the obtained results from

preliminary studies. Then, from these preliminary studies we selected the optimum relation between raw materials (60% wt LG-MgO and 40% wt KH_2PO_4) for the present investigation showed in the attached manuscript. On this manner, **the present manuscript describes the effect of the CSP as a filler on the physical and mechanical properties**. We studied the effect **by design of experiments (DoE) at different ages of curing**. The statistical tool allows to better optimize the study of the effect of water to solid ratio and CSP wt. % on the abovementioned properties.

The main results of the present study showed that sust-MPC formulated with CSP as a filler had promising results. **Also, the present investigation reveals a potential long-term reaction between k-struvite matrix and CSP waste glass filler**. This assumption is **discussed by SEM-EDS, FTIR-ATR spectroscopy, XRD and TGA, where the potential formation of a silicophosphate is argued**.

Then, the present investigation showed that it is possible to use DoE to obtain desired properties when CSP is used as a filler. Last but not least, the potential reaction between the filler and the matrix could suppose a starting point for further studies with this type of waste. Hence the importance of this paper's publication.

Do not hesitate to contact us if you require any additional information related to the paper. We look forward to hearing from you in the near,

Yours sincerely

PhD. Joan Formosa
Tenured-track 2 Lecturer
Departament de Ciència de Materials i Química Física.
Ciència i Enginyeria de Materials.
Chemistry Faculty
Universitat de Barcelona

UNIVERSITAT DE BARCELONA

Ethical declaration of the Authors:

The authors declare under our ethical responsibility that the present paper is original and has not been submitted or is not being considered for publication elsewhere. Besides, we declare that we have seen and approved the manuscript.


S. Huete-Hernández


A. Maldonado-Alameda


PhD J. Giro-Paloma

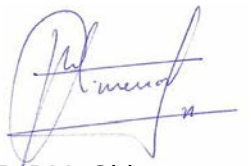
PhD J.M. Chimenos


PhD J. Formosa

Preparation of Sustainable Magnesium Phosphate cement mortars by recycling Ceramic - Stone - Porcelain containing wastes

S. Huete-Hernández[a], A. Maldonado-Alameda[a], J. Giro-Paloma[a], J.M. Chimenos[a], J. Formosa[a*]

[a]Departament de Ciència de Materials i Química Física. Universitat de Barcelona, Martí i Franquès 1, 08028 Barcelona, Spain

*Author to who correspondence should be addressed. Telephone: +34934021316; Fax: +34934035438; E-mail: joanformosa@ub.edu. Departament de Ciència de Materials i Química Física. Universitat de Barcelona, Martí i Franquès 1, 08028 Barcelona, Spain.

Abstract

Magnesium Phosphate Cement (MPC) is a potential sustainable alternative to Ordinary Portland Cement (OPC). The use of a low-grade MgO (LG-MgO) by-product for developing MPC leads to a sustainable MPC (sust-MPC). This research is focused on the incorporation of ceramic, stone, and porcelain waste (CSP) into sust-MPC. CSP is obtained from glass recycling industry, which is landfilled. The percentage of CSP into sust-MPC was analyzed by using design of experiments (DoE). A statistical model was obtained and validated by formulating and testing an Optimal Formulation (OF). The OF was proposed by maximizing compressive strength at 7 and 28 days of curing. The OF compressive strength were 18 and 28 MPa, respectively for the dosage with 15 % wt. of CSP and a water to cement ratio of 0.34. The OF was deeply physico-chemically characterized by SEM-EDS and FTIR-ATR. OF showed good integration of CSP particles in the ceramic matrix. Concluding that a potential reaction between silica and K-struvite matrix may have occurred after one year of curing.

Keywords

B. Microstructure-final; C. Mechanical properties; D. MgO; E. Structural applications; Design of Experiments;

Abbreviations

MPC	Magnesium Phosphate Cement
MPCs	Magnesium Phosphate Cements
OPC	Ordinary Portland Cement
LG-MgO	Low-grade MgO
Sust-MPC	Sustainable Magnesium Phosphate Cement
CSP	Ceramic, Stone, and Porcelain Waste
DoE	Design of Experiments
CS	Compressive Strength
CBCs	Chemically Bonded Ceramics
CBPCs	Chemically Bonded Phosphate Cements
MKP	Monopotassium Phosphate
RSM	Response Surface Methodology
CSP(%)	Ceramic, Stone, and Porcelain Waste percentage in the mortar
R1-13	Mortar formulation from Design of Experiments corresponding run
-7d, -28d, -365d	Days of curing before test and characterization
OF	Optimal Formulation
FA	Fly Ash
BOs	Bridging Oxygens

NBOs Non-Bridging Oxygens

_____

1. Introduction

In terms of pollution and greenhouse gas emissions, the construction and building industry sector has an important challenge for the next years, being this sector responsible of approximately 7-8% of the global CO_2 total emissions [1,2]. This is mainly because OPC is one of the most produced and applied materials on a global scale due to its wide range of properties and its low cost [3,4]. Being known as hydraulic cement, OPC production process consumes extremely high amounts of energy. However, in recent years, new types of alternative cements have emerged with different and improved properties which allow extending their application range in diverse technology areas [5–7]. Those properties can range from mechanic attributes improvements such as compression strength (CS) [8] or enhanced porosity [9], to biocompatibility [10] or environmental sustainability [11]. Among all these types of alternative cements, chemically bonded ceramics (CBCs) and, more specifically, chemically bonded phosphate cements (CBPCs), stand out being an early strength cement with rapid setting [12] and good volume stability [13]. An example of CBPCs could be MPC in which magnesium oxide (MgO) is combined with monopotassium phosphate (KH_2PO_4, MKP) to form magnesium potassium phosphate ($MgKPO_4 \cdot 6H_2O$) also known as K-struvite due to its crystalline structure (Eq. (1)) [14,15]. K-struvite is one type of CBPCs with the best properties as high-performance cement applications [16].

$$MgO + KH_2PO_4 + 5H_2O \leftrightarrow MgKPO_4 \cdot 6H_2O \qquad (1)$$

MPC has advantageous properties enclosing neutral pH due to acid-base formation reaction, low water demand and drying shrinkage, and rapid development of compressive strength [17]. MPC can be applied in cold weather due to the rapid and exothermic nature of its setting chemical reaction (Eq. (1)). It can be used as a repair material to restore damaged roads during traffic and rehabilitations of infrastructure among other applications [13,18,19]. MPC main application is in the field of stabilization and solidification of low-level radioactive wastes containing reactive metals [20] having outstanding encapsulation properties from the point of view of waste management [21,22], and is also used in biomedical implants [12]. Despite all the MPCs assets above-mentioned, the production of MgO in accordance with OPC clinker production process generates excessive CO_2 emissions and consumes an important quantity of energy proceeding from the calcination of natural magnesite ($MgCO_3$) and dolomite ($MgCa(CO_3)_2$). Nevertheless, the MgO process is much less pollutant than OPC clinker fabrication [23].

MgO production starts with $MgCO_3$ and $MgCa(CO_3)_2$ minerals being sieved and fed to the kiln for the calcination process. The by-product LG-MgO is retained as powder cyclone dust in the filters of the air pollution control system during the combustion process. LG-MgO is mainly chemically composed by reactive MgO (40-60 wt.%) proceeding from heavily calcined MgO. Due to its reactive MgO availability and economic cost, LG-MgO must be considered as a sustainable source of material in the MPCs field. Feasibility of using LG-MgO to obtain MPCs was demonstrated on previous studies conducted with outstanding results [24–26]. Considering the above-mentioned, this material can be considered as sust-MPC, a green cement, compared to common MPC. Unreacted particles could be perceived as fine inorganic filler inside the sust-MPC paste, most of them being carbonates and quartz. In consequence, sust-MPC could be considered as a mortar. Furthermore, the addition of inorganic fillers in sust-MPC mortars benefits the binder improving fresh mixture workability, reducing heat development, and production costs [27]. The use of solid waste as inorganic filler in sust-MPC mortars opens a possibility in solid waste treatment encapsulating residual non-profitable or recyclable material. For instance, CSP is the fraction removed from the glass cullet recycling process. CSP fraction is considered a non-valuable waste because it is too small-sized, has glued paper labels, or contains other diverse impurities, among others. CSP is composed approximately by 84 wt.% soda-lime glass, 6 wt.% porcelain, 6 wt.% ceramic, and 4 wt.% of stone, polymer/paper, metals, organic matter, and others [28]. Since CSP is derived from municipal and industrial waste, its composition is heterogeneous along time, depending on weather season, society consuming tendency, and garbage dumping preferences. CSP is definitively a problem for glass cullet recycling companies because its melting point is greater than pure soda-lime glass and inhibits melting process, complicating glass recovery procedure. Nowadays, automated chromatic separators are used to optically sort and classify clean and contaminated shattered glass. Chromatic separators do not detect coarser glass fragments such as bottle bottoms and bottlenecks of a darker tone than the ordinary shattered glass [29,30]. Recycling companies only accept glass cullet if CSP concentration is lower than 20 $g \cdot t^{-1}$. Therefore, CSP is treated as a non-profitable material and dumped to landfill.

The main purpose of this investigation is to develop a sust-MPC mortar using CSP as an inorganic filler and LG-MgO instead of pure MgO. In addition, the interaction between CSP filler and mortar K-struvite matrix is studied over time. This study is based on the research group previous experience in obtaining sust-MPC [24,25,31–33]. When CSP is applied as a filler economic costs are reduced and environmental and sustainable criteria are enhanced. To minimize the number of experiments DoE was used. The

deployment of a factorial design model using DoE enables extracting the maximum information from the experiments performed. Predictive theoretical mathematical models are determined for each response, allowing to estimate the mortars behaviour as well as to find an optimal and adequate formulation with the required properties in the range of the study.

2. Experimental procedure

2.1 Materials

LG-MgO by-product was supplied by Magnesitas Navarras, S.A. located in Navarra (Spain). This plant generates various industrial solid by-products such as LG-MgO. These by-products are treated as dictates the international and Spanish environmental and sustainability normative ISO 14000 embedded in UNE-EN ISO 14001:2015 and UNE-EN ISO 50001:2018.

Phosphate source was food graded KH_2PO_4 with a purity of 99.8 wt.% from Norken, S.L., which is commonly used as a fertilizer and is soluble in water.

CSP waste glass in the form of shattered solid fragments > 2 mm and in an average range of 8-16 mm was provided by Daniel Rosas, S.A. This company is a recycling plant which treats glass cullet from urban and industrial garbage dump containers following the Spanish normatives UNE-EN ISO 9001:2015, UNE-EN ISO 14001:2015, and the European Commission Regulation (EU) Nº 1179/2012. A total amount of 24 kg of CSP waste was quartered and homogenized to ensure a representative chemical composition. To increase reactivity, CSP was cleaned from paper, polymeric, and metallic pieces. The sample was shredded under 2 mm, and milled in alumina ball mill to be sieved under 80 μm.

In order to hydrate the raw materials, deionized water was used to avoid chloride impurities, frequently found in tap water.

2.1.1 Raw materials characterization

A representative sub-samples of about 250 g of LG-MgO and CSP were obtained quartering each of the initial samples. MKP characterization was not conducted since is a commercial product, and it was deeply evaluated in previous studies by the authors [24–26,33]. LG-MgO and CSP characterization were performed using complementary techniques such as X-ray fluoresce (XRF), X-ray diffraction (XRD), and thermogravimetric analysis with simultaneous scanning differential thermal analysis (TGA-SDT). In addition, the citric acid test [34] was completed to evaluate LG-MgO reactivity. A pH-meter was used

instead of the visual evaluation using phenolphthalein. For the citric acid test 2 g of LG-MgO were stirred continuously (500 rpm (min^{-1}) and 30 ºC) in 100 mL of citric acid solution until pH 9 was reached and the elapsed time was measured. The citric acid solution was prepared stirring 28 g of citric acid monohydrate in deionized water in order to obtain 1 l of solution. Samples were tested in triplicate for the citric acid test.

The XRD analysis was carried out using a PANalytical X'Pert PRO MPD Alpha1 powder diffractometer. The XRF analysis was performed using a Philips PW2400 X-ray sequential spectrophotometer to elucidate major and minor elements. To conduct TGA-SDT analysis TA Instruments Q-600 SDT equipment was used. Tests were conducted from 30 °C to 1400 °C at a heating rate of 10 °C·min^{-1} in a nitrogen atmosphere with a gas flow of 100 mL·min^{-1}.

2.2 Design of Experiments

Design of experiments was implemented for reducing the number of experiments and identifying in which manner CSP filler phase influences in the sust-MPC mortars final properties. On one hand, apparent density (ρ), modulus of elasticity (MOE), flexural strength (FS), and compressive strength (CS) were the responses evaluated at 7 days (d). In the present study, CS was also evaluated at 28 d. On the other hand, DoE was used to evaluate if the variables or factors (filler and water percentage) have a synergistic correlation between them, affecting the composite final properties. On this manner it is possible, by using this technique, to obtain a sust-MPC mortar dosage with the convenient mechanical and physical properties for the desired application by varying the factors under study [35,36].

LG-MgO/MKP ratio of 60/40 was fixed as the composition of the cement-based on previous experience [33]. CSP(%) and water to cement ratio (W/C) were variables or factors in this investigation. The total quantity of cement (C) implied in the W/C is the combination of both MKP and LG-MgO mass into the mixture. Hence, CSP is considered as a filler, even though it might partially react with K-struvite. The lowest/highest level for W/C and CSP(%) were 0.34/0.38 and 0 wt.%/15 wt.%, respectively. A CSP increase in the mixture could lead to an extra amount of water to adjust workability, which is usually related to a non-desired decrease of the final mechanical properties of the product. Therefore, the levels were determined after some preliminary experiments to ensure proper workability of the fresh sust-MPC mortar. Consequently, the objective of the preliminary study was to introduce the highest amount of CSP while keeping W/C as low as possible.

The present study was a response surface methodology (RSM) with a D-optimal and quadratic design, in order to further perform an optimization process by using previously obtained results. Design Expert® software was used to perform DoE. The resulting mixtures are summarized in Table 1, where the lowest/highest level of each factor is highlighted in bold.

2.2.1 DoE Optimal formulation

DoE analysis is based on the analysis of variance (ANOVA) to predict an optimal response [35], using the *p*-value to interpret the obtained results. The *p*-value represents the smallest level of significance that would lead to rejection of the null-hypothesis meaning there is no effect of the controllable factor on the response under investigation. If a *p*-value in a test for the significance of a certain factor is smaller than 0.05, this factor is considered statistically significant with confidence superior to 95%.

The ratio of the Model SS/Residual SS (Model SS and residual SS referred to the regression and error sum of squares, respectively) defines the F-value. There is a significant contribution in case of large F-values while small values indicate the variance would be affected by noise. CSP weight percentage (CSP(%)) and water to cement ratio (W/C) were chosen as factors, and their effects on the composite properties were quantified. The model needs to be validated in order to check its feasibility.

2.2.2 Sust-Magnesium phosphate mortar preparation (sust-MPC mortar)

The mortars were mixed in a mortar planetary mixer. A total amount of 3 kg of solids, LG-MgO, KH_2PO_4, and CSP, were weighed and added to the mixer. The raw materials mix was properly dry homogenized in the mixer. Subsequently, water was added and after 10 s, the blend was mixed 30 s on low revolution mode and 30 s on high revolution mode. During the next 20 s, the potential unhydrated solid was checked and removed by using a spatula. Afterwards, the mortar paste was mixed again on high revolution mode during 60 s. The fresh mortar was poured into 40x40x160 mm^3 expanded polystyrene prismatic moulds and vibrated for 10 s on a conventional vibratory table for mortar and concrete. Six prismatic samples of each formulation were obtained. Casted samples were left for 24 h in a curing chamber at a constant temperature of 20 ± 2 °C and relative humidity of 95%. Then, the samples were demoulded and left for further curing in the same conditions until testing (7 d and 28 d).

2.3 Test methods and structure characterization of sust-MPC mortar

Apparent density, MOE, FS, and CS were conducted at 7 d of curing for six specimens of each formulation in order to evaluate the results by means of DoE. The MOE was determined by using an ultrasound test following UNE-EN 12504-4 standard. An ultrasonic pulse velocity tester (C368 by Matest, 55 kHz transceiver sensors) was employed to perform the test measurements. The obtained MOE results were accepted under the presumption that Young's modulus estimation was valid for homogeneous and isotropic media even though sust-MPC mortars do not rigorously fulfil always these conditions.

CS test was conducted for six split specimens obtained from FS test at 7 d and the remaining six parts of the FS test specimens were further cured up to 28 d before the CS test. Test conditions followed UNE-EN 196-1 by using an Incotecnic MULTI-R1 mechanical testing equipment, where the FS test speed was 5 $kg \cdot s^{-1}$ and the CS test speed was 240 $kg \cdot s^{-1}$. After that, an optimal formulation was suggested by analysing the DoE results (see section 3.2.6). The optimal sust-MPC mortar and ordinary sust-MPC without CSP filler as a reference were compared after 365 d of curing, both samples were obtained from the CS test at 28 d. The pieces obtained after the CS tests at 28 d were stored in the curing chamber up to 365 d just for a better evaluation of a potential reaction of the CSP glass phase with K-struvite [37–39]. This potential reaction between K-struvite and siliceous compounds was reported by various authors [37–39]. The evaluation was conducted by means of XRD, TGA-SDT analysis, scanning electron microscopy (SEM), and Fourier transformed infrared spectroscopy in attenuated total reflectance mode (FTIR-ATR). In addition, CSP was evaluated using FTIR-ATR to be compared with the cured sust-MPC mortar pieces. FTIR-ATR spectra of the samples were obtained by a Perkin Elmer Spectrum Two FTIR-ATR spectrometer. Concerning XRD and TGA-SDT measurements both were conducted in the same conditions as raw materials characterization.

In order to perform SEM study to determine the chemical interaction between filler and cement matrix, a JSM-6510 from JEOL Ltd. company scanning electron microscope was used. Various representative broken fragments from the optimal sust-MPC mortar and ordinary sust-MPC without CSP were selected. Fragment samples were fixed on a carbon adhesive and carbon coated for the compilation of SEM images and punctual energy-dispersive scattering (EDS) analysis of the specimens fracture surface. In addition, fragments of both formulations were impregnated in epoxy resin, surface polished, and carbon coated to

reveal the internal configuration of sust-MPC. SEM images and EDS elemental mapping were conducted to the polished fragment samples by collecting various EDS mappings. Each of the EDS mappings were compiled during 1800 s.

3. Results and discussion

3.1 Raw materials characterization

By-products chemical composition was determined by XRF as it is shown in Table 2 for each element as the most stable corresponding oxides, where magnesium was the main element in the case of LG-MgO, with an average content of 61.7 wt.% of MgO. Calcium was the second more abundant element with 9.32 wt.% of CaO. The sulphur found in the sample was mainly attributed to the petroleum coke used as combustible for calcination of the natural magnesite as it was previously stated by Formosa et al. [40]. On the other hand, the XRF results for CSP waste showed in Table 2 denoted high Si elemental concentration (70.78 wt.% of SiO_2) followed by Na (11.15 wt.% of Na_2O), Ca (9.37 wt.% of CaO), and Al (4.81 wt.% of Al_2O_3). The presence of Si, Ca, and Na is related to the high content of soda-lime glass in CSP waste while Al concentration is associated to aluminosilicates present in the ceramic waste.

XRD crystalline spectra of LG-MgO and CSP can be seen in Fig. 1. The presence of glass cullet and ceramic shards in CSP is evidenced by XRD analysis in Fig. 1.a in which quartz (SiO_2, PDF# 01-085-0457) and mullite ($Al_{4.52}Si_{1.48}O_{9.74}$, PDF# 01-079-1457) were found to be the main crystalline phases. The crystallographic spectra also showed important amorphous appearance related to amorphous silica from glass. LG-MgO main crystalline phases are periclase (MgO, PDF# 01-071-1176), brucite ($Mg(OH)_2$, PDF# 01-083-0114), magnesite ($MgCO_3$, PDF# 01-078-2442), dolomite ($CaMg(CO_3)_2$, PDF# 01-084-1208), calcite ($CaCO_3$, PDF# 01-086-0174), and anhydrite ($CaSO_4$, PDF# 00-037-1496) among other minor phases (Fig. 1.b). Other impurities such as iron oxide or silica were also present. The thermal decomposition in nitrogen atmosphere for LG-MgO can be seen in Fig. 2. In the case of CSP the TGA-SDT analysis (not showed) registered a total mass loss of 1.214 wt.% from 30 ºC to 1400 ºC without showing any clear decomposition.TGA-SDT analysis for LG-MgO indicated mass losses attributed to adsorbed water and crystallization water (from 30 ºC to 210 ºC), $Mg(OH)_2$ decomposition resulting in MgO (from 210 ºC to 440 ºC), $MgCO_3$ decarbonation giving MgO and CO_2 as products (from 440 ºC to 660 ºC), $CaMg(CO_3)_2$ decarbonation to MgO, CaO, and CO_2 (from 660 ºC to 740 ºC), $CaCO_3$ decarbonation to CaO and CO_2 (from 740 ºC to 1030 ºC), and desulfurization first $MgSO_4$ (from 1030 ºC

to 1190 ºC) and then $CaSO_4$ (from 1190 ºC to 1400 ºC). TGA-SDT analysis results in combination with XRF and XRD results were used to estimate the chemical actual composition of the by-product. The results of the estimation are shown in Table 3, where MgO total content in LG-MgO was 43.58 wt.%. Considering that $Mg(OH)_2$ (3.77 wt.%) and $MgSO_4$ (2.12 wt.%) are soluble in water in contrast with the carbonate, the total calculated content of available MgO in the by-product is 51.47 wt.%.

The reactivity of MgO can be assessed by the citric acid test where neutralization values under 60 s are specific for highly reactive samples, also known as soft-burnt MgO. Values between 180 and 300 s are defined as medium reactive MgO; while the low reactivity MgO is known as hard-burnt, giving values around 600 s. Finally, values over 900 s are applicable to dead-burnt MgO [34]. LG-MgO acid citric test resulted in a neutralization at 1128 s. Therefore, the LG-MgO value obtained is the proper reactivity to develop K-struvite and no pre-calcination processes is needed [41]. Therefore, the use of LG-MgO by-product instead of pure MgO allows reducing the costs as well as enhancing environmental and sustainable criteria.

3.2 Design of experiments response

The LG-MgO/KH_2PO_4 ratio presented in Table 1 was fixed to 60/40 in weight basis [24–26,42]. The formulations (Runs, i.e.: R15 for run number 15) and a summary of the main experimental and predicted DoE results of the study are described in Table 1. The developed models by using the experimental responses showed *p*-values lower than 0.0001, implying that the proposed models are significant considering the factor relations showed for each response or equation. The best model fitting the experimental results for the apparent density at 7 d, MOE at 7 d, FS at 7 d, CS at 7 d, and CS at 28 d are two factors with interaction, linear, linear, reduced cubic, and reduced quadratic, respectively. A deep discussion about the proposed models for each response under study is presented in the following section.

3.2.1 Apparent Density (ρ)

The best model fitting the experimental values for apparent density response is showed in Eq. (2). The model presented low standard deviation and high R squared statistics value (R^2): 0.01 and 0.87, respectively. The Eq. (2) mathematical model is represented in Fig. 3.a. Both factors under study (W/C and CSP(%)) have a significant effect (p-value = 0.0002 and < 0.0001, respectively) over the response apparent density. According to the results, by increasing W/C ratio the apparent density decreases. The increase of CSP(%) leads to an apparent density response increase. Considering the slope for each

response the effect of CSP(%) is higher than W/C ratio in the range of study. When the combined effect of both factors (W/C ratio and CSP(%)) is considered, the response is minor than the expected from the sum of each one discretely. Therefore, there is a significant negative interaction between both factors (p-value = 0.0196) which explains this performance. The fact that there is a negative interaction of CSP(%) and W/C ratio can be seen by the last term in Eq. (2), where the higher the term, the lower the response. The higher the CSP(%) the higher the apparent density, and at the same time the lower the W/C ratio the higher the apparent density.

As it is well known, an increase in the W/C ratio leads to a decrease in apparent density after curing, because water lightens the material as it leaves pores and/or the cement sets/dries. Besides, an increase in filler amount leads to an increase in apparent density, considering that usually the filler apparent density is higher than the paste apparent density.

$$\rho\ (\mathrm{g \cdot cm^{-3}}) = 1.888 - 0.288 \cdot (W/C) + 0.028 \cdot (CSP) - 0.070 \cdot (W/C) \cdot (CSP) \qquad (2)$$

As it can be seen in Fig. 3.a (on-line version) there are blue and red zones corresponding to lowest and higher apparent density values, respectively.

3.2.2 Modulus of elasticity (MOE)

The model presented low standard deviation and high R squared statistics value (R^2): 0.48 and 0.90, respectively. A response surface linear model was developed for MOE at 7 d response by using the experimental data. MOE surface plot is presented in Fig. 3.b and the corresponding mathematical expression is presented in Eq. (3) The highest MOE values are obtained as CSP(%) (p-value < 0.0001) is increased and W/C ratio (p-value < 0.0001) is decreased. Hence, the MOE model exhibits high values as in the case of apparent density. On the contrary, MOE model is more susceptible to W/C ratio than of CSP(%).

MOE and apparent density are related to the porosity of the samples. Therefore, both responses show similar behaviour, as shown in Fig. 3.a and Fig. 3.b. The higher the W/C ratio the higher the porosity and consequently the lower the MOE and mechanical properties values such as FS and CS [43]. The mathematical approach for density surface plot is presented in Eq. (3).

$$MOE\ (\mathrm{GPa}) = 34.993 - 66.071 \cdot (W/C) + 0.109 \cdot (CSP) \qquad (3)$$

As can be seen in Fig. 3.b (on-line version) there are blue and red zones corresponding to lowest and higher MOE values, respectively. CSP and W/C factors are significant but no interaction between both factors was perceived in the range under study for MOE results.

3.2.3 Flexural strength (FS)

FS at 7 d surface plot is exhibited in Fig. 3.c which was obtained by Eq. (4). The developed model presented a low standard deviation (0.22) and high R^2 statistic value (0.84). The model is a linear model where both factors have a significant effect on the response in the range under study. FS at 7 d augments as W/C ratio (p-value < 0.0001) decreases and while CSP(%) (p-value = 0.0033) augments. It must be noted that FS is more sensitive to W/C ratio variation than of CSP(%) in the mortar as it was already perceived and noted in MOEs 3.2.2 section. Once again, this performance in both MOE and FS could be associated with the formation of pores. If air did not evacuate properly when the mortar was being obtained, this could affect severely the flexural performance. This effect had less impact on CS test due to the enclosure of pores when testing.

$$FS\ (\text{MPa}) = 12.153 - 25.553\cdot(W/C) + 0.033\cdot(CSP) \qquad (4)$$

As can be seen in Fig. 3.c (on-line version) there are blue and red zones corresponding to lowest and higher FS values, respectively.

3.2.4 Compression strength (CS) at 7 d

Compression strength at 7 d (CS-7d) statistical model is presented in Fig. 3.d and Eq. (5). The model showed low standard deviation equal to 0.23 and a model R^2 statistic value of 0.97, which indicated that was properly fitted to experimental data. The proposed model is a reduced cubic model, where the evaluated factors presented significant effect on the response, as follows: W/C ratio (p-value < 0.0001), CSP(%) (p-value = 0.0024), (W/C)·(CSP) (p-value = 0.0836), $(W/C)^2$ (p-value = 0.0061), $(CSP)^2$ (p-value = 0.0227) and $(CSP)^3$ (p-value = 0.0055).

$$CS\text{-}7d\ (\text{MPa}) = 512.470 - 2660.140\cdot(W/C) - 0.719\cdot(CSP) - 2.849\cdot(W/C)\cdot(CSP) + 3529.782\cdot(W/C)^2 + 0.329\cdot(CSP)^2 - 0.014\cdot(CSP)^3 \qquad (5)$$

As can be seen in Fig. 3.d (on-line version) there are blue and red zones corresponding to lowest and higher CS-7d values, respectively. On one hand, the lowest values (see Fig. 3.d blue zone on-line version) were obtained at low CSP(%) and high W/C ratios. This is attributed to the necessity to increase the W/C when CSP was added for improving the workability in the fresh state. On the other hand, the highest values (see Fig. 3.d red zone on-line version) were obtained at high CSP(%) and low W/C ratios. This behaviour is attributed to the effect of the filler in a cement matrix when the proper water was used. In other words, as a result of preliminary work to obtain the range of study, it was concluded that the minimum W/C ratio for acceptable workability was 0.34. When testing the CS of a mortar, the filler particles favour the enclosure of cavities and the propagation of cracks, resulting in an enhanced CS [32].As can be observed in Eq. (5), there is a negative interaction between both factors. This interaction could be observed by following the line when both factors increased together (see Fig. 3.d green zone in the on-line version). Quadratic and cubic terms were used for better fitting the model, as it can be seen by curves instead of line tendencies in the edges of the plotted response surface of Fig. 3.d. In general, it could be assumed that the higher the CSP(%), the higher the CS-7d.

3.2.5 Compression strength (CS) at 28 d

Compression strength at 28 d (CS-28d) model showed a low standard deviation (1.00) and high R^2 statistic value (0.96). Then, the model fitted properly the experimental results for CS-28d. The reduced quadratic model was fitted with Eq. (6) and presented in Fig. 3.e.

$$CS\text{-}28d\ (\text{MPa}) = 64.125 - 134.430\cdot(W/C) + 1.759\cdot(CSP) - 5.863\cdot(W/C)\cdot(CSP) + 0.047\cdot(CSP)^2 \quad (6)$$

The model terms presented p-values as follows: (W/C; < 0.0001), (CSP; < 0.0001), ((W/C)·(CSP); 0.0296), and ($(CSP)^2$; 0.0008). As it can be seen in Fig. 3.e (on-line version) there are blue and red zones corresponding to lowest and higher CS-28d values, respectively. There is a significant negative interaction between both factors which is depicted by a change in the tendency or a valley (green zone in Fig. 3.e in the on-line version) when both factors were increased together. The effect is lower than the expected from the sum of each one separately. As it was expected, an increase of W/C ratio leads to a decrease of CS-28d which is depicted with a negative slope considering W/C axis in Fig. 3.e. However, when CSP(%) is considered there is a minimum region around the middle of this axis (i.e. lower and higher CSP(%) leads to higher CS-28d in the range understudy). Thus, the maximum CS-28d (red zone in Fig. 3.e in the on-line version) was obtained when CSP(%) and W/C ratio were maximum and minimum,

respectively. On the contrary, when CSP(%) was minimized and W/C ratio was maximized the CS-28d value was minimized (blue region in Fig. 3.e in the on-line version). CSP(%) above 15 could lead to an increase of CS-28d, although this value was out of the range of study and it would be further studied. In that case, a new range for W/C ratio it should be considered because of the lack of workability when CSP was added. For future works, some additives may be used to improve the fresh state of these mixtures, such as borax or sodium hexametaphosphate.

3.2.6 Optimal formulation and validation procedure

By using the statistical models presented above, it was possible to optimize the formulation selecting the desired responses. As above-mentioned, the main aim of this study was to enhance the CS as much as possible for developing sust-MPC by using CSP as a filler within the range of study. The optimization idea *per se* involved the concept of reaching a compromise between values. Table 4 shows the optimization criteria used in the optimization process, lower and upper limits were the best and worst values obtained from the tests performed (i.e. experimental values range). CS was treated as the most valuable property since it is the main aspect to contemplate in building materials. Therefore, CS-7d and CS-28d were maximized in the process of optimization. Nonetheless, apparent density, MOE, and FS were in the range limits. In the present research, the importance for each parameter was fixed in 3, where the importance could be ranged from 1 to 5 (i.e. responses had the same importance). Once the desired response values, factors range, and level of importance were selected, two optimal formulations were obtained. The optimal formulation is indicated in Table 4, combined with its modelled predicted properties as well as the desirability. OF coincided with R15 and R7 in terms of W/C ratio and CSP (see Table 1). Comparing the estimated values (see Table 4) with the experimental results of R7 and R15 (see Table 1) the model was validated.

3.3 Mortar structure characterization

In order to evaluate the formation of new mineral phases, R15 was considered as the OF and compared to R11 as the sole dosage without CSP and lower W/C ratio used as a reference or blank. The broken parts obtained after the CS-28d test of R15 and R11 were used to perform the sust-MPC mortar characterization after 365 d of curing. The samples were analyzed using XRD and TGA-SDT in the same conditions as raw materials, SEM combined with EDS chemical microanalysis, and also FTIR-ATR to provide information on the microstructure and whether CSP interacted with MPC matrix in sust-MPC

mortar. For EDS interaction evaluation with matrix, samples were impregnated in epoxy resin and were surface polished to unveil the internal configuration of sust-MPC. Samples were carbon coated and EDS mapping was collected during 1800 s.

Several authors reported the feasibility of a potential reaction when MPC matrixes are used with fly ash (FA) [27]. These authors considered that the reaction would take place after a large period. This research shows R15-365d SEM images because it was related to the potential reaction of MPC matrix with CSP filler.

XRD pattern of both optimal sust-MPC mortar and MPC reference samples showed K-struvite ($KMgPO_4 \cdot 6H_2O$, PDF# 01-075-1076) as the major crystalline phase. Fig. 4. shows the two overlapped patterns. Other phases such as unreacted periclase, dolomite, magnesite, and quartz were detected. Stable phases within LG-MgO did not react and remained unaltered. By means of XRD, only K-struvite was found as the magnesium phosphate phase formed, neither bobierrite ($Mg_3(PO_4)_2 \cdot 8H_2O$) nor newberyite ($MgHPO_4 \cdot 3H_2O$) were identified in the mortar. It must be noted that calcite was expected in the pattern, but peaks could be overlapped with those of magnesite and dolomite. As for possible interactions between CSP particles and the matrix, no differences were perceived in terms of 2θ peaks between the optimal and the reference XRD spectra. There is an exception in R15 (background of higher intensity), which was as a result of the higher CSP, being composed by high amorphous silica content. This presumes that it does not seem to exist chemical combination between the filler and K-struvite matrix in terms of XRD.

TGA-SDT mortars characterization at 365 d can be seen in Fig. 5. The graphs show a higher total mass loss for R11-365d in Fig. 5.a compared to R15-365d in Fig. 5.b, as a result of the reduction of K-struvite due to the filler substitution. TGA-SDT results for both R11-365d and R15-365d showed the same number of mass losses and temperature decomposition ranges. To characterize the mass losses of the mortars, TGA-SDT was analyzed considering the XRD results previously obtained. The mass loss between 30-270 °C was assigned to the loss of H_2O from K-struvite and the mass loss between 270-450 °C was assigned to H_2O from magnesium hydroxide decomposition. The following losses between 450-600 °C, 600-700 °C and 700-1000 °C were assigned to CO_2 derived from magnesite, dolomite, and calcite decomposition, respectively, because of the inert carbonate phases contained in LG-MgO [44,45]. Being K-struvite the main crystalline phase in the mortars, it was quantified using TGA. It was found to be 53.46 wt.% of the total mortar mass in R11-365d and 47.37 wt.% in R15-365d. These results were in

accordance with those found in the bibliography, taking into account that LG-MgO was around 47 wt.% reactive MgO [44–46]. CSP real percentage in R15-365d was calculated by comparing R11-365d and R15-365d mass loss at 30-270 °C and resulting to be 11.70 wt.% of the total mortar mass. It has to be noted that the total mortar mass incorporates water mass, a small part of it lost when mixing.

Images taken with SEM, EDS and mapping analysis of the R15-365d are shown in Fig. 6. In Fig. 6.a the micrograph shows the inner structure appearance of the mortar composed of CSP filler and unreacted LG-MgO particles embedded in a K-struvite matrix. The high degree of microcracking in the sample can be easily detected indicating an elevated level of stress which was endured during CS test [47]. Filler particles can be seen randomly distributed through the mortar matrix providing and enhancing the mechanical properties of the composite. Using XRD crystalline phase analysis, TGA results and observing the relative intensity between EDS chemical elemental peaks [44,45,48] showed in Fig. 6, sharp particles such as dolomite, calcite, magnesite could be situated in the K-struvite sust-MPC mortar matrix between other minor compounds such as sulphates [40]. Unreacted MgO particles and soda-lime glass from CSP were found to be incorporated in the matrix. A few iron oxide particles proceeding from LG-MgO, undermined by XRD, were also detected by means of EDS. Unreacted particles can be considered as filler particles aside from CSP waste filler. Therefore, sust-MPC can be conceived as a micro-mortar. The mortar matrix could trace the path of K-struvite reaction culminating into MgO partially reacted particles embedded in the matrix. The reaction starts on the outside of the particle and advances towards the centre of the particle not reaching its core. Also, prismatic K-struvite crystals were found in the fracture surface of the mortars [49]. Optimal formulation samples were polished to be exhaustively analyzed by means of EDS mapping. Fig. 6.a and Fig. 6.b also show the elemental dispersion and situation of the main elements detected by dispersive energy intensity. In order to spot the CSP filler particles in sust-MPC mortar matrix, a general random zone was subjected to elemental mapping. The main aim was observing the most interesting filler particles. It can be observed S (from sulphates), Mg, P, and K (from K-struvite), Ca (from calcium carbonate and CSP soda-lime glass particles), Na (from CSP soda-lime glass particles), Fe (from a ferrous particle), Al (from CSP phases), and Si (from CSP particles). A magnified zone of interest was analyzed by ESD mapping. This zone was composed by a soda-lime CSP particle surrounded and incorporated into the matrix. This particle was observed with more detail showing an unknown interaction with K-struvite matrix inside the remarked zone in Fig. 6.b. As can be observed, part of the particle outside layer reacted with the matrix and were

integrated . Elemental mapping reinforced this idea can be observed in Fig. 6.b. Si signal overlaps with that of Mg, P, and K. This could be probably because the elemental signal covers a certain volumetric range in the sample. The upper edge of the CPS particle (Fig. 6.b) seemed to have suffered some sort of interaction with the matrix. In order to determine if chemical reactions occurred FTIR-ATR was used. Fig. 7 shows CSP, R15-365d and R11-365d infrared spectra. The lack of sharp peaks in CSP spectrum is related to the disorder of the silicate network [50]. Both mortar spectra presented the same profile which was close to similar materials [51–53]. The most important peak is about 1000 cm^{-1}. Fig. 8.b, Fig. 8.c, and Fig. 8.d show the three deconvoluted spectra (R15-365d, CSP, and R11-365d) in the wavenumber range between 1400 and 700 cm^{-1}. In this range is possible to observe the main vibrations of phosphate group [52], being the same region of Si-O stretching [50]. Fig. 8.a points out the broad band for CSP around 1000 cm^{-1} in comparison with R15-365d and R11-365d spectra. The curves were fitted by using Gaussian shapes, minimizing the number of curves, and obtaining a regression coefficient R^2 higher than 0.999 [54]. In each case, the R^2 obtained was 0.9997, hence the curves were properly fitted. The CSP deconvolution (Fig. 8.c) revealed two main bands at 1025 and 928 cm^{-1} that can be assigned to Si-O asymmetric stretching modes of bridging oxygens (BOs) and non-bridging oxygens (NBOs), respectively [50]. The bands between 1300-800 cm^{-1} were related to the stretching vibrations of SiO_4 tetrahedron depending on the number of shared oxygens [50]. Bands at 788 and 758 cm^{-1} could be assigned to the bending vibration of Si-O-Si at 784 cm^{-1} [55] and Al-O vibration modes due to tetrahedral AlO_4 group [56], respectively. Finally, the deconvoluted broad band at 1158 cm^{-1} could be assigned to Si-O-Al asymmetric stretching vibration [56].

R15-365d and R11-365d deconvoluted spectra (Fig. 8.b and Fig. 8.d) showed that the deconvoluted bands from 923 to 741 cm^{-1} were coincident on both spectra. Because of the unreacted carbonated phases from LG-MgO raw material, some bands attributed to the CO_3^{2-} group were observed (probably due to the presence of magnesite or even dolomite): asymmetrical stretching vibration of the O-C-O about 1450 cm^{-1} (see Fig. 7), as well as 880-879 cm^{-1} and 742-741 cm^{-1} deconvoluted bands determined in Fig. 8.b and Fig. 8.d, assigned to out-of-plane bend and in-plane bend vibrations, respectively, for both samples [57]. The deconvoluted band at 792 cm^{-1} observed in both samples (Fig. 8.b and Fig. 8.d) was assigned to quartz due to the presence of this phase in the LG-MgO raw material and in both R11-365d and R15-365d (see Fig. 1 and Fig. 3.b). Considering the deconvoluted bands for R11-365d, these bands were in concordance with other authors [52,58]. Indeed, the bands at 1102, 1047, 997, and 923 cm^{-1} were

assigned to P-O stretching as the reported bands at 1095-1105, 1054-1075, 978-978, and 916-951 cm^{-1} [52,58]. In the case of R15-365d (see Fig. 8.b), the presented deconvoluted bands differed in comparison with R11-365d. Concretely, the bands at 1119 and 1023 cm^{-1} could be related with a potential substitution of P in the SiO_4 tetrahedron of CSP or Si in the PO_4 tetrahedron of K-struvite matrix due to the shift in both bands to higher frequencies. It is reported that the typical Si-O-P bands due to stretching vibrations appear about 1150-1100 and 1000 cm^{-1} [59]. This assumption is related to SEM evaluation. However, this must not be taken as absolute certainty because of the similar range wavenumber of the SiO_4^{4-} and PO_4^{3-} due to their same tetrahedral structure [60].

XRD results agreed with SEM and EDS analysis results, being K-struvite the main component in the mortars matrix. This was also reinforced and quantified with TGA-SDT results. Other crystalline compounds found in the XRD analysis were identified in SEM images by EDS. Iron oxide was observed in XRF results in LG-MgO sample and also in the form of small particles in the mortars matrix in SEM observation and EDS results. CSP particles showed a remarkably excellent matrix embedment as it can be observed in SEM images. Focusing on the magnified image in Fig. 6.b, an intermediate zone between matrix and the particle is observed, where a colour degradation and an evident blending of the particle-matrix contour is highlighted. The mapping results of this zone was determinant to suppose some reaction degree between the filler and matrix despite XRD results, where no new crystalline phases were found by comparing the R11-365d and R15-365d mortars diffraction spectra. TGA-SDT analysis also did not show any evidence of a new compound formed apart from than K-struvite. Considering TGA-SDT, XRD, and EDS mapping results, it can be concluded that the reaction degree was low and thus in the hypothetical case of the reaction of the filler with matrix either i) the percentage of the new silicophosphate compound was small (inferior to 1 wt.%) or ii) the new compound was in amorphous state and also with a small wt.%. Using and analysing the FTIR-ATR spectra of the samples cured at 365 d, there were slight deviations of the deconvoluted peaks frequencies that could lead to a potential substitution of P in the SiO_4 tetrahedron of CSP or Si in the PO_4 tetrahedron of K-struvite matrix. With that substitution, CSP particles should be partially merged with the matrix as it can be seen in SEM images. More evidence is needed to determine with assertiveness the kind of compound and its possible formation in the reaction of between CSP glass waste filler and matrix.

4. Conclusions

It is plausible to formulate sust-MPC mortars mixed with inorganic glass waste (CSP) as a filler for enhancing the mechanical properties. This is named sust-MPC mortar when formulated with LG-MgO due to its sustainability characteristics. CSP is an inorganic solid waste from industrial and urban glass residues. The main idea when developing sust-MPC mortar using CSP was to enhance not only mechanical properties but to reduce its environmental impact. Revalorization of both residue sources was achieved lowering the price of the final product, promoting circular economy and reducing CO_2 emissions due to the reduction in the magnesia production implied in the use of LG-MgO. Therefore, sust-MPC mortar was developed successfully with CSP upgrading the MPC properties, as expected.

The statistical models generated based on DoE were performed successfully. The results were validated, fitting with the required requirements, and having remarkable accuracies regarding the properties responses of each of the possible formulations compressed within W/C and CSP wt.% studied factor ranges. This set of models based on more than one variable allows estimating the properties of possible formulations, optimizing the whole system, obtaining an optimal formulation with a compromise between properties to perform best according to criteria, and evaluating the variables synergetic effect or factors between them. An optimal formulation was found using the response surface methodology and every DoE model generated was statistically significant.

Optimal formulation was designated to that of the same formulation as R15 with W/C of 0.34 and 15 wt.% of CSP content giving CS values superior to 25 MPa. As for synergetic interaction between factors, it was established that CSP and W/C had certain dependency and synergetic interaction between them.

After one year of curing, optimal formulation and a reference sample without CSP were characterized in order to review their evolution with time. Optimal formulation showed good integration of CSP particles in the matrix. Whereas there was not enough evidence, some CSP particles in sust-MPC mortar matrix presented some degree of chemical reaction between matrix and particles as presented in elemental EDS mapping results and FTIR-ATR spectra analysis, this being yet an uncertain fact.

Future research will need a more detailed structural and chemical characterization to perform sust-MPC mortars to acquire more evidence of the suspected chemical interaction between silica-rich soda-lime glass CSP particles and K-struvite matrix.

Declaration of competing interest

The authors declare that they have no known competing financial interests or personal relationships that could have appeared to influence the work reported in this paper.

Acknowledgements

The authors would like to thank Magnesitas Navarras S.A. for its cooperation in financing and supporting the work. Also, would want to thank Daniel Rosas S.A. for CSP material supplying. The authors are grateful to the Catalan Government for the quality accreditation given to their research group DIOPMA (2017 SGR 118). This work was supported by Magnesitas Navarras S.A. and the Spanish Government (BIA2017-83912-C2-1-R). We specially thank Mr. Eduard Cosialls for getting involved with experimental tasks. Mr. S. Huete-Hernández is grateful to the Government of Catalonia and the University of Barcelona for the research Grant (APIF-DGR 2018). Mr Alex Maldonado-Alameda is grateful to the Government of Catalonia for the research Grant (FI-DGR 2017). Dr Jessica Giro-Paloma is a Serra Húnter Fellow.

References

[1] R.M. Andrew, Global CO_2 emissions from cement production, 1928 – 2018, Earth Syst. Sci. Data. 11 (2019) 1675–1710. doi:10.5194/essd-11-1675-2019.

[2] Z. He, X. Zhu, J. Wang, M. Mu, Y. Wang, Comparison of CO_2 emissions from OPC and recycled cement production, Constr. Build. Mater. 211 (2019) 965–973. doi:10.1016/j.conbuildmat.2019.03.289.

[3] J. Farfan, M. Fasihi, C. Breyer, Trends in the global cement industry and opportunities for long-term sustainable CCU potential for Power-to-X, J. Clean. Prod. 217 (2019) 821–835. doi:10.1016/j.jclepro.2019.01.226.

[4] T. Gao, L. Shen, M. Shen, L. Liu, F. Chen, Analysis of material flow and consumption in cement production process, J. Clean. Prod. 112 (2016) 553–565. doi:10.1016/j.jclepro.2015.08.054.

[5] C. Shi, A.F. Jiménez, A. Palomo, New cements for the 21st century: The pursuit of an alternative to Portland cement, Cem. Concr. Res. 41 (2011) 750–763. doi:10.1016/j.cemconres.2011.03.016.

[6] M.C.G. Juenger, F. Winnefeld, J.L. Provis, J.H. Ideker, Cement and Concrete Research Advances in alternative cementitious binders, Cem. Concr. Res. 41 (2011) 1232–1243. doi:10.1016/j.cemconres.2010.11.012.

[7] E. Gartner, T. Sui, Alternative cement clinkers, Cem. Concr. Res. 114 (2018) 27–39. doi:10.1016/j.cemconres.2017.02.002.

[8] N. Li, C. Shi, Z. Zhang, Understanding the roles of activators towards setting and hardening control of alkali-activated slag cement, Compos. Part B. 171 (2019) 34–45. doi:10.1016/j.compositesb.2019.04.024.

[9] Y.H.M. Amran, N. Farzadnia, A.A.A. Ali, Properties and applications of foamed concrete; A review, Constr. Build. Mater. 101 (2015) 990–1005. doi:10.1016/j.conbuildmat.2015.10.112.

[10] M. Nabiyouni, T. Brückner, H. Zhou, U. Gbureck, S.B. Bhaduri, Magnesium-based bioceramics in orthopedic applications, Acta Biomater. 66 (2018) 23–43. doi:10.1016/j.actbio.2017.11.033.

[11] S. Luo, M. Liu, L. Yang, J. Chang, W. Yang, X. Yan, H. Yu, Y. Shen, Utilization of waste from alumina industry to produce sustainable cement-based materials, Constr. Build. Mater. 229 (2019) 116795. doi:10.1016/j.conbuildmat.2019.116795.

[12] G. Mestres, M.P. Ginebra, Novel magnesium phosphate cements with high early strength and antibacterial properties, Acta Biomater. 7 (2011) 1853–1861. doi:10.1016/j.actbio.2010.12.008.

[13] F. Qiao, C.K. Chau, Z. Li, Property evaluation of magnesium phosphate cement mortar as patch repair material, Constr. Build. Mater. 24 (2010) 695–700. doi:10.1016/j.conbuildmat.2009.10.039.

[14] A.S. Wagh, S.Y. Jeong, Chemically Bonded Phosphate Ceramics: I, A Dissolution Model of Formation, J. Am. Ceram. Soc. 86 (2003) 1838–1844. doi:10.1111/j.1151-2916.2003.tb03569.x.

[15] H. Lahalle, C.C.D. Coumes, A. Mesbah, D. Lambertin, C. Cannes, S. Delpech, S. Gauffinet, Investigation of magnesium phosphate cement hydration in diluted suspension and its retardation by boric acid, Cem. Concr. Res. 87 (2016) 77–86. doi:10.1016/j.cemconres.2016.04.010.

[16] A.S. Wagh, S.Y. Sayenko, A.N. Dovbnya, V.A. Shkuropatenko, R. V. Tarasov, A. V. Rybka, A.A. Zakharchenko, Durability and shielding performance of borated Ceramicrete coatings in beta and gamma radiation fields, J. Nucl. Mater. 462 (2015) 165–172. doi:10.1016/j.jnucmat.2015.03.049.

[17] A.S. Wagh, Chemically Bonded Phosphate Ceramics, First edit, Elsevier Science, Oxford, UK, 2004. doi:10.1016/B978-0-08-044505-2.X5000-5.

[18] N. Roghanian, N. Banthia, Development of a sustainable coating and repair material to prevent bio-corrosion in concrete sewer and waste-water pipes, Cem. Concr. Compos. 100 (2019) 99–107. doi:10.1016/j.cemconcomp.2019.03.026.

[19] X. Jia, J. Li, P. Wang, J. Qian, M. Tang, Preparation and mechanical properties of magnesium phosphate cement for rapid construction repair in ice and snow, Constr. Build. Mater. 229 (2019) 116927. doi:10.1016/j.conbuildmat.2019.116927.

[20] W. Montague, L. Vandeperre, M. Hayes, Processing Characteristics and Strength of Magnesium Phosphate Cement Formulations Compatible with UK Nuclear Waste Treatment Plants, MRS Proc. 1475 (2012) imrc11-1475-nw35-p03. doi:10.1557/opl.2012.588.

[21] Y. Tao, L. Zhenyu, R. Chunrong, W. Yuanyuan, H. Zhichao, H. Xin, W. Jie, L. Mengliang, D. Qiubai, K. Khan, L. Zhongyuan, L. Shuzhen, Study on solidification properties of chemically bonded phosphate ceramics for cesium radionuclides, Ceram. Int. 46 (2020) 14964–14971. https://doi.org/10.1016/j.ceramint.2020.03.025.

[22] A. Viani, A.F. Gualtieri, Preparation of magnesium phosphate cement by recycling the product of thermal transformation of asbestos containing wastes, Cem. Concr. Res. 58 (2014) 56–66. doi:10.1016/j.cemconres.2013.11.016.

[23] A.S. Wagh, Chapter 14: Chemically Bonded Phosphate Ceramic Matrix Compsites, in: Chem. Bond. Phosphate Ceram. Twenty-First Century Mater. With Divers. Appplications, First edit, Elsevier Ltd, Argonne, USA, 2004: pp. 157–176. doi:10.1016/B978-008044505-2/50018-1.

[24] M. Niubó, J. Formosa, A. Maldonado-Alameda, R. del Valle-Zermeño, J.M. Chimenos, Magnesium phosphate cement formulated with low grade magnesium oxide with controlled porosity and low thermal conductivity as a function of admixture, Ceram. Int. 42 (2016) 15049–15056. doi:10.1016/j.ceramint.2016.06.159.

[25] J. Formosa, A.M. Lacasta, A. Navarro, R. del Valle-Zermeño, M. Niubó, J.R. Rosell, J.M. Chimenos, Magnesium Phosphate Cements formulated with a low-grade MgO by-product: Physico-mechanical and durability aspects, Constr. Build. Mater. 91 (2015) 150–157. doi:10.1016/j.conbuildmat.2015.05.071.

[26] M. Morales, J. Formosa, E. Xuriguera, M. Niubó, M. Segarra, J.M. Chimenos, Elastic modulus of a chemically bonded phosphate ceramic formulated with low-grade magnesium oxide determined by Nanoindentation, Ceram. Int. 41 (2015) 12137–12146. doi:10.1016/j.ceramint.2015.06.031.

[27] B. Xu, H. Ma, H. Shao, Z. Li, B. Lothenbach, Influence of fly ash on the compressive strength and micro-characteristics of magnesium potassium phosphate cement mortars, Cem. Concr. Res. 99 (2017) 86–94. doi:10.1016/j.cemconres.2017.05.008.

[28] J. Giro-Paloma, C. Barreneche, A. Maldonado-Alameda, M. Royo, J. Formosa, A.I. Fernández, J.M. Chimenos, Alkali-activated cements for TES materials in buildings' envelops formulated with glass cullet recycling waste and microencapsulated phase change materials, Materials (Basel). 12 (2019) 1–11. doi:10.3390/ma12132144.

[29] M. Ruth, P. Dell'Anno, An industrial ecology of the US glass industry, Resour. Policy. 23 (1997) 109–124. doi:10.1016/s0301-4207(97)00020-2.

[30] N. Dias, I. Garrinhas, A. Maximo, N. Belo, P. Roque, M.T. Carvalho, Recovery of glass from the inert fraction refused by MBT plants in a pilot plant, Waste Manag. 46 (2015) 201–211. doi:10.1016/j.wasman.2015.07.052.

[31] J. Formosa, M.A. Aranda, J.M. Chimenos, J.R. Rosell, A.I. Fernández, O. Ginés, Cementos químicos formulados con subproductos de óxido de magnesio, Boletín La Soc. Española Cerámica y Vidr. 47 (2008) 293–297. doi:10.3989/cyv.2008.v47.i5.169.

[32] A. Maldonado-Alameda, A.M. Lacasta, J. Giro-Paloma, J.M. Chimenos, L. Haurie, J. Formosa,

Magnesium phosphate cements formulated with low grade magnesium oxide incorporating phase change materials for thermal energy storage, Constr. Build. Mater. 155 (2017) 209–216. doi:10.1016/j.conbuildmat.2017.07.227.

[33] J. Formosa, J.M. Chimenos, A.M. Lacasta, M. Niubó, Interaction between low-grade magnesium oxide and boric acid in chemically bonded phosphate ceramics formulation, Ceram. Int. 38 (2012) 2483–2493. doi:10.1016/j.ceramint.2011.11.017.

[34] C.A. Strydom, E.M. Van Der Merwe, M.E. Aphane, The effect of calcining conditions on the rehydration of dead burnt magnesium oxide using magnesium acetate as a hydrating agent, J. Therm. Anal. Calorim. 80 (2005) 659–662. doi:10.1007/s10973-005-0710-x.

[35] D.C. Montgomery, Design and Analysis of Experiments, Sixth edit, John Wiley & Sons, Ltd, New York, USA, 2004.

[36] M. Niubó, A.I. Fernández, L. Haurie, X.G. Capdevila, J.M. Chimenos, J.I. Velasco, Influence of the Electric Arc Furnace Dust in the physical and mechanical properties of EVA–polyethylene–butene blends, Mater. Sci. Eng. A. 528 (2011) 4437–4444. doi:10.1016/j.msea.2011.02.006.

[37] B. Xu, H. Ma, H. Shao, Z. Li, B. Lothenbach, Influence of fly ash on compressive strength and micro-characteristics of magnesium potassium phosphate cement mortars, Cem. Concr. Res. 99 (2017) 86–94. doi:10.1016/j.cemconres.2017.05.008.

[38] L.J. Gardner, S.A. Bernal, S.A. Walling, C.L. Corkhill, J.L. Provis, N.C. Hyatt, Characterisation of magnesium potassium phosphate cements blended with fly ash and ground granulated blast furnace slag, Cem. Concr. Res. 74 (2015) 78–87. doi:10.1016/j.cemconres.2015.01.015.

[39] Y. Xie, X. Lin, X. Pan, T. Ji, Preliminary investigation of the hydration mechanism of the hydration mechanism of MgO-SiO_2-K_2HPO_4 cement, Constr. Build. Mater. 235 (2020) 117471. doi:10.1016/j.conbuildmat.2019.117471.

[40] J. Formosa, J.M. Chimenos, A.M. Lacasta, L. Haurie, Thermal study of low-grade magnesium hydroxide used as fire retardant and in passive fire protection, Thermochim. Acta. 515 (2011) 43–50. doi:10.1016/j.tca.2010.12.018.

[41] D. V. Ribeiro, G.R. Paula, M.R. Morelli, Use of microwave oven in the calcination of MgO and effect on the properties of magnesium phosphate cement, Constr. Build. Mater. 198 (2019) 619–628. doi:10.1016/j.conbuildmat.2018.11.289.

[42] R. del Valle-Zermeño, J. Giro-Paloma, J. Formosa, J.M. Chimenos, Low-grade magnesium oxide

by-products for environmental solutions: Characterization and geochemical performance, J. Geochemical Explor. 152 (2015) 134–144. doi:10.1016/j.gexplo.2015.02.007.

[43] S.A. Emamian, H. Eskandari-Naddaf, Effect of porosity on predicting compressive and flexural strength of cement mortar containing micro and nano-silica by ANN and GEP, Constr. Build. Mater. 218 (2019) 8–27. doi:10.1016/j.conbuildmat.2019.05.092.

[44] B. Xu, B. Lothenbach, A. Leemann, F. Winnefeld, Reaction mechanism of magnesium potassium phosphate cement with high magnesium-to-phosphate ratio, Cem. Concr. Res. 108 (2018) 140–151. doi:10.1016/j.cemconres.2018.03.013.

[45] H. Lahalle, C. Patapy, M. Glid, G. Renaudin, M. Cyr, Microstructural evolution/durability of magnesium phosphate cement paste over time in neutral and basic environments, Cem. Concr. Res. 122 (2019) 42–58. doi:10.1016/j.cemconres.2019.04.011.

[46] C. Yu, Q. Wu, J. Yang, Effect of seawater for mixing on properties of potassium magnesium phosphate cement paste, Constr. Build. Mater. 155 (2017) 217–227. doi:10.1016/j.conbuildmat.2017.08.050.

[47] D.A. Hall, R. Stevens, B. El-Jazairi, The effect of retarders on the microstructure and mechanical properties of magnesia-phosphate cement mortar, Cem. Concr. Res. 31 (2001) 455–465. doi:10.1016/S0008-8846(00)00501-9.

[48] M.R. Ahmad, B. Chen, Effect of silica fume and basalt fiber on the mechanical properties and microstructure of magnesium phosphate cement (MPC) mortar, Constr. Build. Mater. 190 (2018) 466–478. doi:10.1016/j.conbuildmat.2018.09.143.

[49] S. Graeser, W. Postl, H.-P. Bojar, P. Berlepsch, T. Armbruster, T. Raber, K. Ettinger, F. Walter, Struvite-(K), $KMgPO_4 \cdot 6H_2O$, the potassium equivalent of struvite – a new mineral, Eur. J. Miner. 20 (2008) 629–633. doi:10.7868/s002347611506020x.

[50] I. Kansal, A. Reddy, F. Muñoz, S.J. Choi, H.W. Kim, D.U. Tulyaganov, J.M.F. Ferreira, Structure, biodegradation behavior and cytotoxicity of alkali-containing alkaline-earth phosphosilicate glasses, Mater. Sci. Eng. C. 44 (2014) 159–165. doi:10.1016/j.msec.2014.08.016.

[51] B. Lothenbach, B. Xu, F. Winnefeld, Thermodynamic data for magnesium (potassium) phosphates, Appl. Geochemistry. 111 (2019) 104450. doi:10.1016/j.apgeochem.2019.104450.

[52] P. Mácová, A. Viani, Investigation of setting reaction in magnesium potassium phosphate ceramics with time resolved infrared spectroscopy, Mater. Lett. 205 (2017) 62–66.

doi:10.1016/j.matlet.2017.06.063.

[53] D. Leng, X. Li, Y. Lv, H. Tan, N. Li, Z. Liu, W. Jiang, D. Jiang, Cesium immobilization by K-struvite crystal in aqueous solution: Ab initio calculations and experiments, J. Hazard. Mater. 387 (2020) 121872. doi:10.1016/j.jhazmat.2019.121872.

[54] Z. Zhang, H. Wang, J.L. Provis, F. Bullen, A. Reid, Y. Zhu, Quantitative kinetic and structural analysis of geopolymers. Part 1. the activation of metakaolin with sodium hydroxide, Thermochim. Acta. 539 (2012) 23–33. doi:10.1016/j.tca.2012.03.021.

[55] C.Z. Tan, J. Arndt, Interaction of longitudinal and transverse optic modes in silica glass, J. Chem. Phys. 112 (2000) 5970–5974. doi:10.1063/1.481169.

[56] P. Padmaja, G.M. Anilkumar, P. Mukundan, G. Aruldhas, K.G.K. Warrier, Characterisation of stoichiometric sol-gel mullite by fourier transform infrared spectroscopy, Int. J. Inorg. Mater. 3 (2001) 693–698. doi:10.1016/S1466-6049(01)00189-1.

[57] G. Jovanovski, V. Stefov, B. Šoptrajanov, B. Boev, Minerals from Macedonia. IV. Discrimination between some carbonate minerals by FTIR spectroscopy, Neues Jahrb. Fur Mineral. Abhandlungen. 177 (2002) 241–253. doi:10.1127/0077-7757/2002/0177-0241.

[58] A. Viani, P. Mácová, Polyamorphism and frustrated crystallization in the acid-base reaction of magnesium potassium phosphate cements, CrystEngComm. 20 (2018) 4600–4613. doi:10.1039/c8ce00670a.

[59] S. Jähnigen, E. Brendler, U. Böhme, G. Heide, E. Kroke, Silicophosphates containing SiO_6 octahedra-anhydrous synthesis under ambient conditions, New J. Chem. 38 (2014) 744–751. doi:10.1039/c3nj00721a.

[60] A. Udduttula, J. Li, P.Y. Zhao, G.C. Wang, J. V. Zhang, P.G. Ren, Sol-gel derived nanosized $Sr_5(PO_4)_2SiO_4$ powder with enhanced in vitro osteogenesis and angiogenesis for bone regeneration applications, Ceram. Int. 45 (2019) 3148–3158. doi:10.1016/j.ceramint.2018.10.215.

*Declaration of Interest Statement

Declaration of interests

☒ The authors declare that they have no known competing financial interests or personal relationships that could have appeared to influence the work reported in this paper.

☐The authors declare the following financial interests/personal relationships which may be considered as potential competing interests:

Fabrication of Sustainable Magnesium Phosphate Cement Micromortar using Design of Experiments Statistical Modelling: Valorization of Ceramic-Stone-Porcelain containing waste as filler

S. Huete-Hernández[a], A. Maldonado-Alameda[a], J. Giro-Paloma[a], J.M. Chimenos[a], J. Formosa[a*]

[a]Departament de Ciència de Materials i Química Física. Universitat de Barcelona, Martí i Franquès 1, 08028 Barcelona, Spain

*Author to who correspondence should be addressed. Telephone: +34934021316; Fax: +34934035438; E-mail: joanformosa@ub.edu. Departament de Ciència de Materials i Química Física. Universitat de Barcelona, Martí i Franquès 1, 08028 Barcelona, Spain.

Abstract

Magnesium phosphate cement (MPC) is a potential sustainable alternative to Portland cement. It is possible to lower the total CO_2 emissions related to MPC manufacturing by using by-products and wastes as raw materials. When by-products are used to develop MPC, the resultant binder can be referred to as sustainable magnesium phosphate cement (sust-MPC). This research incorporates ceramic, stone, and porcelain waste (CSP) as a filler in sust-MPC to obtain a micromortar. Sust-MPC is formulated with KH_2PO_4 and low-grade MgO (LG-MgO), a by-product composed of 40–60 wt.% MgO. CSP is the non-recyclable glass fraction generated by the glass recycling industry. The effect of water and CSP addition on the mechanical properties of sust-MPC was analyzed using design of experiments (DoE). A statistical model was obtained and validated by testing ideally formulated samples achieved through optimization of the DoE. The optimal formulation (15 wt.% of CSP and a water to cement ratio of 0.34) was realized by maximizing the compressive strength at 7 and 28 days of curing, resulting in values of 18 and 25 MPa respectively. After one year of curing, the micromortar was physico-chemically characterized in-depth using backscattered scanning electron microscopy (BSEM-EDS) and Fourier transform infrared-attenuated total reflectance spectroscopy (FTIR-ATR). The optimal formulation showed good integration of CSP particles in the

ceramic matrix. Thus, a potential reaction between silica and the K-struvite matrix may have occurred after one year of curing.

Keywords

B. Microstructure-final; C. Mechanical properties; D. MgO; E. Structural applications; Design of experiments.

Abbreviations

MPC	Magnesium Phosphate Cement
LG	Low-Grade. Refers to a product containing impurities and of lower quality than the pure product
LG-MgO	Low-grade MgO. MgO containing impurities and of lower quality than pure MgO
Sust-MPC	Sustainable Magnesium Phosphate Cement
CSP	Ceramic, Stone, and Porcelain Waste
DoE	Design of Experiments
CBC	Chemically Bonded Ceramics
CBPC	Chemically Bonded Phosphate Cements
MKP	Monopotassium Phosphate
RSM	Response Surface Methodology
CSP(%)	Ceramic, Stone, and Porcelain Waste percentage in the micromortar
R1-16	Micromortar formulation from the corresponding design of experiments run
-7d, -28d, -365d	Number of days of curing before testing and characterization

---

1. Introduction

In terms of pollution and greenhouse gas emissions, the construction and building industry sector faces an important challenge in the coming years since this sector is responsible for approximately 7–8% of total global CO_2 emissions [1,2]. This is because Portland cement is one of the most produced and widely applied construction materials worldwide owing to its various properties and low cost [3,4]. Also termed hydraulic cement, the production process for Portland cement consumes extremely high amounts of energy, depleting and overexploiting natural resources. However, in recent years, new types of alternative cements have emerged, presenting different and improved properties, extending their application range in diverse technology areas [5–7]. These properties can vary from mechanical attributes such as enhanced compressive strength (CS) [8] and porosity [9] to biocompatibility [10] and environmental sustainability [11]. Among the different types of alternative cements, chemically bonded ceramics (CBC) and, more specifically, chemically bonded phosphate cements (CBPCs), stand out as an early strength cement exhibiting rapid setting [12] and good volume stability [13]. An example of a CBPC is magnesium phosphate cement (MPC), in which magnesium oxide (MgO) is combined with monopotassium phosphate (MKP, KH_2PO_4) to form magnesium potassium phosphate ($MgKPO_4 \cdot 6H_2O$), also known as K-struvite owing to its crystalline structure (Eq. (1)) [14,15]. K-struvite is a type of CBPC that presents superior properties for high-performance cement applications [16].

$$MgO + KH_2PO_4 + 5H_2O \leftrightarrow MgKPO_4 \cdot 6H_2O \quad (1)$$

MPC possesses numerous advantageous properties such as a neutral pH due to an acid-base formation reaction, low water demand and drying shrinkage, and rapid development of the compressive strength [17]. MPC can be applied in cold weather because of the rapid and exothermic nature of its setting chemical reaction (Eq. (1)). It can be used as a repair material to restore roads damaged by traffic, and for the rehabilitation of various infrastructures among other applications [13,18,19]. MPC is primarily applied in the stabilization and solidification of low-level radioactive wastes containing reactive metals [20], with outstanding encapsulation properties from the point of view of waste management [21,22], and is also used in biomedical implants [12]. Despite the advantages of MPC mentioned above, the production of MgO in accordance with the Portland cement clinker production process generates excessive CO_2 emission and consumes vast quantities of energy due to the calcination of natural magnesite ($MgCO_3$) and dolomite

($MgCa(CO_3)_2$). Nevertheless, the MgO process generates much lower pollution than Portland cement clinker fabrication [23].

MgO production begins with sieving of $MgCO_3$ and $MgCa(CO_3)_2$ minerals and feeding these to a kiln for the calcination process. The low-grade MgO (LG-MgO) by-product is retained as powder cyclone dust in the filters of the air pollution control system during the combustion process. LG-MgO is composed of chemically reactive MgO (40–60 wt.%) produced from heavily calcined MgO. Owing to its reactive MgO component and economic cost, LG-MgO must be considered as a sustainable source of material in the MPC field. The feasibility of using LG-MgO to obtain MPC was demonstrated in previous studies with outstanding results obtained [24–26]. Considering the above, this material can be considered as sust-MPC; a green cement compared with common MPC. Unreacted particles such as carbonates and quartz are perceived as fine inorganic fillers inside the sust-MPC paste. Consequently, sust-MPC is considered to be a micromortar. Furthermore, the addition of inorganic fillers in sust-MPC micromortars improves the binder fresh mixture workability and reduces heat development and production costs [27]. The use of solid waste as an inorganic filler in sust-MPC micromortars opens up the possibility of solid waste treatment including residual non-profitable or recyclable materials. For instance, ceramic, stone, and porcelain waste (CSP) is the fraction removed from the glass cullet recycling process. The CSP fraction is considered as non-valuable waste because it is too small, possesses glued paper labels, or contains other diverse impurities. CSP is composed of approximately 84 wt.% soda-lime glass, 6 wt.% porcelain, 6 wt.% ceramic, and 4 wt.% stone, polymer/paper, metals, organic matter, and others [28]. Because CSP is derived from municipal and industrial waste, over time its composition becomes heterogeneous depending on the weather season, society consumption tendencies, and garbage dumping preferences. CSP is a major problem for glass cullet recycling companies because its melting point is higher than that of pure soda-lime glass, inhibiting the melting process and complicating glass recovery procedures. Nowadays, automated chromatic separators are employed to optically sort and classify clean and contaminated shattered glass. However, chromatic separators do not detect coarse glass fragments such as the bottom of bottles and bottlenecks darker in tone than ordinary shattered glass [29,30]. Moreover, recycling companies only accept glass cullet if the CSP concentration is between 20–100 $g \cdot t^{-1}$ or below [31]. Therefore, CSP is treated as a non-profitable material and is dumped in landfill sites.

The primary purpose of this investigation is to develop a sust-MPC micromortar using CSP as an inorganic filler and LG-MgO in place of pure MgO. In addition, the interaction between the CSP filler and the

micromortar K-struvite matrix is studied over time. This study is based on our previous experience in obtaining sust-MPC [24,25,32–34]. When CSP is utilized as a filler, the economic costs are reduced and environmental and sustainable criteria are enhanced. Design of experiments (DoE) was used to minimize the number of experiments carried out. The implementation of a factorial design model using DoE enables extraction of the maximum amount of information from the experiments performed. Predictive theoretical mathematical models are determined for each response, allowing estimation of the micromortar behavior and determination of an optimal and adequate formulation possessing the properties required in the range of the study.

2. Experimental procedure

2.1 Materials

LG-MgO by-product was supplied by Magnesitas Navarras, S.A., located in Navarra (Spain). This plant generates various industrial solid by-products including LG-MgO. These by-products are treated according to the dictates in the international and Spanish environmental and sustainability normative ISO 14000 embedded in UNE-EN ISO 14001:2015 and UNE-EN ISO 50001:2018.

The phosphate source was food-grade KH_2PO_4 with a purity of 99.8 wt.% obtained from Norken, S.L., and is commonly used as a fertilizer and is soluble in water.

CSP waste glass in the form of shattered solid fragments > 2 mm and with an average size range of 8–16 mm was provided by Daniel Rosas, S.A. This company is a recycling plant that treats glass cullet from urban and industrial garbage dump containers following the Spanish normatives UNE-EN ISO 9001:2015, UNE-EN ISO 14001:2015, and the European Commission Regulation (EU) Nº 1179/2012. A total of 24 kg CSP waste was quartered and homogenized to ensure a representative chemical composition. To increase the reactivity, paper, polymeric, and metallic fragments were removed from the CSP. The sample was shredded to a size below 2 mm, milled in an alumina ball mill, and sieved to a size below 80 μm.

In order to hydrate the raw materials, deionized water was employed to avoid chloride impurities, which are frequently present in tap water.

2.1.1 Raw materials characterization

Approximately 250 g representative sub-samples of LG-MgO and CSP were obtained by quartering each of the initial samples. MKP was not characterized since it is a commercial product and was previously

evaluated in-depth by our group [24–26,34]. LG-MgO and CSP were characterized using complementary techniques such as particle size distribution (PSD), X-ray fluorescence (XRF), X-ray diffraction (XRD), and thermogravimetric analysis with derivative thermogravimetry (TG/DTG). In addition, a citric acid test [35] was completed to evaluate the reactivity of LG-MgO. A pH meter was used as an alternative to visual evaluation using phenolphthalein. For the citric acid test, 2 g LG-MgO was continuously stirred (500 rpm min^{-1}) at 30 °C in 100 mL citric acid solution until a pH of 9 was achieved and the elapsed time was measured. The citric acid solution was prepared by stirring 28 g citric acid monohydrate in deionized water to obtain a 1 l solution. Samples were tested in triplicate.

XRD analysis was carried out using a PANalytical X'Pert PRO MPD Alpha1 powder diffractometer. XRF analysis was performed using a Philips PW2400 X-ray sequential spectrophotometer to elucidate the major and minor elements. To conduct TG/DTG analysis, a TA Instruments Q-600 SDT was used. Tests were conducted from 30 to 1400 °C at a heating rate of 10 °C·min^{-1} in a nitrogen atmosphere with a gas flow of 100 mL·min^{-1}.

2.2 Design of experiments

Design of experiments was implemented to reduce the number of experiments and to identify how the CSP filler phase influences the final properties of the sust-MPC micromortar. On the one hand, the apparent density (ρ), modulus of elasticity (MOE), flexural strength (FS), and compressive strength were evaluated at 7 days (d). In this study, the compressive strength was also evaluated at 28 d. On the other hand, design of experiments was employed to evaluate if the variables or factors (filler and water percentage) were synergistically correlated, affecting the final properties of the composite. Using this technique, it is possible to obtain a desired sust-MPC micromortar dosage by varying the factors under study to produce convenient mechanical and physical properties for the preferred application [36,37].

The LG-MgO/MKP ratio of the cement was fixed at 60/40 based on previous experience [34]. The CSP weight percentage (CSP(%)) and water-to-cement ratio (W/C) were the variables or factors studied in this investigation. The total quantity of cement (C) is a combination of both the masses of MKP and LG-MgO in the mixture. Hence, CSP is considered as a filler, although it may slightly react at the interface of K-struvite over a long period of time. The lowest and highest levels for W/C and CSP(%) were 0.34/0.38 and 0/15 wt.%, respectively. An increase in CSP present in the mixture requires additional water to adjust the workability, usually related to a non-desired decrease in the final mechanical properties of the product.

Therefore, the levels were determined after preliminary experiments to ensure proper workability of the fresh sust-MPC micromortar. The objective of the preliminary study was to introduce the highest amount of CSP possible while keeping W/C as low as possible.

The present study employs a response surface methodology (RSM) with a D-optimal and quadratic design to perform a further optimization process using previously obtained results. RSM includes analysis of a response surface plot calculated from statistical polynomic equations that are derived from the experimentally obtained results. One surface was plotted for each measured property (response) of the material studied. Design Expert® software was used for the design of experiments. The resulting mixtures are summarized in Table 1, where the lowest/highest level of each factor is highlighted in bold.

2.2.1 Design of experiments optimal formulation

The design of experiments analysis is based on analysis of variance (ANOVA) to predict an optimal response [36], using p-values to interpret the obtained results. The p-value represents the smallest level of significance that would lead to rejection of the null-hypothesis, indicating that the controllable factor does not affect the response under investigation. If the p-value in a test for the significance of a certain factor is smaller than 0.05, this factor is considered statistically significant with a confidence level above 95%.

The ratio model SS/residual SS (model SS and residual SS refer to the regression and error sum of squares, respectively) defines the F-value. A significant contribution is present in the case of large F-values, while small values indicate that the variance is affected by noise. CSP(%) and W/C were chosen as the factors, and their effects on the composite properties were quantified. The model should be validated to check its feasibility.

2.2.2 Sust-MPC micromortar preparation

The micromortar was mixed in a mortar planetary mixer. LG-MgO, KH_2PO_4, and CSP were added to the mixer summing a total solids mass of 3kg. The raw material mix was dry homogenized in the mixer. Subsequently, water was added and after 10 s the blend was mixed for 30 s in low revolution mode and 30 s in high revolution mode. Over the next 20 s, the unhydrated solid was removed using a spatula. Afterwards, the micromortar paste was mixed in high revolution mode for 60 s. The fresh micromortar was decanted into 40×40×160 mm^3 expanded polystyrene prismatic molds and vibrated for 10 s on a conventional vibratory table. Six prismatic samples of each formulation presented in Table 1 were obtained.

Casted samples were placed in a curing chamber at a constant temperature of 20 ± 2 °C and a relative humidity of 95% for 24 h. Subsequently, the samples were demolded and further curing was performed under the same conditions until testing (7 d and 28 d).

2.3 Test methods and structural characterization of the sust-MPC micromortar

The apparent density, modulus of elasticity, flexural strength, and compressive strength were measured after 7 d of curing for the six formulations in order to evaluate the results by means of design of experiments. The modulus of elasticity was estimated using an ultrasound test following the UNE-EN 12504-4 standard. An ultrasonic pulse velocity tester (C368 by Matest, 55 kHz transceiver sensors) was employed to perform the tests [38]. The obtained modulus of elasticity results were accepted assuming that the estimation of the Young's modulus was valid for homogeneous and isotropic media, even though sust-MPC micromortars do not always satisfy these conditions.

A compressive strength test was conducted for six split specimens obtained from the flexural strength test at 7 d, and the remaining parts of the six test specimens were further cured for 28 d before the compressive strength test. The test conditions followed UNE-EN 196-1 using an Incotecnic MULTI-R1 mechanical testing equipment, where the flexural strength test speed was 5 $kg \cdot s^{-1}$ and the compressive strength test speed was 240 $kg \cdot s^{-1}$. Subsequently, an optimal formulation was determined by analyzing the design of experiments results (see section 3.2.6). The optimal sust-MPC micromortar was compared with an ordinary sust-MPC without CSP filler as a reference, both after 365 d of curing. The samples cured for 365 d were the broken parts of the samples that were tested for compressive strength at 28 d. The obtained fragments were stored in the curing chamber for 365 d at a constant temperature of 20 ± 2 °C and a relative humidity of 50% to evaluate the potential reaction of the CSP glass phase with K-struvite [27,39,40]. This potential reaction between K-struvite and siliceous compounds was reported by various authors [27,39,40]. The evaluation was conducted using XRD, TG/DTG analysis, backscattered scanning electron microscopy (BSEM), and Fourier transformed infrared spectroscopy in attenuated total reflectance mode (FTIR-ATR). In addition, CSP was evaluated using FTIR-ATR and compared with the cured sust-MPC micromortar pieces. FTIR-ATR spectra of the samples were obtained using a Perkin Elmer Spectrum Two FTIR-ATR spectrometer. Both the XRD and TG/DTG measurements were conducted under the same conditions as the raw materials characterization.

In order to perform BSEM analysis to determine the chemical interaction between the filler and the cement matrix, a JSM-6510, JEOL Ltd., scanning electron microscope was used. Various representative broken fragments of the optimal sust-MPC micromortar and the ordinary sust-MPC without CSP were selected. Fragment samples were fixed on a carbon adhesive and coated with carbon to acquire BSEM images and to perform energy-dispersive scattering (EDS) analysis of the fracture surface. In addition, fragments of both formulations were impregnated in epoxy resin, surface polished, and carbon-coated to reveal the internal configuration of sust-MPC. BSEM images and EDS elemental mapping were conducted on the polished fragment samples and numerous EDS maps were collected. Each EDS map was acquired for 1800 s.

3. Results and discussion

3.1 Raw materials characterization

PSD analysis resulted in diameters of 1.666 µm (d_{10}), 12.410 µm (d_{50}), and 39.960 µm (d_{90}) for LG-MgO and 1.763 µm (d_{10}), 14.110 µm (d_{50}), and 40.200 µm (d_{90}) for CSP. The chemical composition of the by-products was determined by XRF. Table 2 shows the most stable oxide of each corresponding element, where magnesium was the predominant element in the case of LG-MgO, with an average MgO content of 61.7 wt.%. Calcium was the second most abundant element with a CaO content of 9.32 wt.%. Sulfur detected in the sample is attributed to the petroleum coke used as combustible material the for calcination of natural magnesite, as previously reported by Formosa et al. [41]. In contrast, the XRF results for CSP waste shown in Table 2 indicate high Si elemental concentrations (70.78 wt.% of SiO_2) followed by Na (11.15 wt.% of Na_2O), Ca (9.37 wt.% of CaO), and Al (4.81 wt.% of Al_2O_3). The presence of Si, Ca, and Na is related to the high content of soda-lime glass in CSP waste, while Al is associated with aluminosilicates present in the ceramic waste.

XRD spectra of LG-MgO and CSP are shown in Fig. 1. The presence of glass cullet and ceramic shards in CSP is demonstrated in Fig. 1.a, where quartz (SiO_2, PDF# 01-085-0457) and mullite ($Al_{4.52}Si_{1.48}O_{9.74}$, PDF# 01-079-1457) were found to be the primary crystalline phases. The spectra also indicated the presence of an amorphous phase related to amorphous silica in glass. The primary crystalline phases of LG-MgO were periclase (MgO, PDF# 01-071-1176), brucite ($Mg(OH)_2$, PDF# 01-083-0114), magnesite ($MgCO_3$, PDF# 01-078-2442), dolomite ($CaMg(CO_3)_2$, PDF# 01-084-1208), calcite ($CaCO_3$, PDF# 01-086-0174), and anhydrite ($CaSO_4$, PDF# 00-037-1496) as well as other minor phases (Fig. 1.b). Other impurities, such

as iron oxide or silica were also present. The thermal decomposition of LG-MgO in a nitrogen atmosphere is shown in Fig. 2. In the case of CSP, the TG/DTG analysis (not shown) registered a total mass loss of 1.214 wt.% when heated from 30 to 1400 °C without any clear decomposition. TG/DTG analysis for LG-MgO indicated mass losses attributed to the crystallization of water (from 30 to 210 °C) [42], $Mg(OH)_2$ decomposition resulting in MgO (from 210 to 440 °C), $MgCO_3$ decarbonation producing MgO and CO_2 products (from 440 to 660 °C), $CaMg(CO_3)_2$ decarbonation to MgO, CaO, and CO_2 (from 660 to 740 °C), $CaCO_3$ decarbonation to CaO and CO_2 (from 740 to 1030 °C), and desulfurization of $MgSO_4$ (from 1030 to 1190 °C), and $CaSO_4$ (from 1190 to 1400 °C) [43]. The TG/DTG analysis results in combination with XRF and XRD results were used to estimate the actual chemical composition of the by-product. First, TG/DTG results were used to estimate the percentage of compounds that thermally decomposed up to 1400 °C by stoichiometric calculation. Second, the remaining composition was calculated using the XRF compositional results considering the outstanding wt.% to estimate. XRD results were used to identify the chemical compounds that thermally decomposed during TG/DTG. The results of the estimation are shown in Table 3, where the MgO total content in LG-MgO was determined to be 43.58 wt.%. Considering that $Mg(OH)_2$ (3.77 wt.%) and $MgSO_4$ (2.12 wt.%) are soluble in water, unlike carbonate, the total calculated content of available reactive magnesium compounds in the unhydrated by-product was 49.47 wt.%.

The reactivity of MgO was assessed using the citric acid test, where neutralization values under 60 s are specific for highly reactive samples, also known as soft-burnt MgO. Values between 180 and 300 s are defined as medium-reactive MgO, while low reactivity MgO is known as hard-burnt, giving values of approximately 600 s. Finally, values over 900 s are observed for dead-burned MgO [35]. The LG-MgO citric acid test resulted in neutralization at 1128 s. Therefore, the obtained reactivity of LG-MgO is suitable to develop K-struvite and no pre-calcination processes are required [44]. Therefore, the use of LG-MgO by-products in place of pure MgO reduces the cost and enhances the environmental and sustainable criteria.

3.2 Design of experiments response

The LG-MgO/KH_2PO_4 ratio presented in Table 1 was fixed at 60/40 based on the weight [24–26,43]. The formulations (runs, i.e., R15 for run number 15) and a summary of the main experimental and predicted design of experiments results of the study are described in Table 1. Predicted values were calculated using the equations obtained after statistical analysis of ANOVA. In this manner, with the help of the design of experiments software and the obtained equations, the predicted responses were obtained as described in the

following sections. The models developed using the experimental responses exhibited p-values below 0.0001, implying that the proposed models are significant considering the factor relations presented for each response or equation. The best model equations for fitting the experimental results are as follows: density at 7 d (two factors with interaction), modulus of elasticity at 7 d (linear), flexural strength at 7 d (linear), compressive strength at 7 d (reduced cubic), and compressive strength at 28 d (reduced quadratic). An in-depth discussion of the proposed models for each response under study is presented in the following sections.

3.2.1 Apparent density

The best model for fitting the experimental values of the apparent density response is shown in Eq. (2). The model presented a low standard deviation and a high R-squared (R^2) value: 0.01 and 0.87, respectively. The mathematical model described in Eq. (2) is represented in Fig. 3.a. Both factors under study (W/C and CSP(%)) have a significant effect (p-value = 0.0002 and < 0.0001, respectively) on the response of the apparent density. According to the results, by increasing the W/C ratio, the apparent density decreases. The increase in CSP(%) leads to an apparent increase in the density response. Considering the slope of each response, the effect of CSP(%) is higher than that of the W/C ratio in the range of study. When the combined effect of both factors (W/C ratio and CSP(%)) is considered, the response is minor compared with the sum of each individual response. Therefore, a significant negative interaction occurs between both factors (p-value = 0.0196), explaining this result. The negative interaction between CSP(%) and the W/C ratio can be understood by the last term in Eq. (2), where the higher the term, the lower the response. The higher the CSP(%), the higher the apparent density, and simultaneously, the lower the W/C ratio, the higher the apparent density.

$$\rho\ (\mathrm{g \cdot cm^{-3}}) = 1.888 - 0.288 \cdot (W/C) + 0.028 \cdot (CSP) - 0.070 \cdot (W/C) \cdot (CSP) \qquad (2)$$

As shown in Fig. 3.a, the blue and red zones correspond to the lowest and highest apparent density values, respectively.

3.2.2 Modulus of elasticity

The model presented a low standard deviation and a high R^2 value: 0.48 and 0.90, respectively. A response surface linear model was developed for the modulus of elasticity at 7 d using the experimental data. The modulus of elasticity surface plot is presented in Fig. 3.b, and the corresponding mathematical expression

is presented in Eq. (3) The highest modulus of elasticity values are obtained as CSP(%) (p-value < 0.0001) increases and the W/C ratio (p-value < 0.0001) decreases. Hence, the modulus of elasticity model exhibits high values, similar to the apparent density. On the contrary, the modulus of elasticity model is more susceptible to the W/C ratio than the CSP(%).

The modulus of elasticity and apparent density are related to the porosity of the samples. Therefore, both responses present similar behavior, as shown in Fig. 3.a and 3.b. The higher the W/C ratio, the higher the porosity and consequently the lower the modulus of elasticity and mechanical properties such as flexural strength and compressive strength [45]. The mathematical approach for the density surface plot is presented in Eq. (3).

$$MOE\ (\text{GPa}) = 34.993 - 66.071\cdot(W/C) + 0.109\cdot(CSP) \quad (3)$$

As shown in Fig. 3.b the blue and red zones correspond to the lowest and highest modulus of elasticity values, respectively. CSP and W/C factors are significant, however, no interaction between both factors was perceived in the range under study for the modulus of elasticity results.

3.2.3 Flexural strength

The surface plot of the flexural strength at 7 d is shown in Fig. 3.c, obtained using Eq. (4). The developed model presented a low standard deviation (0.22) and a high R^2 value (0.84). The model is a linear model in which both factors significantly affect the response in the range under study. The flexural strength at 7 d is augmented as the W/C ratio (p-value < 0.0001) decreases, while CSP(%) (p-value = 0.0033) increases. It must be noted that the flexural strength is more sensitive to the W/C ratio variation than CSP(%) in the micromortar as noted in section 3.2.2. Once again, this performance in terms of both the modulus of elasticity and the flexural strength is associated with the formation of pores. The porosity induced by the increase of the W/C ratio severely affects the flexural performance. This effect had a lower impact on the compressive strength because cavities in the micromortar tend to close during the compressive test, whereas during the flexural test, those cavities tend to open owing to the direction of the internal stresses in the material.

$$FS\ (\text{MPa}) = 12.153 - 25.553\cdot(W/C) + 0.033\cdot(CSP) \quad (4)$$

As shown in Fig. 3.c, the blue and red zones correspond to the lowest and highest flexural strength values, respectively.

3.2.4 Compressive strength at 7 d

The statistical model for the compressive strength at 7 d (CS-7d) is presented in Fig. 3.d and Eq. (5). The model exhibited a low standard deviation of 0.23, and an exemplary R^2 value of 0.97, indicating that it was suitably fitted to the experimental data. The proposed model is a reduced cubic model, in which the evaluated factors significantly affect the response as follows: W/C ratio (p-value < 0.0001), CSP(%) (p-value = 0.0024), (W/C)·(CSP) (p-value = 0.0836), $(W/C)^2$ (p-value = 0.0061), $(CSP)^2$ (p-value = 0.0227), and $(CSP)^3$ (p-value = 0.0055).

$$CS\text{-}7d\ (\text{MPa}) = 512.470 - 2660.140\cdot(W/C) - 0.719\cdot(CSP) - 2.849\cdot(W/C)\cdot(CSP) + 3529.782\cdot(W/C)^2 + 0.329\cdot(CSP)^2 - 0.014\cdot(CSP)^3 \quad (5)$$

As shown in Fig. 3.d, the blue and red zones correspond to the lowest and highest CS-7d values, respectively. On the one hand, the lowest values (see Fig. 3.d blue zone) were obtained at low CSP(%) and high W/C ratios. This is attributed to the necessity to increase W/C when CSP was added to improve the workability in the fresh state. On the other hand, the highest values (see Fig. 3.d red zone) were obtained at high CSP(%) and low W/C ratios. This behavior is attributed to the effect of the filler in a cement matrix, present as long as the W/C ratio is above the stoichiometric amount of water that the cement requires. In other words, as a result of the preliminary work to obtain the range of study, we conclude that the minimum W/C ratio required for acceptable workability is 0.34. Inside the micromortar, during the compressive strength test, the stress transfer mechanism facilitates the closing of pores and cavities and reduces the speed of crack propagation [33]. As observed in Eq. (5), a negative interaction occurs between both factors. This interaction can be observed by following the line generated when both factors increased together (see Fig. 3.d green zone). Quadratic and cubic terms were used for improved model fitting, as can be seen by the tendency to generate curves instead of lines at the edges of the plotted response surface, see Fig. 3.d. In general, it is assumed that the higher the CSP(%), the higher the CS-7d.

3.2.5 Compressive strength at 28 d

The model for the compressive strength at 28 d (CS-28d) showed a low standard deviation (1.00) and a high R^2 value (0.96). Therefore, the model suitably fitted the experimental results obtained for CS-28d. A reduced quadratic model was fitted, as shown in Eq. (6) and presented in Fig. 3.e.

$$CS\text{-}28d\ (\text{MPa}) = 64.125 - 134.430\cdot(W/C) + 1.759\cdot(CSP) - 5.863\cdot(W/C)\cdot(CSP) + 0.047\cdot(CSP)^2 \quad (6)$$

The model terms presented p-values as follows: W/C < 0.0001, CSP < 0.0001, (W/C)·(CSP) = 0.0296, and $(CSP)^2$ = 0.0008. As shown in Fig. 3.e, the blue and red zones correspond to the lowest and highest CS-28d values, respectively. A significant negative interaction occurs between both factors, depicted by a change in the tendency or a valley (green zone in Fig. 3.e) when both factors increased together. The effect is lower than that expected from the sum of each individual factor. As expected, an increase in the W/C ratio leads to a decrease in CS-28d, depicted by a negative slope considering the W/C axis in Fig. 3.e. However, when CSP(%) is considered, a minimum region is observed at approximately the middle of this axis (i.e. lower and higher CSP(%) lead to higher CS-28d in the range under study). Thus, the maximum CS-28d (red zone in Fig. 3.e) is obtained when CSP(%) and the W/C ratio are the maximum and minimum, respectively. On the contrary, when CSP(%) is minimized and the W/C ratio maximized, the CS-28d value is minimized (blue region in Fig. 3.e). CSP(%) above 15 leads to an increase in CS-28d, although this value is outside the range of study and requires further study. In this case, a new range for the W/C ratio should be considered because of the lack of workability when CSP is added. In future studies, additives such as borax or sodium hexametaphosphate may be used to improve the fresh state of these mixtures.

3.2.6 Optimal formulation and validation procedure

By using the statistical models presented above, it was possible to optimize the formulation by selecting the desired responses. As mentioned above, the primary aim of this study was to increase the compressive strength as much as possible in the development of sust-MPC using CSP as a filler within the range of study. The optimization idea involved the concept of reaching a compromise between values. Table 4 shows the criteria used in the optimization process, where the lower and upper limits were the best and worst values obtained from the tests performed (i.e., experimental values). Compressive strength was treated as the most important property because it is the key aspect to consider in building materials. Therefore, CS-7d and CS-28d were maximized in the optimization process. Nonetheless, the apparent density, modulus of elasticity, and flexural strength were within the range limits. In this study, the importance of each parameter was fixed at 3, where the importance could be ranged from 1 to 5 (i.e., responses possessed the

same importance). Once the desired response values, factors range, and level of importance were selected, two optimal formulations were obtained. The optimal formulation is indicated in Table 4, along with its predicted properties as well as the desirability. The optimal formulation coincided with R15 and R7 in terms of the W/C ratio and CSP (0.34 W/C and 15.00 wt.% CSP, see Table 1). The model was validated by comparing the estimated values (see Table 4) with the experimental results obtained for R7 and R15 (see Table 1).

3.3 Micromortar structural characterization

To evaluate the formation of new mineral phases, R15 (0.34 W/C and 15.00 wt.% CSP) was considered as the optimal formulation and compared to R11 as a reference or blank (0.35 W/C and 0.00 wt.% CSP), i.e., without CSP and a lower W/C ratio. The broken fragments obtained after the CS-28d test for R15 and R11 were used to perform the sust-MPC micromortar characterization after 365 d of curing (20 ± 2 °C, relative humidity of 50%). The samples were analyzed using XRD and TG/DTG (under the same conditions as the raw materials), BSEM combined with EDS chemical microanalysis, and FTIR-ATR to provide information on the microstructure and to determine whether CSP interacted with the MPC matrix in the sust-MPC micromortar.

Several authors have reported the feasibility of a potential reaction when MPC matrices are used with fly ash [27]. These authors suggested that the reaction is complete after a period greater than 28 d. This research shows BSEM images of R15-365d since they are related to the potential reaction of the MPC matrix with the CSP filler.

The XRD patterns (Fig. 4) of both the optimal sust-MPC micromortar and the MPC reference samples showed K-struvite ($KMgPO_4 \cdot 6H_2O$, PDF# 01-075-1076) as the major crystalline phase. Other phases such as unreacted periclase, dolomite, magnesite, and quartz were also detected. Stable phases within LG-MgO did not react and remained unaltered. Only K-struvite was found as the magnesium phosphate phase formed, and neither bobierrite ($Mg_3(PO_4)_2 \cdot 8H_2O$) nor newberyite ($MgHPO_4 \cdot 3H_2O$) were identified in the micromortar. It must be noted that calcite was expected in the pattern, however, the calcite peaks may overlap with those of magnesite and dolomite. Regarding possible interactions between CSP particles and the matrix, no differences were observed in terms of 2θ peak positions between the optimal and reference sample spectra. However, R15 exhibited a higher background intensity, which could be related to a higher CSP wt.% in the sample since CSP contains a high amorphous silica content from glass cullet (~84 wt.%

in CSP) as stated in the literature and checked using XRF (Table 1) and XRD (Figure 2) [28]. Thus, it cannot be confirmed the existence of a chemical combination of the filler and the K-struvite matrix from the XRD results shown in Figure 4.

The TG/DTG characterization of the micromortar at 365 d is shown in Fig. 5. Fig. 5.a shows a higher total mass loss for R11-365d compared to R15-365d, as a result of the reduction of K-struvite due to filler substitution. TG/DTG results for both R11-365d and R15-365d exhibited identical mass losses and temperature decomposition ranges. To characterize the mass losses of the micromortar, TG/DTG was analyzed considering the previously obtained XRD results. The mass loss between 30–270 °C was assigned to the loss of H_2O from K-struvite, and the mass loss between 270–450 °C was assigned to H_2O loss due to magnesium hydroxide decomposition. The losses between 450–600 °C, 600–700 °C, and 700–1000 °C were assigned to CO_2 loss from magnesite, dolomite, and calcite decomposition, respectively, because of the inert carbonate phases in LG-MgO [42,46]. K-struvite, the main crystalline phase in the micromortar, was quantified using TG/DTG. It was found to represent 53.46 ± 0.19 wt.% of the total micromortar mass in R11-365d and 47.37 ± 0.33 wt.% in R15-365d. These results were in accordance with those obtained in the literature, taking into account that LG-MgO consisted of approximately 44 wt.% reactive MgO [42,46,47]. The CSP percentage in R15-365d was calculated by comparing the mass losses of R11-365d and R15-365d at 30–270 °C was determined to be 11.70 ± 0.53 wt.% of the total micromortar mass. It should be noted that the total micromortar mass includes water mass, a small part of which is lost during mixing.

BSEM, and EDS elemental mapping analysis images of R15-365d are shown in Fig. 6. The micrograph in Fig. 6.a shows the appearance of the inner structure of the micromortar composed of CSP filler and unreacted LG-MgO particles embedded in a K-struvite matrix. The high degree of microcracking in the sample was induced by exothermic acid-base setting reactions, and shrinkage caused by water evaporation. This added an elevated level of stress endured during the compressive strength test, contributing to the propagation of microcracks [48]. Filler particles are randomly distributed through the micromortar matrix, providing and enhancing the mechanical properties of the composite. In a previous study, sharp shaped particles consisting of dolomite, calcite, and magnesite were observed between other minor particles such as sulphates in the K-struvite matrix [41]. This is in contrast with the XRD, TG/DTG, and EDS elemental mapping results shown in Fig. 6 [42,46,49]. Unreacted MgO particles and soda-lime glass from CSP were incorporated in the matrix. A number of iron oxide particles coming from LG-MgO, confirmed by XRD,

were also detected by EDS. Unreacted particles can also be considered as filler particles in addition to CSP waste filler. Therefore, sust-MPC can be conceived as a micromortar. It was possible to trace the path of the K-struvite reaction in the micromortar matrix, culminating in partially reacted MgO particles embedded in the matrix. The reaction begins on the outside of the particle and advances toward the center of the particle but does not reach its core. Moreover, prismatic K-struvite crystals were observed in the fracture surface of the micromortar [50]. The optimal formulation samples were polished for exhaustive EDS mapping analysis. Fig. 6.a and b show the elemental distribution and location of the primary elements. In order to discern the CSP filler particles in the sust-MPC micromortar matrix, a random zone was subjected to elemental mapping. The primary aim was to observe the most interesting filler particles. S (from sulphates), Mg, P, and K (from K-struvite), Ca (from calcium carbonate and CSP soda-lime glass particles), Na (from CSP soda-lime glass particles), Fe (from ferrous particles), Al (from CSP phases), and Si (from CSP particles) were observed. A magnified zone of interest was subsequently analyzed. This zone contained a soda-lime CSP particle surrounded by and incorporated into the matrix. This particle was observed in detail, showing an unknown interaction with the K-struvite matrix inside the zone indicated in Fig. 6.b. As observed, a region of the particle outer layer reacted with the matrix and was integrated. Elemental mapping shown in Fig. 6.b reinforces this idea. The Si signal overlapped with that of Mg, P, and K. This was most likely because the elemental signal covers a certain volumetric area of the sample. The upper edge of the CPS particle (Fig. 6.b) seems to have interacted with the matrix. In order to determine if chemical reactions occurred, FTIR-ATR was employed. Fig. 7 shows the infrared spectra of CSP, R15-365d and R11-365d. The lack of sharp peaks in the CSP spectrum is related to the disordered silicate network [51]. Both micromortar spectra presented identical profiles, similar to analogous materials [52–54]. The most important peak is located at approximately 1000 cm^{-1}. Fig. 8.b, c, and d show the three deconvoluted spectra (R15-365d, CSP, and R11-365d) between 1400 and 700 cm^{-1}. In this range it is possible to observe the primary vibrations of the phosphate group [53], the same region where Si–O stretching occurs [51]. Fig. 8.a shows a broad band for CSP at approximately 1000 cm^{-1} compared with the spectra for R15-365d and R11-365d. The curves were fitted using a Gaussian function, minimizing the number of curves, and obtaining a regression coefficient, R^2, above 0.999 [55]. In each case, the obtained R^2 value was 0.9997; hence, the curves were suitably fitted. Deconvolution of the CSP peak (Fig. 8.c) revealed two primary bands at 1025 and 928 cm^{-1} that are assigned to the Si–O asymmetric stretching modes of bridging and non-bridging oxygen, respectively [51]. The bands between 1300–800 cm^{-1} are related to the stretching

vibrations of SiO_4 tetrahedron depending on the number of shared oxygens [51]. Bands at 788 and 758 cm^{-1} are assigned to the bending vibration of Si–O–Si at 784 cm^{-1} [56] and the Al-O vibration modes due to the tetrahedral AlO_4 group [57], respectively. Finally, the deconvoluted broad band at 1158 cm^{-1} is assigned to the Si–O–Al asymmetric stretching vibration [57].

The deconvoluted spectra for R15-365d and R11-365d (Fig. 8.b and d) showed that the bands from 923 to 741 cm^{-1} were present in both spectra. Because of the presence of unreacted carbonate phases from the LG-MgO raw material, a number of bands attributed to the CO_3^{2-} group were observed (most likely due to the presence of magnesite or even dolomite): asymmetrical stretching vibration of O–C–O at approximately 1450 cm^{-1} (see Fig. 7) as well as bands at 880–879 cm^{-1} and 742–741 cm^{-1} as shown in Fig. 8.b and d, assigned to out-of-plane and in-plane bending vibrations, respectively [58]. The deconvoluted band at 792 cm^{-1} was observed in both samples (Fig. 8.b and d) and is assigned to quartz owing to the presence of this phase in the LG-MgO raw material and in both R11-365d and R15-365d (see Fig. 1 and 3.b). Considering the deconvoluted bands for R11-365d, these bands were in accordance with those observed by other authors [53,59]. Indeed, the bands at 1102, 1047, 997, and 923 cm^{-1} were assigned to P–O stretching similar to the reported bands at 1095–1105, 1054–1075, 978–978, and 916–951 cm^{-1} [53,59]. In the case of R15-365d (see Fig. 8.b), the deconvoluted bands differed to R11-365d. Specifically, the bands at 1119 and 1023 cm^{-1} are related to the potential substitution of P in the SiO_4 tetrahedron present in CSP or Si in the PO_4 tetrahedron present in the K-struvite matrix owing to the shift in both bands to higher frequencies. It was reported that the typical Si–O–P bands due to stretching vibrations appear at approximately 1150–1100 and 1000 cm^{-1} [60]. This assumption is related to the BSEM evaluation. However, this must not be considered absolutely certain because of the similar wavenumber range at which the peaks for SiO_4^{4-} and PO_4^{3-} groups appear, as a result of their tetrahedral structure [61].

The XRD results agreed with the BSEM and EDS analyses, with K-struvite the main component in the micromortar matrix. This was also supported and quantified by the TG/DTG results. Other crystalline compounds observed in the XRD analysis were identified in the BSEM images by EDS. Iron oxide was observed in the XRF results for the LG-MgO sample and was also present in the form of small particles in the micromortar matrix as determined from the BSEM and EDS results. CSP particles were remarkably embedded in the matrix, as observed in the BSEM images. The magnified image in Fig. 6.b shows an intermediate zone between the matrix and the particle, where color degradation and evident blending of the particle-matrix contour are indicated. The mapping results of this zone allow determination of the degree

of reaction between the filler and the matrix despite the XRD results indicating that no new crystalline phases were formed by comparing the R11-365d and R15-365d micromortar diffraction spectra. TG/DTG analysis also did not show any evidence of a new compound formed in addition to K-struvite. Considering the TG/DTG, XRD, and EDS mapping results, we conclude that the reaction degree was low, and thus in the hypothetical case of the reaction between the filler and the matrix, either i) the percentage of the new silicophosphate compound was small (less than 1 wt.%) or ii) the new compound was present in an amorphous state also with a small wt.%. Analyzing the FTIR-ATR spectra of the samples cured at 365 d revealed slight deviations in the deconvoluted peak frequencies that may indicate the potential substitution of P in the SiO_4 tetrahedron of CSP or Si in the PO_4 tetrahedron of the K-struvite matrix. With this substitution, CSP particles should be partially merged with the matrix, as observed in the BSEM images. More evidence is required to determine the type of compound and its possible formation during the reaction between CSP glass waste filler and the matrix.

4. Conclusions

It is plausible to formulate a sust-MPC micromortar mixed with inorganic glass waste (CSP) as a filler that enhances the mechanical properties. This is termed sust-MPC micromortar when formulated with LG-MgO because of its sustainability characteristics. CSP is an inorganic solid waste from industrial and urban glass residues. The primary idea behind the development of a sust-MPC micromortar using CSP was not only to enhance the mechanical properties but also to reduce the environmental impact. Revalorization of both residue sources was achieved, thereby lowering the price of the final product, promoting a circular economy, and reducing CO_2 emissions due to the reduced amount of magnesia product inherent in the use of LG-MgO. Therefore, a sust-MPC micromortar was successfully developed using CSP to improve the properties of MPC, as expected.

The statistical models generated based on the design of experiments performed successfully. The results were validated, fitted with the desired requirements, and displayed remarkable accuracy regarding the property responses of each of the possible formulations within the studied W/C and CSP wt.% factor ranges. This set of models was based on more than one variable and allows estimation of the properties of possible formulations and improvements in the entire system. Moreover, the models enable determination of an optimal formulation with a compromise required between properties in order to achieve maximum performance according to the criteria. They also allow evaluation of the synergetic effect of variables or factors between them. An optimal formulation was found achieved using the response surface methodology, and every design of experiments model generated was statistically significant.

The optimal formulation was designated the same formulation as that of R15 with a W/C ratio of 0.34 and a CSP content of 15 wt.%, reaching compressive strength values above 25 MPa. Regarding the synergetic interaction between the factors, CSP and W/C possessed a certain dependency on and synergetic interaction between each other.

After one year of curing, the optimal formulation and a reference sample without CSP were characterized in order to review their evolution over time. The optimal formulation exhibited excellent integration of CSP particles in the matrix. Although more evidence is required, a number of CSP particles in the sust-MPC micromortar matrix presented a certain degree of chemical reaction with the matrix as observed in elemental EDS mapping results and FTIR-ATR analysis, yet an uncertain observation.

Future research requires highly detailed structural and chemical characterization of the sust-MPC micromortar to acquire more evidence of the suspected chemical interaction between silica-rich soda-lime glass CSP particles and the K-struvite matrix.

Declaration of competing interest

The authors declare that they have no known competing financial interests or personal relationships that influenced the work reported in this paper.

Acknowledgements

The authors would like to thank Magnesitas Navarras S.A. for their cooperation in financing and supporting the work. We would also like to thank Daniel Rosas S.A. for supplying the CSP material. The authors are grateful to the Catalan government for the DIOPMA (2017 SGR 118) quality accreditation awarded to their research group. This work was supported by Magnesitas Navarras S.A. and the Spanish government (BIA2017-83912-C2-1-R). We would like to thank Mr. Eduard Cosialls in particular for aiding with the experiments. Mr. S. Huete-Hernández is grateful to the government of Catalonia and the University of Barcelona for the research grant (APIF-DGR 2018). Mr. Alex Maldonado-Alameda is grateful to the government of Catalonia for the research Grant (FI-DGR 2017). Dr. Jessica Giro-Paloma is a Serra Húnter Fellow.

References

[1] Z. He, X. Zhu, J. Wang, M. Mu, Y. Wang, Comparison of CO_2 emissions from OPC and recycled cement production, Constr. Build. Mater. 211 (2019) 965–973. doi:10.1016/j.conbuildmat.2019.03.289.

[2] R.M. Andrew, Global CO_2 emissions from cement production , 1928 – 2018, Earth Syst. Sci. Data. 11 (2019) 1675–1710. doi:10.5194/essd-11-1675-2019.

[3] J. Farfan, M. Fasihi, C. Breyer, Trends in the global cement industry and opportunities for long-term sustainable CCU potential for Power-to-X, J. Clean. Prod. 217 (2019) 821–835. doi:10.1016/j.jclepro.2019.01.226.

[4] T. Gao, L. Shen, M. Shen, L. Liu, F. Chen, Analysis of material flow and consumption in cement production process, J. Clean. Prod. 112 (2016) 553–565. doi:10.1016/j.jclepro.2015.08.054.

[5] C. Shi, A.F. Jiménez, A. Palomo, New cements for the 21st century: The pursuit of an alternative to Portland cement, Cem. Concr. Res. 41 (2011) 750–763. doi:10.1016/j.cemconres.2011.03.016.

[6] M.C.G. Juenger, F. Winnefeld, J.L. Provis, J.H. Ideker, Advances in alternative cementitious binders, Cem. Concr. Res. 41 (2011) 1232–1243. doi:10.1016/j.cemconres.2010.11.012.

[7] E. Gartner, T. Sui, Alternative cement clinkers, Cem. Concr. Res. 114 (2018) 27–39. doi:10.1016/j.cemconres.2017.02.002.

[8] N. Li, C. Shi, Z. Zhang, Understanding the roles of activators towards setting and hardening control of alkali-activated slag cement, Compos. Part B Eng. 171 (2019) 34–45. doi:10.1016/j.compositesb.2019.04.024.

[9] Y.H.M. Amran, N. Farzadnia, A.A.A. Ali, Properties and applications of foamed concrete; A review, Constr. Build. Mater. 101 (2015) 990–1005. doi:10.1016/j.conbuildmat.2015.10.112.

[10] M. Nabiyouni, T. Brückner, H. Zhou, U. Gbureck, S.B. Bhaduri, Magnesium-based bioceramics in orthopedic applications, Acta Biomater. 66 (2018) 23–43. doi:10.1016/j.actbio.2017.11.033.

[11] S. Luo, M. Liu, L. Yang, J. Chang, W. Yang, X. Yan, H. Yu, Y. Shen, Utilization of waste from alumina industry to produce sustainable cement-based materials, Constr. Build. Mater. 229 (2019) 116795. doi:10.1016/j.conbuildmat.2019.116795.

[12] G. Mestres, M.P. Ginebra, Novel magnesium phosphate cements with high early strength and antibacterial properties, Acta Biomater. 7 (2011) 1853–1861. doi:10.1016/j.actbio.2010.12.008.

[13] F. Qiao, C.K. Chau, Z. Li, Property evaluation of magnesium phosphate cement mortar as patch repair material, Constr. Build. Mater. 24 (2010) 695–700. doi:10.1016/j.conbuildmat.2009.10.039.

[14] A.S. Wagh, S.Y. Jeong, Chemically Bonded Phosphate Ceramics: I, A Dissolution Model of Formation, J. Am. Ceram. Soc. 86 (2003) 1838–1844. doi:10.1111/j.1151-2916.2003.tb03569.x.

[15] H. Lahalle, C.C.D. Coumes, A. Mesbah, D. Lambertin, C. Cannes, S. Delpech, S. Gauffinet, Investigation of magnesium phosphate cement hydration in diluted suspension and its retardation by boric acid, Cem. Concr. Res. 87 (2016) 77–86. doi:10.1016/j.cemconres.2016.04.010.

[16] A.S. Wagh, S.Y. Sayenko, A.N. Dovbnya, V.A. Shkuropatenko, R. V. Tarasov, A. V. Rybka, A.A. Zakharchenko, Durability and shielding performance of borated Ceramicrete coatings in beta and gamma radiation fields, J. Nucl. Mater. 462 (2015) 165–172. doi:10.1016/j.jnucmat.2015.03.049.

[17] A.S. Wagh, Chemically Bonded Phosphate Ceramics, First edit, Elsevier Science, Oxford, UK, 2004. doi:10.1016/B978-0-08-044505-2.X5000-5.

[18] N. Roghanian, N. Banthia, Development of a sustainable coating and repair material to prevent bio-corrosion in concrete sewer and waste-water pipes, Cem. Concr. Compos. 100 (2019) 99–107. doi:10.1016/j.cemconcomp.2019.03.026.

[19] X. Jia, J. Li, P. Wang, J. Qian, M. Tang, Preparation and mechanical properties of magnesium phosphate cement for rapid construction repair in ice and snow, Constr. Build. Mater. 229 (2019) 116927. doi:10.1016/j.conbuildmat.2019.116927.

[20] W. Montague, L. Vandeperre, M. Hayes, Processing Characteristics and Strength of Magnesium Phosphate Cement Formulations Compatible with UK Nuclear Waste Treatment Plants, MRS Proc. 1475 (2012) imrc11-1475-nw35-p03. doi:10.1557/opl.2012.588.

[21] Y. Tao, L. Zhenyu, R. Chunrong, W. Yuanyuan, H. Zhichao, H. Xin, W. Jie, L. Mengliang, D. Qiubai, K. Khan, L. Zhongyuan, L. Shuzhen, Study on solidification properties of chemically bonded phosphate ceramics for cesium radionuclides, Ceram. Int. 46 (2020) 14964–14971. doi:10.1016/j.ceramint.2020.03.025.

[22] A. Viani, A.F. Gualtieri, Preparation of magnesium phosphate cement by recycling the product of thermal transformation of asbestos containing wastes, Cem. Concr. Res. 58 (2014) 56–66. doi:10.1016/j.cemconres.2013.11.016.

[23] A.S. Wagh, Chapter 14: Chemically Bonded Phosphate Ceramic Matrix Compsites, in: Chem. Bond. Phosphate Ceram. Twenty-First Century Mater. With Divers. Appplications, First edit, Elsevier Ltd, Argonne, USA, 2004: pp. 157–176. doi:10.1016/B978-008044505-2/50018-1.

[24] M. Niubó, J. Formosa, A. Maldonado-Alameda, R. del Valle-Zermeño, J.M. Chimenos, Magnesium phosphate cement formulated with low grade magnesium oxide with controlled porosity and low thermal conductivity as a function of admixture, Ceram. Int. 42 (2016) 15049–15056. doi:10.1016/j.ceramint.2016.06.159.

[25] J. Formosa, A.M. Lacasta, A. Navarro, R. Del Valle-Zermeño, M. Niubó, J.R. Rosell, J.M. Chimenos, Magnesium Phosphate Cements formulated with a low-grade MgO by-product: Physico-mechanical and durability aspects, Constr. Build. Mater. 91 (2015) 150–157. doi:10.1016/j.conbuildmat.2015.05.071.

[26] M. Morales, J. Formosa, E. Xuriguera, M. Niubó, M. Segarra, J.M. Chimenos, Elastic modulus of a chemically bonded phosphate ceramic formulated with low-grade magnesium oxide determined by Nanoindentation, Ceram. Int. 41 (2015) 12137–12146. doi:10.1016/j.ceramint.2015.06.031.

[27] B. Xu, H. Ma, H. Shao, Z. Li, B. Lothenbach, Influence of fly ash on the compressive strength and micro-characteristics of magnesium potassium phosphate cement mortars, Cem. Concr. Res. 99 (2017) 86–94. doi:10.1016/j.cemconres.2017.05.008.

[28] J. Giro-Paloma, C. Barreneche, A. Maldonado-Alameda, M. Royo, J. Formosa, A.I. Fernández, J.M. Chimenos, Alkali-activated cements for TES materials in buildings' envelops formulated with glass cullet recyclingwaste and microencapsulated phase change materials, Materials (Basel). 12 (2019) 1–11. doi:10.3390/ma12132144.

[29] M. Ruth, P. Dell'Anno, An industrial ecology of the US glass industry, Resour. Policy. 23 (1997) 109–124. doi:10.1016/s0301-4207(97)00020-2.

[30] N. Dias, I. Garrinhas, A. Maximo, N. Belo, P. Roque, M.T. Carvalho, Recovery of glass from the inert fraction refused by MBT plants in a pilot plant, Waste Manag. 46 (2015) 201–211.

doi:10.1016/j.wasman.2015.07.052.

[31] E.R. Vieitez, P. Eder, A. Villanueva, H. Saveyn, End-of-waste criteria for glass cullet: Technical proposals, 2011. doi:10.2791/7150.

[32] J. Formosa, M.A. Aranda, J.M. Chimenos, J.R. Rosell, A.I. Fernández, O. Ginés, Cementos químicos formulados con subproductos de óxido de magnesio, Boletín La Soc. Española Cerámica y Vidr. 47 (2008) 293–297. doi:10.3989/cyv.2008.v47.i5.169.

[33] A. Maldonado-Alameda, A.M. Lacasta, J. Giro-Paloma, J.M. Chimenos, L. Haurie, J. Formosa, Magnesium phosphate cements formulated with low grade magnesium oxide incorporating phase change materials for thermal energy storage, Constr. Build. Mater. 155 (2017) 209–216. doi:10.1016/j.conbuildmat.2017.07.227.

[34] J. Formosa, J.M. Chimenos, A.M. Lacasta, M. Niubó, Interaction between low-grade magnesium oxide and boric acid in chemically bonded phosphate ceramics formulation, Ceram. Int. 38 (2012) 2483–2493. doi:10.1016/j.ceramint.2011.11.017.

[35] C.A. Strydom, E.M. Van Der Merwe, M.E. Aphane, The effect of calcining conditions on the rehydration of dead burnt magnesium oxide using magnesium acetate as a hydrating agent, J. Therm. Anal. Calorim. 80 (2005) 659–662. doi:10.1007/s10973-005-0710-x.

[36] D.C. Montgomery, Design and Analysis of Experiments, Sixth edit, John Wiley & Sons, Ltd, New York, USA, 2004.

[37] M. Niubó, A.I. Fernández, L. Haurie, X.G. Capdevila, J.M. Chimenos, J.I. Velasco, Influence of the Electric Arc Furnace Dust in the physical and mechanical properties of EVA–polyethylene–butene blends, Mater. Sci. Eng. A. 528 (2011) 4437–4444. doi:10.1016/j.msea.2011.02.006.

[38] J.R. Rosell, I.R. Cantalapiedra, Simple method of dynamic Young's modulus determination in lime and cement mortars, Mater. Constr. 61 (2011) 39–48. doi:10.3989/mc.2010.53509.

[39] L.J. Gardner, S.A. Bernal, S.A. Walling, C.L. Corkhill, J.L. Provis, N.C. Hyatt, Characterisation of magnesium potassium phosphate cements blended with fly ash and ground granulated blast furnace slag, Cem. Concr. Res. 74 (2015) 78–87. doi:10.1016/j.cemconres.2015.01.015.

[40] Y. Xie, X. Lin, X. Pan, T. Ji, Preliminary investigation of the hydration mechanism of MgO-SiO_2-

K_2HPO_4 cement, Constr. Build. Mater. 235 (2020) 117471. doi:10.1016/j.conbuildmat.2019.117471.

[41] J. Formosa, J.M. Chimenos, A.M. Lacasta, L. Haurie, Thermal study of low-grade magnesium hydroxide used as fire retardant and in passive fire protection, Thermochim. Acta. 515 (2011) 43–50. doi:10.1016/j.tca.2010.12.018.

[42] H. Lahalle, C. Patapy, M. Glid, G. Renaudin, M. Cyr, Microstructural evolution/durability of magnesium phosphate cement paste over time in neutral and basic environments, Cem. Concr. Res. 122 (2019) 42–58. doi:10.1016/j.cemconres.2019.04.011.

[43] R. del Valle-Zermeño, J. Giro-Paloma, J. Formosa, J.M. Chimenos, Low-grade magnesium oxide by-products for environmental solutions: Characterization and geochemical performance, J. Geochemical Explor. 152 (2015) 134–144. doi:10.1016/j.gexplo.2015.02.007.

[44] D. V. Ribeiro, G.R. Paula, M.R. Morelli, Use of microwave oven in the calcination of MgO and effect on the properties of magnesium phosphate cement, Constr. Build. Mater. 198 (2019) 619–628. doi:10.1016/j.conbuildmat.2018.11.289.

[45] S.A. Emamian, H. Eskandari-Naddaf, Effect of porosity on predicting compressive and flexural strength of cement mortar containing micro and nano-silica by ANN and GEP, Constr. Build. Mater. 218 (2019) 8–27. doi:10.1016/j.conbuildmat.2019.05.092.

[46] B. Xu, B. Lothenbach, A. Leemann, F. Winnefeld, Reaction mechanism of magnesium potassium phosphate cement with high magnesium-to-phosphate ratio, Cem. Concr. Res. 108 (2018) 140–151. doi:10.1016/j.cemconres.2018.03.013.

[47] C. Yu, Q. Wu, J. Yang, Effect of seawater for mixing on properties of potassium magnesium phosphate cement paste, Constr. Build. Mater. 155 (2017) 217–227. doi:10.1016/j.conbuildmat.2017.08.050.

[48] D.A. Hall, R. Stevens, B. El-Jazairi, The effect of retarders on the microstructure and mechanical properties of magnesia-phosphate cement mortar, Cem. Concr. Res. 31 (2001) 455–465. doi:10.1016/S0008-8846(00)00501-9.

[49] M.R. Ahmad, B. Chen, Effect of silica fume and basalt fiber on the mechanical properties and

microstructure of magnesium phosphate cement (MPC) mortar, Constr. Build. Mater. 190 (2018) 466–478. doi:10.1016/j.conbuildmat.2018.09.143.

[50] S. Graeser, W. Postl, H.-P. Bojar, P. Berlepsch, T. Armbruster, T. Raber, K. Ettinger, F. Walter, Struvite-(K), $KMgPO_4 \cdot 6H_2O$, the potassium equivalent of struvite – a new mineral, Eur. J. Miner. 20 (2008) 629–633. doi:10.7868/s002347611506020x.

[51] I. Kansal, A. Reddy, F. Muñoz, S.J. Choi, H.W. Kim, D.U. Tulyaganov, J.M.F. Ferreira, Structure, biodegradation behavior and cytotoxicity of alkali-containing alkaline-earth phosphosilicate glasses, Mater. Sci. Eng. C. 44 (2014) 159–165. doi:10.1016/j.msec.2014.08.016.

[52] B. Lothenbach, B. Xu, F. Winnefeld, Thermodynamic data for magnesium (potassium) phosphates, Appl. Geochemistry. 111 (2019) 104450. doi:10.1016/j.apgeochem.2019.104450.

[53] P. Mácová, A. Viani, Investigation of setting reaction in magnesium potassium phosphate ceramics with time resolved infrared spectroscopy, Mater. Lett. 205 (2017) 62–66. doi:10.1016/j.matlet.2017.06.063.

[54] D. Leng, X. Li, Y. Lv, H. Tan, N. Li, Z. Liu, W. Jiang, D. Jiang, Cesium immobilization by K-struvite crystal in aqueous solution: Ab initio calculations and experiments, J. Hazard. Mater. 387 (2020) 121872. doi:10.1016/j.jhazmat.2019.121872.

[55] Z. Zhang, H. Wang, J.L. Provis, F. Bullen, A. Reid, Y. Zhu, Quantitative kinetic and structural analysis of geopolymers. Part 1. the activation of metakaolin with sodium hydroxide, Thermochim. Acta. 539 (2012) 23–33. doi:10.1016/j.tca.2012.03.021.

[56] C.Z. Tan, J. Arndt, Interaction of longitudinal and transverse optic modes in silica glass, J. Chem. Phys. 112 (2000) 5970–5974. doi:10.1063/1.481169.

[57] P. Padmaja, G.M. Anilkumar, P. Mukundan, G. Aruldhas, K.G.K. Warrier, Characterisation of stoichiometric sol-gel mullite by fourier transform infrared spectroscopy, Int. J. Inorg. Mater. 3 (2001) 693–698. doi:10.1016/S1466-6049(01)00189-1.

[58] P. Makreski, G. Jovanovski, MINERALS FROM MACEDONIA IX . DISTINCTION BETWEEN SOME, (2003).

[59] A. Viani, P. Mácová, Polyamorphism and frustrated crystallization in the acid-base reaction of

magnesium potassium phosphate cements, CrystEngComm. 20 (2018) 4600–4613. doi:10.1039/c8ce00670a.

[60] S. Jähnigen, E. Brendler, U. Böhme, G. Heide, E. Kroke, Silicophosphates containing SiO_6 octahedra-anhydrous synthesis under ambient conditions, New J. Chem. 38 (2014) 744–751. doi:10.1039/c3nj00721a.

[61] A. Udduttula, J. Li, P.Y. Zhao, G.C. Wang, J. V. Zhang, P.G. Ren, Sol-gel derived nanosized $Sr_5(PO_4)_2SiO_4$ powder with enhanced in vitro osteogenesis and angiogenesis for bone regeneration applications, Ceram. Int. 45 (2019) 3148–3158. doi:10.1016/j.ceramint.2018.10.215.

Title: Fabrication of Sustainable Magnesium Phosphate Cement micromortar using Design of Experiments Statistical Modelling: valorization of Ceramic - Stone - Porcelain containing waste as filler.

Authors: S. Huete-Hernández, A. Maldonado-Alameda, J. Giro-Paloma, J.M. Chimenos, J. Formosa

The authors would like to thank the reviewer for all the positive feedback, comments, and suggestions to improve the overall quality of the manuscript. The reviewer's contribution is very helpful for the better understanding of the investigation. All the responses of the reviewer comments and questions are presented below. Hopefully, we answered all the questions and clarified all issues. Please, check the attached revised manuscript to see all the modifications marked in color. Thank you again for your comments and suggestions.

Note from assistant editor:

For possible final paper acceptance, English of the whole paper requires considerable revision efforts. Authors are suggested to make use of Elsevier language services, and are advised to write in colour any technical and language improvement made in their revised text.

Thank you very much for the suggestion, the English of the manuscript has been revised and checked by Elsevier Language Editing services (Project number: 11410, Invoice reference: CS114056). Language improvements are marked in blue, the improvements related to the reviewer comments are marked in red. We hope the English of the paper is now correct and easy to understand.

Answer to the comments of Reviewer

REVIEWER 1:

This article addresses an interesting topic, such as the design of new MgO phosphate cements, using low grade MgO. Although the topic is very interesting, there are some major concerns that authors should address before its publication. Attached is the manuscript with my suggestions and comments.

Thank you very much. We agree on the relevance of the topic, in particular, on the use of by-products and wastes as raw materials. The authors are really grateful for your comments and suggestions. We are also open to introduce some changes to improve the quality of the manuscript.

Title. * The title is very generic, and do not sump up the main objective of this study, which is a to apply a statistical model in MPC, incorporating different proportions of wastes...Authors should be more specific.

We really appreciate this suggestion. In order to further specify the subject of the investigation the title has been modified from:

"*Preparation of Sustainable Magnesium Phosphate cement mortars by recycling Ceramic - Stone - Porcelain containing wastes*"

To:

"*Fabrication of Sustainable Magnesium Phosphate Cement Micromortar using Design of Experiments Statistical Modelling: Valorization of Ceramic-Stone-Porcelain containing waste as filler*"

Keywords. * This key-word is odd, what is microstructure-final?

The keyword "*microstructure-final*" refers to the characterization of the final microstructure of the mortar performed via scanning electron microscopy. The keyword might seem odd due to the dash between words but it is enclosed inside the list of suitable keywords for Ceramics International listed inside the guide for authors. In particular, the keyword "*microstructure-final*" is included in segment "*B. Structure and Microstructure*".

Abstract. * What is sust-MPC?

Please we encourage you to check the new abstract to ensure it is better defined now. The abbreviation Sust-MPC refers to Sustainable Magnesium Phosphate Cement. As it is defined in the abstract, the authors consider magnesium phosphate cement (MPC) as Sust-MPC when MgO by-products are used in substitution of pure MgO as raw material.

Line 1, Title. * This title is very far from the main objective of the manuscript, change it for one more specific.

Thank you for your comment. The title of the manuscript has been changed as you can check in previous answers. We hope it fits better and more specifically the main objectives now.

Line 14, Abstract. * This abstract is very difficult to follow. Please, re-write it.

The abstract:

"*Magnesium Phosphate Cement (MPC) is a potential sustainable alternative to Ordinary Portland Cement (OPC). The use of a low-grade MgO (LG-MgO) by-product for developing MPC leads to a sustainable MPC (sust-MPC). This research is focused on the incorporation of ceramic, stone, and porcelain waste (CSP) into sust-MPC. CSP is obtained from glass recycling industry, which is landfilled. The percentage of CSP into sust-MPC was analyzed by using design of experiments (DoE). A statistical model was obtained and validated by formulating and testing an Optimal Formulation (OF). The OF was proposed by maximizing compressive strength at 7 and 28 days of curing. The OF compressive strength were 18 and 28 MPa, respectively for the dosage with 15 % wt. of CSP and a water to cement ratio of 0.34. The OF was deeply physico-chemically characterized by SEM-EDS and FTIR-ATR. OF showed good integration of CSP particles in the ceramic matrix. Concluding that a potential reaction between silica and K-struvite matrix may have occurred after one year of curing."*

Has been replaced by:

"Magnesium phosphate cement (MPC) is a potential sustainable alternative to Portland cement. It is possible to lower the total CO_2 emissions related to MPC manufacturing by using by-products and wastes as raw materials. When by-products are used to develop MPC, the resultant binder

can be referred to as sustainable magnesium phosphate cement (sust-MPC). This research incorporates ceramic, stone, and porcelain waste (CSP) as a filler in sust-MPC to obtain a micromortar. Sust-MPC is formulated with KH_2PO_4 and low-grade MgO (LG-MgO), a by-product composed of 40–60 wt.% MgO. CSP is the non-recyclable glass fraction generated by the glass recycling industry. The effect of water and CSP addition on the mechanical properties of sust-MPC was analyzed using design of experiments (DoE). A statistical model was obtained and validated by testing ideally formulated samples achieved through optimization of the DoE. The optimal formulation (15 wt.% of CSP and a water to cement ratio of 0.34) was realized by maximizing the compressive strength at 7 and 28 days of curing, resulting in values of 18 and 25 MPa respectively. After one year of curing, the micromortar was physico-chemically characterized in-depth using backscattered scanning electron microscopy (BSEM-EDS) and Fourier transform infrared-attenuated total reflectance spectroscopy (FTIR-ATR). The optimal formulation showed good integration of CSP particles in the ceramic matrix. Thus, a potential reaction between silica and the K-struvite matrix may have occurred after one year of curing."

Line 28, Keywords. * What is that? Please, choose another Keyword, or simply remove final.

The authors think we are not allowed to change the keyword. The keyword is enclosed inside the list of suitable keywords for Ceramics International listed inside the guide for authors. Authors must choose keywords as they are in the list. This is a quote from the keywords section linked below: "*Authors should select a maximum of four keywords from this list. Each keyword should be accompanied by the capital letter denoting the category from which the keyword has been selected. Authors may also choose one keyword not appearing in this list*"

https://www.elsevier.com/__data/promis_misc/ceri_keywords.pdf

As it is answered above, the keyword "*microstructure-final*" refers to the characterization of the final microstructure of the mortar performed via scanning electron microscopy.

Line 31. * Too many acronyms, please try to reduce the number of these in the manuscript.

Thank you for your recommendation, we have reduced the number of acronyms in the list of abbreviations as well as in the manuscript to make the paper easier to follow.

"*Abbreviations*

MPC	*Magnesium Phosphate Cement*
MPCs	*Magnesium Phosphate Cements*
OPC	*Ordinary Portland Cement*
LG-MgO	*Low-grade MgO*
Sust-MPC	*Sustainable Magnesium Phosphate Cement*
CSP	*Ceramic, Stone, and Porcelain Waste*
DoE	*Design of Experiments*
CS	*Compressive Strength*
CBCs	*Chemically Bonded Ceramics*

CBPCs	*Chemically Bonded Phosphate Cements*
MKP	*Monopotassium Phosphate*
RSM	*Response Surface Methodology*
CSP(%)	*Ceramic, Stone, and Porcelain Waste percentage in the mortar*
R1-16	*Mortar formulation from Design of Experiments corresponding run*
-7d, -28d, -365d	*Days of curing before test and characterization*
OF	*Optimal Formulation*
FA	*Fly Ash*
BOs	*Bridging Oxygens*
NBOs	*Non-Bridging Oxygens*"

Has been replaced by:

"Abbreviations

MPC	*Magnesium Phosphate Cement*
LG	*Low-Grade. Refers to a product containing impurities and of lower quality than the pure product*
LG-MgO	*Low-grade MgO. MgO containing impurities and of lower quality than pure MgO*
Sust-MPC	*Sustainable Magnesium Phosphate Cement*
CSP	*Ceramic, Stone, and Porcelain Waste*
DoE	*Design of Experiments*
CBC	*Chemically Bonded Ceramics*
CBPC	*Chemically Bonded Phosphate Cements*
MKP	*Monopotassium Phosphate*
RSM	*Response Surface Methodology*
CSP(%)	*Ceramic, Stone, and Porcelain Waste percentage in the micromortar*
R1-16	*Micromortar formulation from the corresponding design of experiments run*
-7d, -28d, -365d	*Number of days of curing before testing and characterization"*

Line 34. * OPC is not used anymore, please replace OPC by PC.

Thank you very much for this correction. The authors decided not to use any acronyms referring to Portland cement in the manuscript, using "*Portland Cement*" instead of the abbreviation PC.

Line 35. * Define low grade.

Low-grade MgO is now better defined in the abstract, we also included a brief definition in the abbreviation section as well as for low-grade (LG) alone. We hope it is understood much better now.

Line 43. * Define what is this....

Response Surface Methodology definition was added in the manuscript after first mention.

"RSM includes analysis of a response surface plot calculated from statistical polynomic equations that are derived from the experimentally obtained results. One surface was plotted for each measured property (response) of the material studied."

Line 46. * Is that correct?

It is correct. The abbreviation is referred to the curing period of the samples before testing and/or before physicochemical characterization. For example, CS-28d refers to compressive strength test performed at 28 days of curing, and R15-365d corresponds to the R15 formulation samples R15 cured 365 days.

Line 49. * The s is not necessary.

Thank you for your suggestion, BOs abbreviation was removed from the abbreviation list to reduce the number of acronyms used throughout the manuscript.

Line 95. * See comment above.

Thank you for your suggestion, NBOs abbreviation was removed from the abbreviation list to reduce the number of acronyms used throughout the manuscript.

Line 56. * Construction.

We really appreciate the recommendation. Construction was added to further specify the type of material.

The sentence*:*

"This is mainly because Portland cement is one of the most produced and applied materials on a global scale due to its wide range of properties and its low cost [3,4]."

Was replaced by:

"This is because Portland cement is one of the most produced and widely applied construction materials worldwide owing to its various properties and low cost [3,4]."

Line 57. * Apart of the CO_2 prodcution and the E consume, OPC fabriacation face another problems, such as the overexplotation of the natural resources.

The authors totally agree on this, to improve the quality of the manuscript the sentence:

"Being known as hydraulic cement, Portland cement production process consumes extremely high amounts of energy"

Was replaced by:

"Also termed hydraulic cement, the production process for Portland cement consumes extremely high amounts of energy, depleting and overexploiting natural resources."

Line 65. * Define before writting the acronym.

Thank you for the suggestion. The acronym was previously defined at the first mention in the abstract and in the abbreviations section. The authors considered MPC was already defined in this segment. Nevertheless, the definition *"magnesium phosphate cement (MPC)"* was added in this sentence.

Line 80. * Do you have some data? What is the proportion of CO2 released to the atmosphere due to the dolomite calcination....? I guess is quite similar than in the CaCO3, probably is less contaminant because the production of MgO is much more lower than the production of PC.

Thank you for bringing up this point. You can calculate the CO_2 released from $CaCO_3$, $MgCa(CO_3)_2$ and $MgCO_3$ using the wt. % decomposition in their calcination process. The CO_2 released from thermal decomposition is quite similar as you can see.

								CO_2 released from raw material calcination
900ºC	$CaCO_3$	→	CaO	+	CO_2			g CO_2/g $CaCO_3$
(g)	100,09		56,1		44,01			**0,44**
750 ºC	$CaMg(CO_3)_2$	→	CaO	+	MgO	+	2 CO_2	g CO_2/g $CaMg(CO_3)_2$
(g)	184,4		56,1		40,3		88,02	0,48
600 ºC	$MgCO_3$	→	MgO	+	CO_2			g CO_2/g $MgCO_3$
(g)	84,31		40,3		44,01			**0,52**

The decisive factor is the energy input in the rotary kiln to calcinate raw materials. CO_2 released to reach calcination temperatures inside the kiln comes from fuel burning, this releases much higher amounts of CO_2 into the atmosphere than CO_2 from thermal decomposition. The higher the temperature, the higher the energy needed and the higher the CO_2 released. MgO total global production is lower than PC, from this point of view MgO produces less total amount of CO_2 emissions than PC globally, but the authors are referring to the process itself in the manuscript. The lower calcination temperature in MgO production process make it less pollutant than PC production process.

Line 89. * Depending, of the secondary products that you are going to have in the Low grade MgO.

Thank you for the comment. The authors agree on this point. Based in our experience working with this by-product over the years, low-grade MgO secondary products composition have remained unchanged and in a controlled range. Carbonates proceeding from unreacted raw materials, quartz and silicates from raw materials impurities are the main two secondary products in the low-grade MgO we work with.

Line 90. * I am not convinced that can be considered a mortar, the particle size of these secondary phases is going to be much more lower than the normalized sand used in the preparation of a standar PC (beteen 0.5 and 2 mm aprox.).

We really appreciate this comment. We were also doubting between using micromortar instead of mortar in the manuscript. We see magnesium phosphate cement as a mortar or micromortar when ceramic- stone-porcelain waste CSP is added as an inert filler or aggregate. It is true that the particle size is much lower than that of normalized PC mortar. For these reasons, the word *"mortar"* has been replaced by *"micromortar"* in the manuscript when required.

Line 90. * What kinf of fillers?

In this case we refer to any kind of inert inorganic filler, improves workability by the bearing ball effect, reduces heat development since is does not react exothermically like the cement and reduces production costs by replacing more expensive material in the cement.

Line 93. * Define the acronym in the text first.

As well as in the response to the comment in line 65, the authors considered CSP was already defined in this segment. The acronym was previously defined at the first mention in the abstract and in the abbreviations as it is required in the guide for authors. Nevertheless, the definition *"ceramic, stone, and porcelain waste (CSP)"* was added in this line. Thank you very much for the recommendation.

Line 93. * Fine fraction I guess.

CSP is the fraction of the glass cullet recycling process that cannot be classified by optical sorting machinery. CSP is not the fine fraction. In line 123 of the manuscript we explain how CSP is delivered to us in the form of shattered solid fragments superior to 2 mm of length and in an average range of 8-16 mm.

Line 97. * What kind of stone?.

The stones found in CSP come from pebbles found in the storage ground. These pebbles inevitably are introduced in the waste glass when shoveling and handling the waste.

Line 100. * Temperature?.

CSP melting point temperature is unknown for the authors. We could not find any references pointing this feature in the literature while in the process of writing the manuscript. Soda-lime glass melting point ranges from 1450 to 1800 ºC. Ceramic, stone and porcelain melting point could reach up to 3000 ºC approximately. Since CSP is around 80 wt.% soda-lime glass it can be assumed that CSP melting point will increase considerably.

Line 105. * I guess this amount is highly dependent of the country...isn´t it? Please, include a reference.

Thank you very much. The recycling company has the last decision in this matter. European Union federations related to glass recycling set concentration standards or recommendations. CSP standard concentration ranges between 20 to 100 $g \cdot t^{-1}$, but the recycling companies decide how much CSP accept in their process based on their process, infrastructure and other different

reasons. The authors added a reference in this sentence and modified it to be more rigorous. The sentence:

"Recycling companies only accept glass cullet if CSP concentration is lower than 20 g·t^{-1}."

Has been replaced by:

"Moreover, recycling companies only accept glass cullet if the CSP concentration is between 20–100 g·t^{-1} or below [31]."

Line 107. * See my previpus comment about mortar...i do not think this is a mortar...in any case it would be a amicromortar.

Thank you very much for the suggestion. The use of mortar has been already corrected to micromortar throughout all the manuscript.

Line 109. * ,

We are sorry for this. A comma was added:

"When CSP is utilized as a filler, the economic costs are reduced and environmental and sustainable criteria are enhanced."

Line 110. * See my previous comments about the acronyms...

Thank you for the suggestion, the use of the acronym DoE has been reduced in the manuscript. Instead it is used now *"design of experiments"* when the authors consider it appropriate.

Line 121. * ???

Food grade is the terminology commercially used for KH_2PO_4 suitable for its use as a fertilizer for example for growing vegetables, it is of a lower quality than laboratory reactive K_2HPO_4. The authors believe that the use of food grade K_2HPO_4 excess production to develop Magnesium Phosphate Cement could be beneficious from the point of view of sustainability and costs savings.

Line 128. * Which was the cleaning process?

The cleaning process consisted on the next steps:

- Soaking CSP with water and soap during 5 days. Every day the water was replaced with fresh water and soap.
- Drying CSP during 24h (105ºC).
- Milling CSP in alumina ball mill until all particles are under 0,75 mm.
- Removing the solids retained by the sieve (paper, plastics and metallic pieces).

Line 130. * I do not understand this step, what do you need to hydrate the raw mateirials?? What kind of materials are you talking about?

Sorry for this misunderstanding. To hydrate the raw materials and develop the micromortar we used deionized water. In that sentence we are referring to the kneading water used in developing

magnesium phosphate micromortar. Raw materials are defined in the manuscript as LG-MgO, KH_2PO_4, and CSP.

Line 153. * Too many acronyms...

Thank you for the recommendation. The number of acronyms throughout the manuscript has been reduced.

Line 160. * What do you consider as cement? The LgMgO or the mixture of LgMgO + CSP??

Sorry for this misunderstanding. As it is explained in the referred sentence (line 160) the authors consider cement (C) the combination of LG-MgO and monopotassium phosphate (MKP, KH_2O_4) in a proportion of 60/40 LG-MgO/MKP (line 158). The cement alone can be considered as a micromortar due to all the unreacted carbonates and quartz particles inside the matrix among others, but the authors always refer to it as cement (magnesium phosphate cement, MPC) and use micromortar only when CSP is added (MPC micromortar). We hope we have answered or clarified this issue.

Line 161. * Fillers are usually consider as inert materilas in pastes and mortars, but I guess this is not the case....

Thank you for the observation, we are sorry if this sentence could lead to a misunderstanding. We totally agree, fillers are considered inert materials. The authors consider CSP as a filler because it behaves like one during mixing, molding and micromortar application, being CSP an inert material at first glance. This study focused on the possibility that CSP particles and K-struvite matrix could slightly interact in the interlayer between them forming some type of phoshposilicate compound. The authors really want to highlight this possible reaction could take years, and would slightly affect only the interlayer between filler particle and matrix, enhancing the embeddedness of the filler in the cement. That is why authors consider CSP as an inert filler to formulate the micromortar using Design of Expermients, and why the characterization of the micromortar takes place at 28 days of curing and after one year of curing.

To make more understandable the use of filler in this sentence, the text in the manuscript:

"Hence, CSP is considered as a filler, even though it might partially react with K-struvite."

Has been replaced by:

"Hence, CSP is considered as a filler, although it may slightly react at the interface of K-struvite over a long period of time."

Line 166. * Same again, I do not think this is a mortar per se...

Thank you for the recommendation. The word mortar has been replaced by "micromortar" throughout the manuscript as it is resolved in a previous comment.

Line 168. * I am not familiar with this methodology, please briefly describe it.

We really appreciate this suggestion.

The description:

"RSM includes analysis of a response surface plot calculated from statistical polynomic equations that are derived from the experimentally obtained results. One surface was plotted for each measured property (response) of the material studied."

Has been added to the manuscript after RSM first mention.

Line 195. * I can not remember what was MOE...

MOE stands for modulus of elasticity. The number of acronyms has been reduced in the paper, now "*modulus of elasticity*" is used instead of "*MOE*" when considered necessary.

Line 195. * Why this particular age? These properties are usually reported after 2 and 28 days....

Thank you for the observation. There are several authors that work at 7 and 28 days of age, especially when working with magnesium phosphate cement. This is mainly due to the early setting of the cement, being known as a repair material. Here are some recent publications in this field, in these, cements are cured and tested after 7 days of curing among other curing ages:

https://doi.org/10.1016/j.conbuildmat.2020.119893

https://doi.org/10.1016/j.conbuildmat.2019.117501

https://doi.org/10.3390/ma12162561

https://doi.org/10.3390/ma13173692

https://doi.org/10.1007/s40891-020-00212-3

Line 196. * Do you have some reference where this MOE has been determined for MPC usin this procedure? I have some reservations... see next comment.

Yes, we included the reference in the manuscript. Thank you very much.

Line 199. * To calculate the Young´s modulus is necessary the Poison Coeficient...which is standar PC concrete is usally 0.2...however this systems is very different to the PC, so...what value have you used?

To estimate the modulus of elasticity of the samples a Poisson Coefficient value of 0.22 was used following the procedure described in the reference recently added to the manuscript, which at the same time followed UNE-EN 12504-4. The authors think Poisson Coefficient does not change severely between materials of the same classification, although is true sust-MPC Poisson coefficient can not be the same as PC Poisson coefficient. For this reason, the authors modified the use of *"determinated"* or *"calculated" to "estimatied"* in reference to modulus of elasticity, it is more accurate since the value 0.22 was used for the calculations of modulus of elasticity estimation.

Line 207. * I do not follow this sentence...

We are sorry this sentence not totally clear for the reader. The samples characterized after one year of curing were the same as the samples tested by means of compressive strength test after 28 days of curing. The characterization was performed on the cured broken parts of the micromortar samples. To make this part more understandable the manuscript has been modified:

"The optimal sust-MPC micromortar and ordinary sust-MPC without CSP filler as a reference were compared after 365 d of curing, both samples were obtained from the compressive strength test at 28 d"

Has been replaced by:

"The optimal sust-MPC micromortar was compared with an ordinary sust-MPC without CSP filler as a reference, both after 365 d of curing. The samples cured for 365 d were the broken parts of the samples that were tested for compressive strength at 28 d."

Line 213. * The raw materials or the same material after 1 year??

In this case the authors are referring to the raw material CSP. It was evaluated using FTIR as well as the micromortar one year cured samples. This evaluation was performed in order to compare the spectra of both and see differences between the peaks and bands corresponding to phosphates and silicates.

Line 235. * As these wastes were collected from dump containers, have you analysed the presence of minoritary elements, such as heavy metals?

We are glad you bring up this point. Yes, we have measured the leaching metals of CSP waste in deionized water after 24 h of constant stirring following UNE-EN 12457-2 (EN 12457-2). The pH of the final slurries was 10.68±0.05.

Leached metals in CSP waste.

(ppm)	**Ba**	**As**	**Cr**	**Pb**	**Cd**	**Ni**	**Hg**	**Cu**	**Zn**	**Mo**	**Sb**	**Se**	**Sn**	**V**
EU limits for non-hazardous waste*	**100**	**2**	**10**	**10**	1	**10**	0.2	**50**	**50**	**10**	**0.7**	**0.5**	-	-
CSP	**0,72**	**0,65**	**0,06**	**0,01**	0,00	**0,07**	0,00	**0,74**	**0,17**	**0,02**	**0,37**	**0,20**	0,00	**0,06**

* EU, 2003. Council decision of 19 December 2002 establishing criteria and procedures for the acceptance of waste at landfills pursuant to Article 16 of and Annex II to Directive 1999/31/EC. European Council

The authors decided not showing leaching metals results because the article was considered long enough.

Line 240. * Have you quantify the amount of amorphous glass in the CPS?

Yes, we have partially quantified the amorphous glass in CSP using ICP-OES analysis, analyzing the Si and Al dissolved in NaOH solution at different concentrations. This analysis is based in the idea that amorphous phases are more susceptible to chemical attack than crystalline phases. The experiments were run by triplicated. 1 g of sample was added to 100 ml of NaOH solution in a Teflon beaker. The beaker was heated via water bath at 80° and the solution was constantly stirred during 5 h at 500 rpm. The authors would like to save these results to be published with Rietveld analysis in other future investigations. Also, the authors decided not showing these results because the manuscript was considered long enough.

The results are showed below:

Amorphous SiO_2 and Al_2O_3 in CSP waste, analyzed via NaOH chemical attack.

	4M	6M	8M
SiO_2 (%)	16,13	16,15	25,68
Al_2O_3 (%)	0,81	0,77	0,70

Line 241. * It would be quite interesting to have data corresponding to the particle size distribution (i.e d10, d50 and d90).

We really appreciate this comment. The authors decided not showing particle size distribution graphics because the article was considered long enough. Particle size distribution (PSD) information d_{10}, d_{50} and d_{90} was added in the manuscript. The requested data can be seen below, included graphs:

d_{10}, d_{50} and d_{90} of raw materials.

	d_{10}	d_{50}	d_{90}
Raw material	(µm)	(µm)	(µm)
CSP	1.666	12.410	39.960
LG-MgO	1.763	14.110	40.200

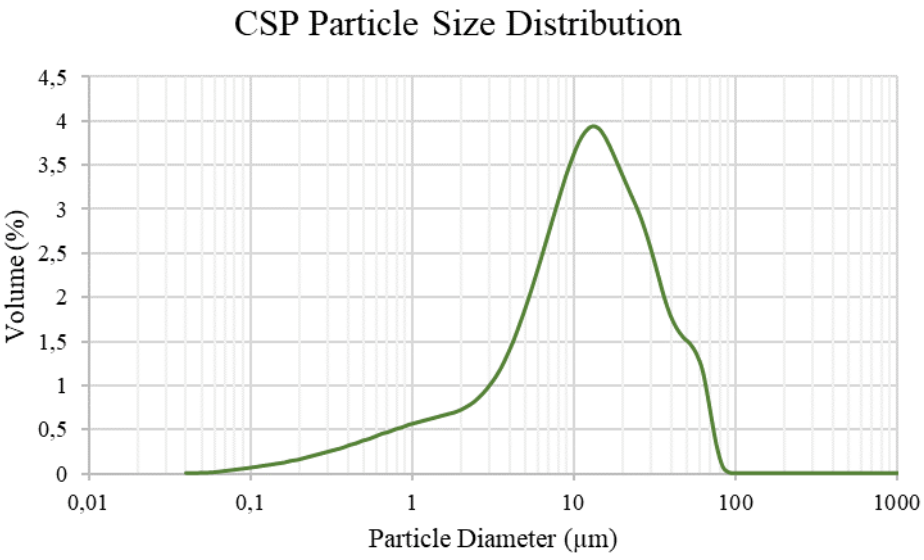

Particle size distribution of aconditioned CSP.

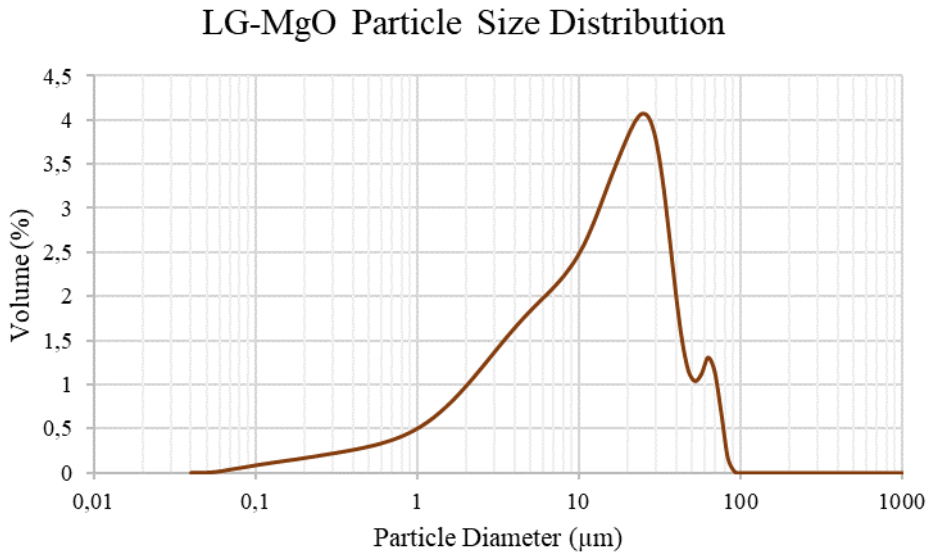

Particle size distribution of aconditioned LG-MgO.

The sentence:

"LG-MgO and CSP characterization were performed using complementary techniques such as X-ray fluoresce (XRF), X-ray diffraction (XRD), and thermogravimetric analysis with derivative thermogravimetry (TG/DTG)."

Has been replaced by:

"LG-MgO and CSP were characterized using complementary techniques such as particle size distribution (PSD), X-ray fluorescence (XRF), X-ray diffraction (XRD), and thermogravimetric analysis with derivative thermogravimetry (TG/DTG)."

The sentence:

"PSD analysis resulted in diameters of 1.666 µm (d10), 12.410 µm (d50), and 39.960 µm (d90) for LG-MgO and 1.763 µm (d10), 14.110 µm (d50), and 40.200 µm (d90) for CSP."

Has been added to the manuscript.

Line 247. * There are several peaks in the DTG analysisis , corresponding to the decarbonation of MgCO3 and CaCO3, as well another peak associated to the dehydroxilation of the Mg(OH)2...I would not say "without showing any clear decomposition".

In this sentence the authors are not referring to TGA analysis of LG-MgO, the sentence refers to the TGA analysis of CSP which is not showed in the figures. The analysis did not show any clear mass loss that could be identified and CSP only lost a total of 1,214 wt.%. The authors attach to this answer the TGA overlaid analysis of LG-MgO and CSP:

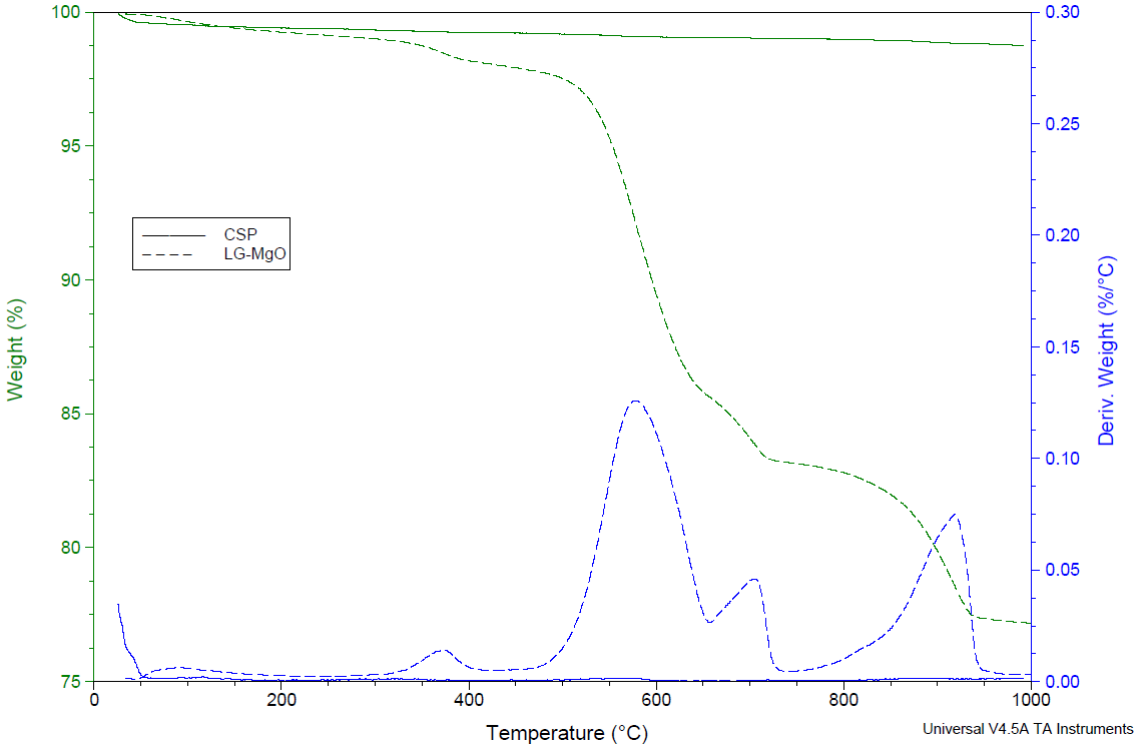

TG/DTG analysis of CSP and LG-MgO

Line 247. * Fig. 2 only shows the TG curves and the DTG curves, so I would replcae TGA-SDT bt TG/DTG analysis...

We really appreciate this recommendation, thank you very much. We agree, "*TGA-SDT*" has been replaced with "*TG/DTG*" analysis throughout the manuscript, figures and tables. Also, the definition was changed in the first mention:

"LG-MgO and CSP characterization were performed using complementary techniques such as X-ray fluoresce (XRF), X-ray diffraction (XRD), and thermogravimetric analysis with simultaneous scanning differential thermal analysis (TGA-SDT)."

Has been replaced by:

"LG-MgO and CSP were characterized using complementary techniques such as particle size distribution (PSD), X-ray fluorescence (XRF), X-ray diffraction (XRD), and thermogravimetric analysis with derivative thermogravimetry (TG/DTG)."

Line 248. * Please, specify.

Thank you for the recommendation. Cements tend to retain some adsorbed water in their porous structure, although after one year of curing most of this adsorbed water should be evaporated. For that reason, the authors decided to remove *"adsorbed water"* from the text.

This section from sentence in the manuscript:

"TG/DTG analysis for LG-MgO indicated mass losses attributed to adsorbed water and crystallization water (from 30 ºC to 210 ºC)"

has been replaced by:

"TG/DTG analysis for LG-MgO indicated mass losses attributed to the crystallization of water (from 30 to 210 °C) [42]"

Line 252. * Include references for these assigments.

Thank you for the suggestion. The references are now included in the manuscript.

Line 252. * See my previous comment.

Thank you very much. *"TGA-SDT"* has been replaced by *"TG/DTG"* throughout the manuscript, figures and tables.

Line 253. * Please, comment these calculations. For next time I would recommend to perform a Rietveld analysis.

Thank you for your recommendation, we will consider Rietveld analysis for next investigations.

The estimation of the actual composition of LG-MgO has been conducted firstly by stoichiometric calculation of the wt. % of each compound thermally decomposed in TG / DTG analysis. Then, the remaining wt. % of components is estimated from XRF composition results in proportion to the wt. % left to complete the characterization. XRD results were used to identify the chemical compounds being thermically decomposed in TG/DTG analysis in combination with the experience our research group has characterizing LG-MgO.

In order to add this explanation in the manuscript, the segment:

"*First, TG/DTG results were used to estimate the percentage of compounds that thermally decomposed up to 1400 °C by stoichiometric calculation. Second, the remaining composition was calculated using the XRF compositional results considering the outstanding wt.% to estimate. XRD results were used to identify the chemical compounds that thermally decomposed during TG/DTG."*

Has been added to the manuscript.

Line 256. * After solubilization Mg would be as Mg2+....I do not think is correct to include as MgO....

We really appreciate this comment. In this sentence we are referring to the magnesium available in the by-product before hydration. Nevertheless, it is a matter of fact that it is not correct to refer to $Mg(OH)_2$ and $MgSO_4$ as available MgO. We also detected that the total wt.% of magnesium compounds did not sum up, and we corrected it. For those reasons, the sentence:

"Considering that $Mg(OH)_2$ (3.77 wt.%) and $MgSO_4$ (2.12 wt.%) are soluble in water in contrast with the carbonate, the total calculated content of available MgO in the by-product is 51.47 wt.%."

Has been replaced by:

"Considering that $Mg(OH)_2$ (3.77 wt.%) and $MgSO_4$ (2.12 wt.%) are soluble in water, unlike carbonate, the total calculated content of available reactive magnesium compounds in the unhydrated by-product was 49.47 wt.%.

Line 258. * references?

The sentence is already referenced a bit ahead in the manuscript. Thank you very much.

Line 267. * I do not follow this terminology.

We are sorry for this inconvenient, but we think this could be mainly because the formulations are randomized. The different formulations of the micromortar are established using Design of Experiments software. Each one of the formulations are experimental trials also called runs inside the software. If you take a look in Table 1 you will observe how some of those runs are exactly the same formulation. This is because in Design of Experiments modelling some formulations are duplicated, triplicated or quadruplicated near the zone where it is thought to statistically find the optimal formulation before proceeding with the experimental, reducing the results (responses) deviation of the hypothetical optimal formulation. The randomization of the experimental trials performed using Design of Experiments software makes it difficult to find a proper terminology for every formulation designed. For this reason, the formulations remained with the terminology "Run" in the manuscript, and are abbreviated as R1, R2, …, R15, R16 since there exist 16 different runs. We hope we have clarified this issue.

Line 270. * This part is difficult to follow for a reader non familiar with this kind of analysis, please re-write.

We are sorry for this inconvenient. The number of acronyms has been reduced and also we modified the text to make it more understandable for readers non familiar with Design of Experiments. We hope the sentence is easier to follow now.

The sentence:

"The best model fitting the experimental results for the apparent density at 7 d, MOE at 7 d, FS at 7 d, CS at 7 d, and CS at 28 d are two factors with interaction, linear, linear, reduced cubic, and reduced quadratic, respectively."

Has been replaced by:

"The best model equations for fitting the experimental results are as follows: density at 7 d (two factors with interaction), modulus of elasticity at 7 d (linear), flexural strength at 7 d (linear), compressive strength at 7 d (reduced cubic), and compressive strength at 28 d (reduced quadratic)."

Line 275. * How do you get this Eq.?

This equation is calculated from statistical analysis of the experimental results derived from Design of Experiments experimental methodology. The equation is a polynomic equation generated by adding or removing terms and variables to adjust the surface equation the best to the experimental results, minimizing standard deviation and optimizing R^2.

Line 276. * AS far as I know R2 has to be close to 0.99, 0.87 does´t seem a very high value...

We agree on the fact that R^2 has to be as high as possible being 1 the ideal value. But, since the surface model equation has to fit all the experimental responses points it is really difficult to reach such high values. The model is considered to fit when Lack of Fit is not significant and Model F Value is significant. If the F value is high, the probability (*p*-value) will fall below 0.05, indicating that there is a significant difference between the response surface points. The value of 0.05 is a typical accepted risk value. Below you can see the statistical results of density at 7 days of curing.

Density-7d Analysis of variance table (Partial sum of squares - Type III)

Source	Sum of Squares	df	Mean Square	F Value	p-value Prob > F	
Model	0,009706	3	0,003235	**27,96414**	**< 0.0001**	**significant**
A-W/C	0,003047	1	0,003047	26,34044	0.0002	
B-CSP	0,006069	1	0,006069	52,45331	< 0.0001	
AB	0,00089	1	0,00089	7,691684	0.0169	
Residual	0,001388	12	0,000116			
Lack of Fit	0,001117	7	0,00016	**2,940772**	**0.1265**	**not significant**
Pure Error	0,000271	5	5,43E-05			
Cor Total	0,011094	15				

The Model F-value of 27.96 implies the model is significant. There is only a 0.01% chance that a "Model F-Value" this large could occur due to noise. The "Lack of Fit F-value" of 2.94 implies the Lack of Fit is not significant relative to the pure error. There is only a 12.65% chance that a "Lack of Fit F-value" this large could occur due to noise. Non-significant lack of fit is good since we want the model to fit. We hope this issue is clarified now.

Line 288. * This is what the reader expect, so I do not see any novelty in this section…

Thank you for your observation. We agree, we wanted to provide some explanation to the water and filler effect on density but, the effect is very basic. For this reason, the sentence:

"As it is well known, an increase in the W/C ratio leads to a decrease in apparent density after curing, because water lightens the material as it leaves pores and/or the cement sets/dries. Besides, an increase in filler amount leads to an increase in apparent density, considering that usually the filler apparent density is higher than the paste apparent density."

Has been removed from the manuscript.

Line 296. * In this case the standard deviation is much higher than in the previous section...which was 0.01, so for me 0.48 seems a lot...what is the maximum values to be considered as adequate?

We are sorry for this misunderstanding. The standard deviation showed in the manuscript is the standard deviation of the whole surface model, it does not refer to the individual standard deviation of the variables measured. The authors think this value is not high at all for the model. The maximum values to be considered as adequate highly depends on the response analyzed, density at 7 days tend to vary less between formulations in contrast with compressive strength at 28 days that is more sensitive to changes in the formulation. Also, response value is the key parameter to be considered for a high or low standard deviation. As an example, a response of 15 ± 5 and 15000 ± 5 have the same standard deviation. The standard deviation ± 5 can be considered high or low depending on the main response value. We hope we have resolved this question.

Line 314. * It would be convenient specify some ranges to consider as valid...or to define what the authors consider as valid…

We are sorry, the maximum values to be considered as adequate highly depends on the response analyzed. We hope we have resolved this question in the previous answer to the review in line 296 of the revised manuscript. Thank you.

Line 314. * See my previus comments with respect to the standar deviation and the R2 values...

Thank you, we address this issue in the answer to comment in line 276 and 296.

Line 318. * Non surprising.

Thank you for the comment. The authors agree this is not a surprising result but also believe that the results have to be explained and related to the structure of the micromortar somehow. If you believe this kind of explanations is not needed, please let us know. Thank you very much again.

Line 319. * What does the authors mean with this sentence?

Sorry if this sentence was unclear. In this sentence the authors are trying to explain how porosity affects to flexural strength, modulus of elasticity, and compressive strength, being flexural strength and modulus of elasticity more sensitive to porosity than compressive strength. The direction of stresses in flexural test tend to open the pores of the material while in the compressive strength test tend to close the pore cavities. In consequence modulus of elasticity and flexural strength are more sensitive to W/C ratio since water affects porosity severely. In order make this sentence more understandable, the sentence:

"If air did not evacuate properly when the mortar was being obtained, this could affect severely the flexural performance. This effect had less impact on CS test due to the enclosure of pores when testing."

Has been replaced by:

"The porosity induced by the increase of the W/C ratio severely affects the flexural performance. This effect had a lower impact on the compressive strength because cavities in the micromortar tend to close during the compressive test, whereas during the flexural test, those cavities tend to open owing to the direction of the internal stresses in the material."

Line 323. *?????

"On-line version" is used in the manuscript just for the editorial-publication process. It was used in case the paper was read printed in black and white. "On-line version" has been removed from the manuscript. Thank you for the comment.

Line 334. *????

The authors address the same issue in the previous answer (line 323). Thank you.

Line 335. *???

The authors address the same issue in the previous answer (line 323). Thank you.

Line 339. * What do you mean by proper water? Are you referring to w/c ratio?

By "proper water" the authors are referring to the stoichiometric water. The authors wanted to explain how increasing CSP% while decreasing of W/C ratio increases compressive strength, as long as W/C ratio does not go lower than the stoichiometric water needed. In order to explain better this feature the sentence:

"This behaviour is attributed to the effect of the filler in a cement matrix when the proper water was used"

Has been replaced by:

"This behavior is attributed to the effect of the filler in a cement matrix, present as long as the W/C ratio is above the stoichiometric amount of water that the cement requires."

Line 342. * Speculative, you would have to prove it using some characterization technique , such as BSEM…

We really appreciate this comment, thank you. The sentence:

"When testing the compressive strength of a mortar, the filler particles favour the enclosure of cavities and the propagation of cracks, resulting in an enhanced compressive strength [32]."

Has been replaced by:

"Inside the micromortar, during the compressive strength test, the stress transfer mechanism facilitates the closing of pores and cavities and reduces the speed of crack propagation [33]."

Line 346. * This is quite susprising! Have you actually tested?

The authors think this is not surprising when talking about a micromortar considering that the sentence refers to the DoE results, always inside the range of study. We tested formulations with higher CSP% but it was hard to work with the binder, for this reason the range of study was set between 0-15 CSP% and between 0.34-0.38 W/C ratio. I hope this answer helped to clarify this point. Thank you very much for the comment.

Line 349. *????

We are sorry, the maximum values to be considered as adequate highly depends on the response analyzed. We hope we have resolved this question it the previous answer to the review in line 296 of the revised manuscript. Thank you.

Line 371. * Increase.

Thank you for this correction. The word "enhance" has been replaced by *"increase"* throughout the manuscript when considered, to improve the quality of the manuscript.

Line 378. * Why this particula value?

The importance value used in the optimization was selected in order to give the same importance to all the responses analyzed, in order to obtain a balanced micromortar in terms of density, modulus of elasticity, flexural strength and, compressive strength. It wouldn't have mattered using 1 or 5 as long as it was the same value for all the responses. If a higher value of importance is given to certain response among all the responses, the optimization will prioritize optimizing that response or property of the micromortar over the rest of properties of the selected optimal formulation. We hope we answered your question.

Line 382. * It would be quite convenient for the reader a brief reminder about the main features of these two mixtures (% of component, w/c ratios or Compressive strength values…).

I am glad you raised this issue since runs nomenclature in Design of Experiments can be confusing for the reader. We really appreciate the suggestion. In order to remind the main features of R15 and R7 the sentence:

"Optimal formulation coincided with R15 and R7 in terms of W/C ratio and CSP (see Table 1)."

Has been replaced by:

"The optimal formulation coincided with R15 and R7 in terms of the W/C ratio and CSP (0.34 W/C and 15.00 wt.% CSP, see Table 1)."

In addition, the reader has all the runs information available in Table 1, wt. % of component, W/C ratios and compressive strength included. Thank you for bringing up this issue.

Line 387. * See previous comment, is neccesary to reming which are the main features of R15 and R11.

The authors are really thankful for this suggestion. In order to improve the overall quality of the manuscript, the sentence:

"In order to evaluate the formation of new mineral phases, R15 was considered as the optimal formulation and compared to R11 as the sole dosage without CSP and lower W/C ratio used as a reference or blank."

Has been replaced by:

"To evaluate the formation of new mineral phases, R15 (0.34 W/C and 15.00 wt.% CSP) was considered as the optimal formulation and compared to R11 as a reference or blank (0.35 W/C and 0.00 wt.% CSP), i.e., without CSP and a lower W/C ratio."

Line 388. * From the 28 days of testing to the 365 days of curing...how are the samples conserved? Is the further hydration stopped? Is the CO2 avoided?.

Part of the answer to this question is addressed in line 208 of the manuscript section 2.3, although it could be further specified. The samples were cured in a curing chamber at a constant temperature of 20 ± 2 °C and relative humidity of 50%, CO_2 was not avoided since the chamber is often opened to introduce or take out samples. Hydration was not stopped in order to further cure the samples. With the aim of further specify the cure conditions of the 365 d cured samples, the sentence in line 208:

"The pieces obtained after the compressive strength tests at 28 d were stored in the curing chamber up to 365 d just for a better evaluation of a potential reaction of the CSP glass phase with K-struvite [37–39]."

Has been replaced by:

"The obtained fragments were stored in the curing chamber for 365 d at a constant temperature of 20 ± 2 °C and a relative humidity of 50% to evaluate the potential reaction of the CSP glass phase with K-struvite [27,39,40]."

And the sentence in line 388:

"The broken parts obtained after the CS-28d test of R15 and R11 were used to perform the sust-MPC micromortar characterization after 365 d of curing."

Has been replaced by:

"The broken fragments obtained after the CS-28d test for R15 and R11 were used to perform the sust-MPC micromortar characterization after 365 d of curing (20 ± 2 °C, relative humidity of 50%)"

Thank you very much.

Line 396. * Define large.

Thank you for the recommendation. The sentence:

"These authors considered that the reaction would take place after a large period."

Has been replaced by:

"These authors suggested that the reaction is complete after a period greater than 28 d."

Line 404. * See my previous comments about the mortars.

We really appreciate the suggestion about replacing "mortar" by "micromortar". This issue has been already addressed. We hope the nomenclature is correct now.

Line 408. * Is not possible to identify the chemical composition of an amorphous hump using exclusively XRD.

We agree it is not possible to identify the chemical composition of higher amorphous background with XRD alone. In this case we related the amorphous hump with amorphous silica associating XRF results (Table 2), which showed silica as the main elemental composition of CSP (70.78 wt.%), and also we know CSP is usually composed by ~84 wt.% soda-lime glass in average. CSP amorphous structure can be appreciated in XRD patter showed Figure 1. The fact that this higher background appeared only in the optimal formulation R15 (15 wt. % CSP) when compared with blank formulation R11 (0 wt. % CSP), could be easily related to the glassy composition of CSP. The authors believe that the way used to explain in the manuscript all the abovementioned could be improved. In order to do so, the sentence:

"There is an exception in R15 (background of higher intensity), which was as a result of the higher CSP, being composed by high amorphous silica content."

Has been replaced by:

"However, R15 exhibited a higher background intensity, which could be related to a higher CSP wt.% in the sample since CSP contains a high amorphous silica content from glass cullet (~84 wt.% in CSP) as stated in the literature and checked using XRF (Table 1) and XRD (Figure 2) [28]."

Line 409. * What does the authors mean by chemical composition? Again, this kind of affirmations are quite complicated to believe using exclusively XRD.

We agree that is not possible to identify the chemical composition of a sample based on XRD alone. We would like to underline the authors referred to chemical combination, not chemical composition. After 1 year of curing, the authors expected the products of the possible reaction between CSP and matrix to be crystalline due to the large period of curing. Potential products of this reaction could be in amorphous structure due to the incompletion of the possible reaction or be below the intensity limit of detection of XRD technique as it is mentioned later in the manuscript, in both cases undetectable under our XRD results. For these reasons, the authors were very careful when writing this part and added *"in terms of XRD"* at the end of the sentence. Nonetheless, we thought the sentence could be improved for a better understanding. To strengthen our point, the sentence:

"This presumes that it does not seem to exist chemical combination between the filler and K-struvite matrix in terms of XRD."

Has been replaced by:

"Thus, it cannot be confirmed the existence of a chemical combination of the filler and the K-struvite matrix from the XRD results shown in Figure 4."

Thank you very much for bringing up this issue.

Line 410. * DTG.

Thank you very much. *"TGA-SDT"* has been replaced by *"TG/DTG"* throughout the manuscript, figures and tables.

Line 423. * Which are the standar deviation in these values? Were the samples run by triplicated?

Yes, samples were run by triplicated. Standard deviation of the calculated values has been added to the manuscript. The sentences:

"It was found to be 53.46 wt.% of the total micromortar mass in R11-365d and 47.37 wt.% in R15-365d."

"CSP real percentage in R15-365d was calculated by comparing R11-365d and R15-365d mass loss at 30-270 °C and resulting to be 11.70 wt.% of the total micromortar mass."

Have been respectively replaced by:

"It was found to represent 53.46 ± 0.19 wt.% of the total micromortar mass in R11-365d and 47.37 ± 0.33 wt.% in R15-365d."

"The CSP percentage in R15-365d was calculated by comparing the mass losses of R11-365d and R15-365d at 30–270 °C was determined to be 11.70 ± 0.53 wt.% of the total micromortar mass."

Line 425. * SEM or BSEM?

The Scanning Electron Microscope characterization of the samples was performed using backscattered electrons image microscopy, also EDX mapping was conducted in backscattering mode. The authors think the use of SEM is correct in the manuscript although to further specify

the characteristics of the technique used, the use of "*SEM*" has been replaced with "*BSEM*" throughout the manuscript. Thank you for the suggestion.

Line 425. * Elemental mappings are usually taken in polished samples in the BSEM mode. EDX analysis in SEM is not representative and cannot be consider as a quantitative analysis.

We agree in this subject. The elemental mappings in the investigation were taken in BSEM mode. Although EDX analysis is not a quantitative analysis the authors consider it as a semi-quantitative analysis and can be used to see the distribution of elements among the sample surface. The strict quantification of elements using BSEM or EDX mapping is never stated in the manuscript.

We modified "mapping" in this sentence which has been replaced by "elemental mapping"

Thank you, we hope we have correctly addressed this issue.

Line 428. * Are you sure of this? Have you measured the shrinkage? Chemically bonds cements usually show thermally induced stresses caused by the exothermic acid-base setting reactions and successive the shrinkage.

Thank you for the comment. No, we have not measured shrinkage in this particular investigation but we agree that the exothermic acid-base setting reactions and shrinkage caused by water evaporation can induce microcracks in the micromortar matrix. Compressive strength test induced stresses help the propagation of such microcracks through the micromomortar structure. In order to further specify this subject, the sentence:

"The high degree of microcracking in the sample can be easily detected indicating an elevated level of stress which was endured during compressive strength test [47]."

Has been replaced by:

"The high degree of microcracking in the sample was induced by exothermic acid-base setting reactions, and shrinkage caused by water evaporation. This added an elevated level of stress endured during the compressive strength test, contributing to the propagation of microcracks [48]."

Line 432 *. I do not follow this sentence.

We are sorry for this inconvenience, we also think the writing in this segment can be improved. I order to make this sentence easier to follow, the sentence:

"Using XRD crystalline phase analysis, TG/DTG results and observing the relative intensity between EDS chemical elemental peaks [44,45,48] showed in Fig. 6, sharp particles such as dolomite, calcite, magnesite could be situated in the K-struvite sust-MPC micromortar matrix between other minor compounds such as sulphates [40]."

Has been replaced by:

"In a previous study, sharp shaped particles consisting of dolomite, calcite, and magnesite were observed between other minor particles such as sulphates in the K-struvite matrix [41]. This is in contrast with the XRD, TG/DTG, and EDS elemental mapping results shown in Fig. 6 [42,46,49]."

TABLE 1. * What is the difference between R7 and R15? Apparently both have the same %CSP content and the same w/c ratio…

There is no difference at all, R7 and R15 are duplicates of the same formulation. This subject is addressed in the answer to the comment in line 267. Some of the runs are exactly the same formulation. This is because, in Design of Experiments modelling, some formulations are duplicated, triplicated or quadruplicated near the zone where it is thought to statistically find the optimal formulation before proceeding with the experimental, reducing the results (responses) deviation of the hypothetical optimal formulation. We hope we have clarified this issue.

TABLE 1. * Explain better how the predicted value is calculated…

Thank you for the suggestion. The predicted values were calculated by using the equations obtained after statistical study of ANOVA. On this manner, with the help of the Design of Experiments software and the obtained equations the predicted responses were obtained. In order to explain this feature better, the sentence :

"Predicted values were calculated using the equations obtained after statistical analysis of ANOVA. In this manner, with the help of the design of experiments software and the obtained equations, the predicted responses were obtained as described in the following sections."

Has been added to the manuscript in section 3.2 Design of Experiments response

TABLE 3. * Please include the standar deviation (+-...).

We really appreciate this comment. Standard deviation is now included.

TABLE 4. * All the parameters have the same importance?

Yes, all the parameters were granted the same importance in order to optimize the micromortar. All the properties measured were equal maximized in the optimization process. This subject is also addressed in the answer to the comment in line 378. Thank you.

FIGURE CAPTIONS-FIG 5. * It would be easier to see the differences, if you plot in one graph the Weight loss of R11 and R 15 and in the other graph the DTG curves.

Thank you for your recommendation, we really appreciate it. Figure 5 has been modified to implement your suggestion, now DTG and TG curves are separated and R15-365d curves are overlapped with R11-365d curves.

FIGURE CAPTIONS-FIG 6. * Elemental mappings are usually taken in polished samples in the BSEM mode. EDX analysis in SEM is not representative and cannot be consider as a quantitative analysis.

As it is addressed previously, the authors consider EDX elemental mapping in BSEM as a semi-quantitative analysis and can be used to see the distribution of elements among the sample surface. The strict quantification of elements using BSEM or EDX mapping is never stated in the manuscript. Thank you very much, we hope we have solved this matter.

FIG 4. * The figures are too small to identify any differences...he legend is almost impossible to read.

Thank you for this comment. Figure 4 size has been incremented from small column size (90 mm width) to one and a half page width size (140 mm width). We hope the figure looks better now.

FIG 5. * Only the Weight loss and the Derivative of the weight curves are shown, so I would say that these are TG/DTG analysis.

The authors really appreciate this correction, thank you very much. *"TGA-SDT"* has been replaced by *"TG/DTG"* in the manuscript, figures and tables. Thank you again for all these helpful recommendations.

Fabrication of Sustainable Magnesium Phosphate Cement Micromortar using Design of Experiments Statistical Modelling: Valorization of Ceramic-Stone-Porcelain containing waste as filler

S. Huete-Hernández[a], A. Maldonado-Alameda[a], J. Giro-Paloma[a], J.M. Chimenos[a], J. Formosa[a*]

[a]Departament de Ciència de Materials i Química Física. Universitat de Barcelona, Martí i Franquès 1, 08028 Barcelona, Spain

*Author to who correspondence should be addressed. Telephone: +34934021316; Fax: +34934035438; E-mail: joanformosa@ub.edu. Departament de Ciència de Materials i Química Física. Universitat de Barcelona, Martí i Franquès 1, 08028 Barcelona, Spain.

Abstract

Magnesium phosphate cement (MPC) is a potential sustainable alternative to Portland cement. It is possible to lower the total CO_2 emissions related to MPC manufacturing by using by-products and wastes as raw materials. When by-products are used to develop MPC, the resultant binder can be referred to as sustainable magnesium phosphate cement (sust-MPC). This research incorporates ceramic, stone, and porcelain waste (CSP) as a filler in sust-MPC to obtain a micromortar. Sust-MPC is formulated with KH_2PO_4 and low-grade MgO (LG-MgO), a by-product composed of 40–60 wt.% MgO. CSP is the non-recyclable glass fraction generated by the glass recycling industry. The effect of water and CSP addition on the mechanical properties of sust-MPC was analyzed using design of experiments (DoE). A statistical model was obtained and validated by testing ideally formulated samples achieved through optimization of the DoE. The optimal formulation (15 wt.% of CSP and a water to cement ratio of 0.34) was realized by maximizing the compressive strength at 7 and 28 days of curing, resulting in values of 18 and 25 MPa respectively. After one year of curing, the micromortar was physico-chemically characterized in-depth using backscattered scanning electron microscopy (BSEM-EDS) and Fourier transform infrared-attenuated total reflectance spectroscopy (FTIR-ATR). The optimal formulation showed good integration of CSP particles in the

ceramic matrix. Thus, a potential reaction between silica and the K-struvite matrix may have occurred after one year of curing.

Keywords

B. Microstructure-final; C. Mechanical properties; D. MgO; E. Structural applications; Design of experiments.

_____

Abbreviations

MPC	Magnesium Phosphate Cement
LG	Low-Grade. Refers to a product containing impurities and of lower quality than the pure product
LG-MgO	Low-grade MgO. MgO containing impurities and of lower quality than pure MgO
Sust-MPC	Sustainable Magnesium Phosphate Cement
CSP	Ceramic, Stone, and Porcelain Waste
DoE	Design of Experiments
CBC	Chemically Bonded Ceramics
CBPC	Chemically Bonded Phosphate Cements
MKP	Monopotassium Phosphate
RSM	Response Surface Methodology
CSP(%)	Ceramic, Stone, and Porcelain Waste percentage in the micromortar
R1-16	Micromortar formulation from the corresponding design of experiments run
-7d, -28d, -365d	Number of days of curing before testing and characterization

_____

1. Introduction

In terms of pollution and greenhouse gas emissions, the construction and building industry sector faces an important challenge in the coming years since this sector is responsible for approximately 7–8% of total global CO_2 emissions [1,2]. This is because Portland cement is one of the most produced and widely applied construction materials worldwide owing to its various properties and low cost [3,4]. Also termed hydraulic cement, the production process for Portland cement consumes extremely high amounts of energy, depleting and overexploiting natural resources. However, in recent years, new types of alternative cements have emerged, presenting different and improved properties, extending their application range in diverse technology areas [5–7]. These properties can vary from mechanical attributes such as enhanced compressive strength (CS) [8] and porosity [9] to biocompatibility [10] and environmental sustainability [11]. Among the different types of alternative cements, chemically bonded ceramics (CBC) and, more specifically, chemically bonded phosphate cements (CBPCs), stand out as an early strength cement exhibiting rapid setting [12] and good volume stability [13]. An example of a CBPC is magnesium phosphate cement (MPC), in which magnesium oxide (MgO) is combined with monopotassium phosphate (MKP, KH_2PO_4) to form magnesium potassium phosphate ($MgKPO_4 \cdot 6H_2O$), also known as K-struvite owing to its crystalline structure (Eq. (1)) [14,15]. K-struvite is a type of CBPC that presents superior properties for high-performance cement applications [16].

$$MgO + KH_2PO_4 + 5H_2O \leftrightarrow MgKPO_4 \cdot 6H_2O \quad (1)$$

MPC possesses numerous advantageous properties such as a neutral pH due to an acid-base formation reaction, low water demand and drying shrinkage, and rapid development of the compressive strength [17]. MPC can be applied in cold weather because of the rapid and exothermic nature of its setting chemical reaction (Eq. (1)). It can be used as a repair material to restore roads damaged by traffic, and for the rehabilitation of various infrastructures among other applications [13,18,19]. MPC is primarily applied in the stabilization and solidification of low-level radioactive wastes containing reactive metals [20], with outstanding encapsulation properties from the point of view of waste management [21,22], and is also used in biomedical implants [12]. Despite the advantages of MPC mentioned above, the production of MgO in accordance with the Portland cement clinker production process generates excessive CO_2 emission and consumes vast quantities of energy due to the calcination of natural magnesite ($MgCO_3$) and dolomite

($MgCa(CO_3)_2$). Nevertheless, the MgO process generates much lower pollution than Portland cement clinker fabrication [23].

MgO production begins with sieving of $MgCO_3$ and $MgCa(CO_3)_2$ minerals and feeding these to a kiln for the calcination process. The low-grade MgO (LG-MgO) by-product is retained as powder cyclone dust in the filters of the air pollution control system during the combustion process. LG-MgO is composed of chemically reactive MgO (40–60 wt.%) produced from heavily calcined MgO. Owing to its reactive MgO component and economic cost, LG-MgO must be considered as a sustainable source of material in the MPC field. The feasibility of using LG-MgO to obtain MPC was demonstrated in previous studies with outstanding results obtained [24–26]. Considering the above, this material can be considered as sust-MPC; a green cement compared with common MPC. Unreacted particles such as carbonates and quartz are perceived as fine inorganic fillers inside the sust-MPC paste. Consequently, sust-MPC is considered to be a micromortar. Furthermore, the addition of inorganic fillers in sust-MPC micromortars improves the binder fresh mixture workability and reduces heat development and production costs [27]. The use of solid waste as an inorganic filler in sust-MPC micromortars opens up the possibility of solid waste treatment including residual non-profitable or recyclable materials. For instance, ceramic, stone, and porcelain waste (CSP) is the fraction removed from the glass cullet recycling process. The CSP fraction is considered as non-valuable waste because it is too small, possesses glued paper labels, or contains other diverse impurities. CSP is composed of approximately 84 wt.% soda-lime glass, 6 wt.% porcelain, 6 wt.% ceramic, and 4 wt.% stone, polymer/paper, metals, organic matter, and others [28]. Because CSP is derived from municipal and industrial waste, over time its composition becomes heterogeneous depending on the weather season, society consumption tendencies, and garbage dumping preferences. CSP is a major problem for glass cullet recycling companies because its melting point is higher than that of pure soda-lime glass, inhibiting the melting process and complicating glass recovery procedures. Nowadays, automated chromatic separators are employed to optically sort and classify clean and contaminated shattered glass. However, chromatic separators do not detect coarse glass fragments such as the bottom of bottles and bottlenecks darker in tone than ordinary shattered glass [29,30]. Moreover, recycling companies only accept glass cullet if the CSP concentration is between 20–100 $g \cdot t^{-1}$ or below [31]**.** Therefore, CSP is treated as a non-profitable material and is dumped in landfill sites.

The primary purpose of this investigation is to develop a sust-MPC micromortar using CSP as an inorganic filler and LG-MgO in place of pure MgO. In addition, the interaction between the CSP filler and the

micromortar K-struvite matrix is studied over time. This study is based on our previous experience in obtaining sust-MPC [24,25,32–34]. When CSP is utilized as a filler, the economic costs are reduced and environmental and sustainable criteria are enhanced. Design of experiments (DoE) was used to minimize the number of experiments carried out. The implementation of a factorial design model using DoE enables extraction of the maximum amount of information from the experiments performed. Predictive theoretical mathematical models are determined for each response, allowing estimation of the micromortar behavior and determination of an optimal and adequate formulation possessing the properties required in the range of the study.

2. Experimental procedure

2.1 Materials

LG-MgO by-product was supplied by Magnesitas Navarras, S.A., located in Navarra (Spain). This plant generates various industrial solid by-products including LG-MgO. These by-products are treated according to the dictates in the international and Spanish environmental and sustainability normative ISO 14000 embedded in UNE-EN ISO 14001:2015 and UNE-EN ISO 50001:2018.

The phosphate source was food-grade KH_2PO_4 with a purity of 99.8 wt.% obtained from Norken, S.L., and is commonly used as a fertilizer and is soluble in water.

CSP waste glass in the form of shattered solid fragments > 2 mm and with an average size range of 8–16 mm was provided by Daniel Rosas, S.A. This company is a recycling plant that treats glass cullet from urban and industrial garbage dump containers following the Spanish normatives UNE-EN ISO 9001:2015, UNE-EN ISO 14001:2015, and the European Commission Regulation (EU) Nº 1179/2012. A total of 24 kg CSP waste was quartered and homogenized to ensure a representative chemical composition. To increase the reactivity, paper, polymeric, and metallic fragments were removed from the CSP. The sample was shredded to a size below 2 mm, milled in an alumina ball mill, and sieved to a size below 80 μm.

In order to hydrate the raw materials, deionized water was employed to avoid chloride impurities, which are frequently present in tap water.

2.1.1 Raw materials characterization

Approximately 250 g representative sub-samples of LG-MgO and CSP were obtained by quartering each of the initial samples. MKP was not characterized since it is a commercial product and was previously

evaluated in-depth by our group [24–26,34]. LG-MgO and CSP were characterized using complementary techniques such as particle size distribution (PSD), X-ray fluorescence (XRF), X-ray diffraction (XRD), and thermogravimetric analysis with derivative thermogravimetry (TG/DTG). In addition, a citric acid test [35] was completed to evaluate the reactivity of LG-MgO. A pH meter was used as an alternative to visual evaluation using phenolphthalein. For the citric acid test, 2 g LG-MgO was continuously stirred (500 rpm min^{-1}) at 30 °C in 100 mL citric acid solution until a pH of 9 was achieved and the elapsed time was measured. The citric acid solution was prepared by stirring 28 g citric acid monohydrate in deionized water to obtain a 1 l solution. Samples were tested in triplicate.

XRD analysis was carried out using a PANalytical X'Pert PRO MPD Alpha1 powder diffractometer. XRF analysis was performed using a Philips PW2400 X-ray sequential spectrophotometer to elucidate the major and minor elements. To conduct TG/DTG analysis, a TA Instruments Q-600 SDT was used. Tests were conducted from 30 to 1400 °C at a heating rate of 10 °C·min^{-1} in a nitrogen atmosphere with a gas flow of 100 mL·min^{-1}.

2.2 Design of experiments

Design of experiments was implemented to reduce the number of experiments and to identify how the CSP filler phase influences the final properties of the sust-MPC micromortar. On the one hand, the apparent density (ρ), modulus of elasticity (MOE), flexural strength (FS), and compressive strength were evaluated at 7 days (d). In this study, the compressive strength was also evaluated at 28 d. On the other hand, design of experiments was employed to evaluate if the variables or factors (filler and water percentage) were synergistically correlated, affecting the final properties of the composite. Using this technique, it is possible to obtain a desired sust-MPC micromortar dosage by varying the factors under study to produce convenient mechanical and physical properties for the preferred application [36,37].

The LG-MgO/MKP ratio of the cement was fixed at 60/40 based on previous experience [34]. The CSP weight percentage (CSP(%)) and water-to-cement ratio (W/C) were the variables or factors studied in this investigation. The total quantity of cement (C) is a combination of both the masses of MKP and LG-MgO in the mixture. Hence, CSP is considered as a filler, although it may slightly react at the interface of K-struvite over a long period of time. The lowest and highest levels for W/C and CSP(%) were 0.34/0.38 and 0/15 wt.%, respectively. An increase in CSP present in the mixture requires additional water to adjust the workability, usually related to a non-desired decrease in the final mechanical properties of the product.

Therefore, the levels were determined after preliminary experiments to ensure proper workability of the fresh sust-MPC micromortar. The objective of the preliminary study was to introduce the highest amount of CSP possible while keeping W/C as low as possible.

The present study employs a response surface methodology (RSM) with a D-optimal and quadratic design to perform a further optimization process using previously obtained results. RSM includes analysis of a response surface plot calculated from statistical polynomic equations that are derived from the experimentally obtained results. One surface was plotted for each measured property (response) of the material studied. Design Expert® software was used for the design of experiments. The resulting mixtures are summarized in Table 1, where the lowest/highest level of each factor is highlighted in bold.

2.2.1 Design of experiments optimal formulation

The design of experiments analysis is based on analysis of variance (ANOVA) to predict an optimal response [36], using p-values to interpret the obtained results. The p-value represents the smallest level of significance that would lead to rejection of the null-hypothesis, indicating that the controllable factor does not affect the response under investigation. If the p-value in a test for the significance of a certain factor is smaller than 0.05, this factor is considered statistically significant with a confidence level above 95%.

The ratio model SS/residual SS (model SS and residual SS refer to the regression and error sum of squares, respectively) defines the F-value. A significant contribution is present in the case of large F-values, while small values indicate that the variance is affected by noise. CSP(%) and W/C were chosen as the factors, and their effects on the composite properties were quantified. The model should be validated to check its feasibility.

2.2.2 Sust-MPC micromortar preparation

The micromortar was mixed in a mortar planetary mixer. LG-MgO, KH_2PO_4, and CSP were added to the mixer summing a total solids mass of 3kg. The raw material mix was dry homogenized in the mixer. Subsequently, water was added and after 10 s the blend was mixed for 30 s in low revolution mode and 30 s in high revolution mode. Over the next 20 s, the unhydrated solid was removed using a spatula. Afterwards, the micromortar paste was mixed in high revolution mode for 60 s. The fresh micromortar was decanted into 40×40×160 mm^3 expanded polystyrene prismatic molds and vibrated for 10 s on a conventional vibratory table. Six prismatic samples of each formulation presented in Table 1 were obtained.

Casted samples were placed in a curing chamber at a constant temperature of 20 ± 2 °C and a relative humidity of 95% for 24 h. Subsequently, the samples were demolded and further curing was performed under the same conditions until testing (7 d and 28 d).

2.3 Test methods and structural characterization of the sust-MPC micromortar

The apparent density, modulus of elasticity, flexural strength, and compressive strength were measured after 7 d of curing for the six formulations in order to evaluate the results by means of design of experiments. The modulus of elasticity was estimated using an ultrasound test following the UNE-EN 12504-4 standard. An ultrasonic pulse velocity tester (C368 by Matest, 55 kHz transceiver sensors) was employed to perform the tests [38]. The obtained modulus of elasticity results were accepted assuming that the estimation of the Young's modulus was valid for homogeneous and isotropic media, even though sust-MPC micromortars do not always satisfy these conditions.

A compressive strength test was conducted for six split specimens obtained from the flexural strength test at 7 d, and the remaining parts of the six test specimens were further cured for 28 d before the compressive strength test. The test conditions followed UNE-EN 196-1 using an Incotecnic MULTI-R1 mechanical testing equipment, where the flexural strength test speed was 5 $kg \cdot s^{-1}$ and the compressive strength test speed was 240 $kg \cdot s^{-1}$. Subsequently, an optimal formulation was determined by analyzing the design of experiments results (see section 3.2.6). The optimal sust-MPC micromortar was compared with an ordinary sust-MPC without CSP filler as a reference, both after 365 d of curing. The samples cured for 365 d were the broken parts of the samples that were tested for compressive strength at 28 d. The obtained fragments were stored in the curing chamber for 365 d at a constant temperature of 20 ± 2 °C and a relative humidity of 50% to evaluate the potential reaction of the CSP glass phase with K-struvite [27,39,40]. This potential reaction between K-struvite and siliceous compounds was reported by various authors [27,39,40]. The evaluation was conducted using XRD, TG/DTG analysis, backscattered scanning electron microscopy (BSEM), and Fourier transformed infrared spectroscopy in attenuated total reflectance mode (FTIR-ATR). In addition, CSP was evaluated using FTIR-ATR and compared with the cured sust-MPC micromortar pieces. FTIR-ATR spectra of the samples were obtained using a Perkin Elmer Spectrum Two FTIR-ATR spectrometer. Both the XRD and TG/DTG measurements were conducted under the same conditions as the raw materials characterization.

In order to perform BSEM analysis to determine the chemical interaction between the filler and the cement matrix, a JSM-6510, JEOL Ltd., scanning electron microscope was used. Various representative broken fragments of the optimal sust-MPC micromortar and the ordinary sust-MPC without CSP were selected. Fragment samples were fixed on a carbon adhesive and coated with carbon to acquire BSEM images and to perform energy-dispersive scattering (EDS) analysis of the fracture surface. In addition, fragments of both formulations were impregnated in epoxy resin, surface polished, and carbon-coated to reveal the internal configuration of sust-MPC. BSEM images and EDS elemental mapping were conducted on the polished fragment samples and numerous EDS maps were collected. Each EDS map was acquired for 1800 s.

3. Results and discussion

3.1 Raw materials characterization

PSD analysis resulted in diameters of 1.666 μm (d_{10}), 12.410 μm (d_{50}), and 39.960 μm (d_{90}) for LG-MgO and 1.763 μm (d_{10}), 14.110 μm (d_{50}), and 40.200 μm (d_{90}) for CSP. The chemical composition of the by-products was determined by XRF. Table 2 shows the most stable oxide of each corresponding element, where magnesium was the predominant element in the case of LG-MgO, with an average MgO content of 61.7 wt.%. Calcium was the second most abundant element with a CaO content of 9.32 wt.%. Sulfur detected in the sample is attributed to the petroleum coke used as combustible material the for calcination of natural magnesite, as previously reported by Formosa et al. [41]. In contrast, the XRF results for CSP waste shown in Table 2 indicate high Si elemental concentrations (70.78 wt.% of SiO_2) followed by Na (11.15 wt.% of Na_2O), Ca (9.37 wt.% of CaO), and Al (4.81 wt.% of Al_2O_3). The presence of Si, Ca, and Na is related to the high content of soda-lime glass in CSP waste, while Al is associated with aluminosilicates present in the ceramic waste.

XRD spectra of LG-MgO and CSP are shown in Fig. 1. The presence of glass cullet and ceramic shards in CSP is demonstrated in Fig. 1.a, where quartz (SiO_2, PDF# 01-085-0457) and mullite ($Al_{4.52}Si_{1.48}O_{9.74}$, PDF# 01-079-1457) were found to be the primary crystalline phases. The spectra also indicated the presence of an amorphous phase related to amorphous silica in glass. The primary crystalline phases of LG-MgO were periclase (MgO, PDF# 01-071-1176), brucite ($Mg(OH)_2$, PDF# 01-083-0114), magnesite ($MgCO_3$, PDF# 01-078-2442), dolomite ($CaMg(CO_3)_2$, PDF# 01-084-1208), calcite ($CaCO_3$, PDF# 01-086-0174), and anhydrite ($CaSO_4$, PDF# 00-037-1496) as well as other minor phases (Fig. 1.b). Other impurities, such

as iron oxide or silica were also present. The thermal decomposition of LG-MgO in a nitrogen atmosphere is shown in Fig. 2. In the case of CSP, the TG/DTG analysis (not shown) registered a total mass loss of 1.214 wt.% when heated from 30 to 1400 °C without any clear decomposition. TG/DTG analysis for LG-MgO indicated mass losses attributed to the crystallization of water (from 30 to 210 °C) [42], $Mg(OH)_2$ decomposition resulting in MgO (from 210 to 440 °C), $MgCO_3$ decarbonation producing MgO and CO_2 products (from 440 to 660 °C), $CaMg(CO_3)_2$ decarbonation to MgO, CaO, and CO_2 (from 660 to 740 °C), $CaCO_3$ decarbonation to CaO and CO_2 (from 740 to 1030 °C), and desulfurization of $MgSO_4$ (from 1030 to 1190 °C), and $CaSO_4$ (from 1190 to 1400 °C) [43]. The TG/DTG analysis results in combination with XRF and XRD results were used to estimate the actual chemical composition of the by-product. First, TG/DTG results were used to estimate the percentage of compounds that thermally decomposed up to 1400 °C by stoichiometric calculation. Second, the remaining composition was calculated using the XRF compositional results considering the outstanding wt.% to estimate. XRD results were used to identify the chemical compounds that thermally decomposed during TG/DTG. The results of the estimation are shown in Table 3, where the MgO total content in LG-MgO was determined to be 43.58 wt.%. Considering that $Mg(OH)_2$ (3.77 wt.%) and $MgSO_4$ (2.12 wt.%) are soluble in water, unlike carbonate, the total calculated content of available reactive magnesium compounds in the unhydrated by-product was 49.47 wt.%.

The reactivity of MgO was assessed using the citric acid test, where neutralization values under 60 s are specific for highly reactive samples, also known as soft-burnt MgO. Values between 180 and 300 s are defined as medium-reactive MgO, while low reactivity MgO is known as hard-burnt, giving values of approximately 600 s. Finally, values over 900 s are observed for dead-burned MgO [35]. The LG-MgO citric acid test resulted in neutralization at 1128 s. Therefore, the obtained reactivity of LG-MgO is suitable to develop K-struvite and no pre-calcination processes are required [44]. Therefore, the use of LG-MgO by-products in place of pure MgO reduces the cost and enhances the environmental and sustainable criteria.

3.2 Design of experiments response

The LG-MgO/KH_2PO_4 ratio presented in Table 1 was fixed at 60/40 based on the weight [24–26,43]. The formulations (runs, i.e., R15 for run number 15) and a summary of the main experimental and predicted design of experiments results of the study are described in Table 1. Predicted values were calculated using the equations obtained after statistical analysis of ANOVA. In this manner, with the help of the design of experiments software and the obtained equations, the predicted responses were obtained as described in the

following sections. The models developed using the experimental responses exhibited p-values below 0.0001, implying that the proposed models are significant considering the factor relations presented for each response or equation. The best model equations for fitting the experimental results are as follows: density at 7 d (two factors with interaction), modulus of elasticity at 7 d (linear), flexural strength at 7 d (linear), compressive strength at 7 d (reduced cubic), and compressive strength at 28 d (reduced quadratic). An in-depth discussion of the proposed models for each response under study is presented in the following sections.

3.2.1 Apparent density

The best model for fitting the experimental values of the apparent density response is shown in Eq. (2). The model presented a low standard deviation and a high R-squared (R^2) value: 0.01 and 0.87, respectively. The mathematical model described in Eq. (2) is represented in Fig. 3.a. Both factors under study (W/C and CSP(%)) have a significant effect (p-value = 0.0002 and < 0.0001, respectively) on the response of the apparent density. According to the results, by increasing the W/C ratio, the apparent density decreases. The increase in CSP(%) leads to an apparent increase in the density response. Considering the slope of each response, the effect of CSP(%) is higher than that of the W/C ratio in the range of study. When the combined effect of both factors (W/C ratio and CSP(%)) is considered, the response is minor compared with the sum of each individual response. Therefore, a significant negative interaction occurs between both factors (p-value = 0.0196), explaining this result. The negative interaction between CSP(%) and the W/C ratio can be understood by the last term in Eq. (2), where the higher the term, the lower the response. The higher the CSP(%), the higher the apparent density, and simultaneously, the lower the W/C ratio, the higher the apparent density.

$$\rho\ (\mathrm{g \cdot cm^{-3}}) = 1.888 - 0.288 \cdot (W/C) + 0.028 \cdot (CSP) - 0.070 \cdot (W/C) \cdot (CSP) \qquad (2)$$

As shown in Fig. 3.a, the blue and red zones correspond to the lowest and highest apparent density values, respectively.

3.2.2 Modulus of elasticity

The model presented a low standard deviation and a high R^2 value: 0.48 and 0.90, respectively. A response surface linear model was developed for the modulus of elasticity at 7 d using the experimental data. The modulus of elasticity surface plot is presented in Fig. 3.b, and the corresponding mathematical expression

is presented in Eq. (3) The highest modulus of elasticity values are obtained as CSP(%) (p-value < 0.0001) increases and the W/C ratio (p-value < 0.0001) decreases. Hence, the modulus of elasticity model exhibits high values, similar to the apparent density. On the contrary, the modulus of elasticity model is more susceptible to the W/C ratio than the CSP(%).

The modulus of elasticity and apparent density are related to the porosity of the samples. Therefore, both responses present similar behavior, as shown in Fig. 3.a and 3.b. The higher the W/C ratio, the higher the porosity and consequently the lower the modulus of elasticity and mechanical properties such as flexural strength and compressive strength [45]. The mathematical approach for the density surface plot is presented in Eq. (3).

$$MOE\ (\text{GPa}) = 34.993 - 66.071\cdot(W/C) + 0.109\cdot(CSP) \quad (3)$$

As shown in Fig. 3.b the blue and red zones correspond to the lowest and highest modulus of elasticity values, respectively. CSP and W/C factors are significant, however, no interaction between both factors was perceived in the range under study for the modulus of elasticity results.

3.2.3 Flexural strength

The surface plot of the flexural strength at 7 d is shown in Fig. 3.c, obtained using Eq. (4). The developed model presented a low standard deviation (0.22) and a high R^2 value (0.84). The model is a linear model in which both factors significantly affect the response in the range under study. The flexural strength at 7 d is augmented as the W/C ratio (p-value < 0.0001) decreases, while CSP(%) (p-value = 0.0033) increases. It must be noted that the flexural strength is more sensitive to the W/C ratio variation than CSP(%) in the micromortar as noted in section 3.2.2. Once again, this performance in terms of both the modulus of elasticity and the flexural strength is associated with the formation of pores. The porosity induced by the increase of the W/C ratio severely affects the flexural performance. This effect had a lower impact on the compressive strength because cavities in the micromortar tend to close during the compressive test, whereas during the flexural test, those cavities tend to open owing to the direction of the internal stresses in the material.

$$FS\ (\text{MPa}) = 12.153 - 25.553\cdot(W/C) + 0.033\cdot(CSP) \quad (4)$$

As shown in Fig. 3.c, the blue and red zones correspond to the lowest and highest flexural strength values, respectively.

3.2.4 Compressive strength at 7 d

The statistical model for the compressive strength at 7 d (CS-7d) is presented in Fig. 3.d and Eq. (5). The model exhibited a low standard deviation of 0.23, and an exemplary R^2 value of 0.97, indicating that it was suitably fitted to the experimental data. The proposed model is a reduced cubic model, in which the evaluated factors significantly affect the response as follows: W/C ratio (p-value < 0.0001), CSP(%) (p-value = 0.0024), (W/C)·(CSP) (p-value = 0.0836), $(W/C)^2$ (p-value = 0.0061), $(CSP)^2$ (p-value = 0.0227), and $(CSP)^3$ (p-value = 0.0055).

$$CS\text{-}7d\ (\text{MPa}) = 512.470 - 2660.140\cdot(W/C) - 0.719\cdot(CSP) - 2.849\cdot(W/C)\cdot(CSP) + 3529.782\cdot(W/C)^2 + 0.329\cdot(CSP)^2 - 0.014\cdot(CSP)^3 \quad (5)$$

As shown in Fig. 3.d, the blue and red zones correspond to the lowest and highest CS-7d values, respectively. On the one hand, the lowest values (see Fig. 3.d blue zone) were obtained at low CSP(%) and high W/C ratios. This is attributed to the necessity to increase W/C when CSP was added to improve the workability in the fresh state. On the other hand, the highest values (see Fig. 3.d red zone) were obtained at high CSP(%) and low W/C ratios. This behavior is attributed to the effect of the filler in a cement matrix, present as long as the W/C ratio is above the stoichiometric amount of water that the cement requires. In other words, as a result of the preliminary work to obtain the range of study, we conclude that the minimum W/C ratio required for acceptable workability is 0.34. Inside the micromortar, during the compressive strength test, the stress transfer mechanism facilitates the closing of pores and cavities and reduces the speed of crack propagation [33]. As observed in Eq. (5), a negative interaction occurs between both factors. This interaction can be observed by following the line generated when both factors increased together (see Fig. 3.d green zone). Quadratic and cubic terms were used for improved model fitting, as can be seen by the tendency to generate curves instead of lines at the edges of the plotted response surface, see Fig. 3.d. In general, it is assumed that the higher the CSP(%), the higher the CS-7d.

3.2.5 Compressive strength at 28 d

The model for the compressive strength at 28 d (CS-28d) showed a low standard deviation (1.00) and a high R^2 value (0.96). Therefore, the model suitably fitted the experimental results obtained for CS-28d. A reduced quadratic model was fitted, as shown in Eq. (6) and presented in Fig. 3.e.

$$CS\text{-}28d\ (\text{MPa}) = 64.125 - 134.430\cdot(W/C) + 1.759\cdot(CSP) - 5.863\cdot(W/C)\cdot(CSP) + 0.047\cdot(CSP)^2 \quad (6)$$

The model terms presented p-values as follows: W/C < 0.0001, CSP < 0.0001, (W/C)·(CSP) = 0.0296, and $(CSP)^2$ = 0.0008. As shown in Fig. 3.e, the blue and red zones correspond to the lowest and highest CS-28d values, respectively. A significant negative interaction occurs between both factors, depicted by a change in the tendency or a valley (green zone in Fig. 3.e) when both factors increased together. The effect is lower than that expected from the sum of each individual factor. As expected, an increase in the W/C ratio leads to a decrease in CS-28d, depicted by a negative slope considering the W/C axis in Fig. 3.e. However, when CSP(%) is considered, a minimum region is observed at approximately the middle of this axis (i.e. lower and higher CSP(%) lead to higher CS-28d in the range under study). Thus, the maximum CS-28d (red zone in Fig. 3.e) is obtained when CSP(%) and the W/C ratio are the maximum and minimum, respectively. On the contrary, when CSP(%) is minimized and the W/C ratio maximized, the CS-28d value is minimized (blue region in Fig. 3.e). CSP(%) above 15 leads to an increase in CS-28d, although this value is outside the range of study and requires further study. In this case, a new range for the W/C ratio should be considered because of the lack of workability when CSP is added. In future studies, additives such as borax or sodium hexametaphosphate may be used to improve the fresh state of these mixtures.

3.2.6 Optimal formulation and validation procedure

By using the statistical models presented above, it was possible to optimize the formulation by selecting the desired responses. As mentioned above, the primary aim of this study was to increase the compressive strength as much as possible in the development of sust-MPC using CSP as a filler within the range of study. The optimization idea involved the concept of reaching a compromise between values. Table 4 shows the criteria used in the optimization process, where the lower and upper limits were the best and worst values obtained from the tests performed (i.e., experimental values). Compressive strength was treated as the most important property because it is the key aspect to consider in building materials. Therefore, CS-7d and CS-28d were maximized in the optimization process. Nonetheless, the apparent density, modulus of elasticity, and flexural strength were within the range limits. In this study, the importance of each parameter was fixed at 3, where the importance could be ranged from 1 to 5 (i.e., responses possessed the same importance). Once the desired response values, factors range, and level of importance were selected, two optimal formulations were obtained. The optimal formulation is indicated in Table 4, along with its predicted properties as well as the desirability. The optimal formulation coincided with R15 and R7 in terms of the W/C ratio and CSP (0.34 W/C and 15.00 wt.% CSP, see Table 1). The model was validated by

comparing the estimated values (see Table 4) with the experimental results obtained for R7 and R15 (see Table 1).

3.3 Micromortar structural characterization

To evaluate the formation of new mineral phases, R15 (0.34 W/C and 15.00 wt.% CSP) was considered as the optimal formulation and compared to R11 as a reference or blank (0.35 W/C and 0.00 wt.% CSP), i.e., without CSP and a lower W/C ratio. The broken fragments obtained after the CS-28d test for R15 and R11 were used to perform the sust-MPC micromortar characterization after 365 d of curing (20 ± 2 °C, relative humidity of 50%). The samples were analyzed using XRD and TG/DTG (under the same conditions as the raw materials), BSEM combined with EDS chemical microanalysis, and FTIR-ATR to provide information on the microstructure and to determine whether CSP interacted with the MPC matrix in the sust-MPC micromortar.

Several authors have reported the feasibility of a potential reaction when MPC matrices are used with fly ash [27]. These authors suggested that the reaction is complete after a period greater than 28 d. This research shows BSEM images of R15-365d since they are related to the potential reaction of the MPC matrix with the CSP filler.

The XRD patterns (Fig. 4) of both the optimal sust-MPC micromortar and the MPC reference samples showed K-struvite ($KMgPO_4 \cdot 6H_2O$, PDF# 01-075-1076) as the major crystalline phase. Other phases such as unreacted periclase, dolomite, magnesite, and quartz were also detected. Stable phases within LG-MgO did not react and remained unaltered. Only K-struvite was found as the magnesium phosphate phase formed, and neither bobierrite ($Mg_3(PO_4)_2 \cdot 8H_2O$) nor newberyite ($MgHPO_4 \cdot 3H_2O$) were identified in the micromortar. It must be noted that calcite was expected in the pattern, however, the calcite peaks may overlap with those of magnesite and dolomite. Regarding possible interactions between CSP particles and the matrix, no differences were observed in terms of 2θ peak positions between the optimal and reference sample spectra. However, R15 exhibited a higher background intensity, which could be related to a higher CSP wt.% in the sample since CSP contains a high amorphous silica content from glass cullet (~84 wt.% in CSP) as stated in the literature and checked using XRF (Table 1) and XRD (Figure 2) [28]. Thus, it cannot be confirmed the existence of a chemical combination of the filler and the K-struvite matrix from the XRD results shown in Figure 4.

The TG/DTG characterization of the micromortar at 365 d is shown in Fig. 5. Fig. 5.a shows a higher total mass loss for R11-365d compared to R15-365d, as a result of the reduction of K-struvite due to filler substitution. TG/DTG results for both R11-365d and R15-365d exhibited identical mass losses and temperature decomposition ranges. To characterize the mass losses of the micromortar, TG/DTG was analyzed considering the previously obtained XRD results. The mass loss between 30–270 °C was assigned to the loss of H_2O from K-struvite, and the mass loss between 270–450 °C was assigned to H_2O loss due to magnesium hydroxide decomposition. The losses between 450–600 °C, 600–700 °C, and 700–1000 °C were assigned to CO_2 loss from magnesite, dolomite, and calcite decomposition, respectively, because of the inert carbonate phases in LG-MgO [42,46]. K-struvite, the main crystalline phase in the micromortar, was quantified using TG/DTG. It was found to represent 53.46 ± 0.19 wt.% of the total micromortar mass in R11-365d and 47.37 ± 0.33 wt.% in R15-365d. These results were in accordance with those obtained in the literature, taking into account that LG-MgO consisted of approximately 44 wt.% reactive MgO [42,46,47]. The CSP percentage in R15-365d was calculated by comparing the mass losses of R11-365d and R15-365d at 30–270 °C was determined to be 11.70 ± 0.53 wt.% of the total micromortar mass. It should be noted that the total micromortar mass includes water mass, a small part of which is lost during mixing.

BSEM, and EDS elemental mapping analysis images of R15-365d are shown in Fig. 6. The micrograph in Fig. 6.a shows the appearance of the inner structure of the micromortar composed of CSP filler and unreacted LG-MgO particles embedded in a K-struvite matrix. The high degree of microcracking in the sample was induced by exothermic acid-base setting reactions, and shrinkage caused by water evaporation. This added an elevated level of stress endured during the compressive strength test, contributing to the propagation of microcracks [48]. Filler particles are randomly distributed through the micromortar matrix, providing and enhancing the mechanical properties of the composite. In a previous study, sharp shaped particles consisting of dolomite, calcite, and magnesite were observed between other minor particles such as sulphates in the K-struvite matrix [41]. This is in contrast with the XRD, TG/DTG, and EDS elemental mapping results shown in Fig. 6 [42,46,49]. Unreacted MgO particles and soda-lime glass from CSP were incorporated in the matrix. A number of iron oxide particles coming from LG-MgO, confirmed by XRD, were also detected by EDS. Unreacted particles can also be considered as filler particles in addition to CSP waste filler. Therefore, sust-MPC can be conceived as a micromortar. It was possible to trace the path of the K-struvite reaction in the micromortar matrix, culminating in partially reacted MgO particles embedded

in the matrix. The reaction begins on the outside of the particle and advances toward the center of the particle but does not reach its core. Moreover, prismatic K-struvite crystals were observed in the fracture surface of the micromortar [50]. The optimal formulation samples were polished for exhaustive EDS mapping analysis. Fig. 6.a and b show the elemental distribution and location of the primary elements. In order to discern the CSP filler particles in the sust-MPC micromortar matrix, a random zone was subjected to elemental mapping. The primary aim was to observe the most interesting filler particles. S (from sulphates), Mg, P, and K (from K-struvite), Ca (from calcium carbonate and CSP soda-lime glass particles), Na (from CSP soda-lime glass particles), Fe (from ferrous particles), Al (from CSP phases), and Si (from CSP particles) were observed. A magnified zone of interest was subsequently analyzed. This zone contained a soda-lime CSP particle surrounded by and incorporated into the matrix. This particle was observed in detail, showing an unknown interaction with the K-struvite matrix inside the zone indicated in Fig. 6.b. As observed, a region of the particle outer layer reacted with the matrix and was integrated. Elemental mapping shown in Fig. 6.b reinforces this idea. The Si signal overlapped with that of Mg, P, and K. This was most likely because the elemental signal covers a certain volumetric area of the sample. The upper edge of the CPS particle (Fig. 6.b) seems to have interacted with the matrix. In order to determine if chemical reactions occurred, FTIR-ATR was employed. Fig. 7 shows the infrared spectra of CSP, R15-365d and R11-365d. The lack of sharp peaks in the CSP spectrum is related to the disordered silicate network [51]. Both micromortar spectra presented identical profiles, similar to analogous materials [52–54]. The most important peak is located at approximately 1000 cm^{-1}. Fig. 8.b, c, and d show the three deconvoluted spectra (R15-365d, CSP, and R11-365d) between 1400 and 700 cm^{-1}. In this range it is possible to observe the primary vibrations of the phosphate group [53], the same region where Si–O stretching occurs [51]. Fig. 8.a shows a broad band for CSP at approximately 1000 cm^{-1} compared with the spectra for R15-365d and R11-365d. The curves were fitted using a Gaussian function, minimizing the number of curves, and obtaining a regression coefficient, R^2, above 0.999 [55]. In each case, the obtained R^2 value was 0.9997; hence, the curves were suitably fitted. Deconvolution of the CSP peak (Fig. 8.c) revealed two primary bands at 1025 and 928 cm^{-1} that are assigned to the Si–O asymmetric stretching modes of bridging and non-bridging oxygen, respectively [51]. The bands between 1300–800 cm^{-1} are related to the stretching vibrations of SiO_4 tetrahedron depending on the number of shared oxygens [51]. Bands at 788 and 758 cm^{-1} are assigned to the bending vibration of Si–O–Si at 784 cm^{-1} [56] and the Al-O vibration modes due to the

tetrahedral AlO_4 group [57], respectively. Finally, the deconvoluted broad band at 1158 cm^{-1} is assigned to the Si–O–Al asymmetric stretching vibration [57].

The deconvoluted spectra for R15-365d and R11-365d (Fig. 8.b and d) showed that the bands from 923 to 741 cm^{-1} were present in both spectra. Because of the presence of unreacted carbonate phases from the LG-MgO raw material, a number of bands attributed to the CO_3^{2-} group were observed (most likely due to the presence of magnesite or even dolomite): asymmetrical stretching vibration of O–C–O at approximately 1450 cm^{-1} (see Fig. 7) as well as bands at 880–879 cm^{-1} and 742–741 cm^{-1} as shown in Fig. 8.b and d, assigned to out-of-plane and in-plane bending vibrations, respectively [58]. The deconvoluted band at 792 cm^{-1} was observed in both samples (Fig. 8.b and d) and is assigned to quartz owing to the presence of this phase in the LG-MgO raw material and in both R11-365d and R15-365d (see Fig. 1 and 3.b). Considering the deconvoluted bands for R11-365d, these bands were in accordance with those observed by other authors [53,59]. Indeed, the bands at 1102, 1047, 997, and 923 cm^{-1} were assigned to P–O stretching similar to the reported bands at 1095–1105, 1054–1075, 978–978, and 916–951 cm^{-1} [53,59]. In the case of R15-365d (see Fig. 8.b), the deconvoluted bands differed to R11-365d. Specifically, the bands at 1119 and 1023 cm^{-1} are related to the potential substitution of P in the SiO_4 tetrahedron present in CSP or Si in the PO_4 tetrahedron present in the K-struvite matrix owing to the shift in both bands to higher frequencies. It was reported that the typical Si–O–P bands due to stretching vibrations appear at approximately 1150–1100 and 1000 cm^{-1} [60]. This assumption is related to the BSEM evaluation. However, this must not be considered absolutely certain because of the similar wavenumber range at which the peaks for SiO_4^{4-} and PO_4^{3-} groups appear, as a result of their tetrahedral structure [61].

The XRD results agreed with the BSEM and EDS analyses, with K-struvite the main component in the micromortar matrix. This was also supported and quantified by the TG/DTG results. Other crystalline compounds observed in the XRD analysis were identified in the BSEM images by EDS. Iron oxide was observed in the XRF results for the LG-MgO sample and was also present in the form of small particles in the micromortar matrix as determined from the BSEM and EDS results. CSP particles were remarkably embedded in the matrix, as observed in the BSEM images. The magnified image in Fig. 6.b shows an intermediate zone between the matrix and the particle, where color degradation and evident blending of the particle-matrix contour are indicated. The mapping results of this zone allow determination of the degree of reaction between the filler and the matrix despite the XRD results indicating that no new crystalline phases were formed by comparing the R11-365d and R15-365d micromortar diffraction spectra. TG/DTG

analysis also did not show any evidence of a new compound formed in addition to K-struvite. Considering the TG/DTG, XRD, and EDS mapping results, we conclude that the reaction degree was low, and thus in the hypothetical case of the reaction between the filler and the matrix, either i) the percentage of the new silicophosphate compound was small (less than 1 wt.%) or ii) the new compound was present in an amorphous state also with a small wt.%. Analyzing the FTIR-ATR spectra of the samples cured at 365 d revealed slight deviations in the deconvoluted peak frequencies that may indicate the potential substitution of P in the SiO_4 tetrahedron of CSP or Si in the PO_4 tetrahedron of the K-struvite matrix. With this substitution, CSP particles should be partially merged with the matrix, as observed in the BSEM images. More evidence is required to determine the type of compound and its possible formation during the reaction between CSP glass waste filler and the matrix.

4. Conclusions

It is plausible to formulate a sust-MPC micromortar mixed with inorganic glass waste (CSP) as a filler that enhances the mechanical properties. This is termed sust-MPC micromortar when formulated with LG-MgO because of its sustainability characteristics. CSP is an inorganic solid waste from industrial and urban glass residues. The primary idea behind the development of a sust-MPC micromortar using CSP was not only to enhance the mechanical properties but also to reduce the environmental impact. Revalorization of both residue sources was achieved, thereby lowering the price of the final product, promoting a circular economy, and reducing CO_2 emissions due to the reduced amount of magnesia product inherent in the use of LG-MgO. Therefore, a sust-MPC micromortar was successfully developed using CSP to improve the properties of MPC, as expected.

The statistical models generated based on the design of experiments performed successfully. The results were validated, fitted with the desired requirements, and displayed remarkable accuracy regarding the property responses of each of the possible formulations within the studied W/C and CSP wt.% factor ranges. This set of models was based on more than one variable and allows estimation of the properties of possible formulations and improvements in the entire system. Moreover, the models enable determination of an optimal formulation with a compromise required between properties in order to achieve maximum performance according to the criteria. They also allow evaluation of the synergetic effect of variables or factors between them. An optimal formulation was found achieved using the response surface methodology, and every design of experiments model generated was statistically significant.

The optimal formulation was designated the same formulation as that of R15 with a W/C ratio of 0.34 and a CSP content of 15 wt.%, reaching compressive strength values above 25 MPa. Regarding the synergetic interaction between the factors, CSP and W/C possessed a certain dependency on and synergetic interaction between each other.

After one year of curing, the optimal formulation and a reference sample without CSP were characterized in order to review their evolution over time. The optimal formulation exhibited excellent integration of CSP particles in the matrix. Although more evidence is required, a number of CSP particles in the sust-MPC micromortar matrix presented a certain degree of chemical reaction with the matrix as observed in elemental EDS mapping results and FTIR-ATR analysis, yet an uncertain observation.

Future research requires highly detailed structural and chemical characterization of the sust-MPC micromortar to acquire more evidence of the suspected chemical interaction between silica-rich soda-lime glass CSP particles and the K-struvite matrix.

Declaration of competing interest

The authors declare that they have no known competing financial interests or personal relationships that influenced the work reported in this paper.

Acknowledgements

The authors would like to thank Magnesitas Navarras S.A. for their cooperation in financing and supporting the work. We would also like to thank Daniel Rosas S.A. for supplying the CSP material. The authors are grateful to the Catalan government for the DIOPMA (2017 SGR 118) quality accreditation awarded to their research group. This work was supported by Magnesitas Navarras S.A. and the Spanish government (BIA2017-83912-C2-1-R). We would like to thank Mr. Eduard Cosialls in particular for aiding with the experiments. Mr. S. Huete-Hernández is grateful to the government of Catalonia and the University of Barcelona for the research grant (APIF-DGR 2018). Mr. Alex Maldonado-Alameda is grateful to the government of Catalonia for the research Grant (FI-DGR 2017). Dr. Jessica Giro-Paloma is a Serra Húnter Fellow.

References

[1] Z. He, X. Zhu, J. Wang, M. Mu, Y. Wang, Comparison of CO_2 emissions from OPC and recycled cement production, Constr. Build. Mater. 211 (2019) 965–973. doi:10.1016/j.conbuildmat.2019.03.289.

[2] R.M. Andrew, Global CO_2 emissions from cement production , 1928 – 2018, Earth Syst. Sci. Data. 11 (2019) 1675–1710. doi:10.5194/essd-11-1675-2019.

[3] J. Farfan, M. Fasihi, C. Breyer, Trends in the global cement industry and opportunities for long-term sustainable CCU potential for Power-to-X, J. Clean. Prod. 217 (2019) 821–835. doi:10.1016/j.jclepro.2019.01.226.

[4] T. Gao, L. Shen, M. Shen, L. Liu, F. Chen, Analysis of material flow and consumption in cement production process, J. Clean. Prod. 112 (2016) 553–565. doi:10.1016/j.jclepro.2015.08.054.

[5] C. Shi, A.F. Jiménez, A. Palomo, New cements for the 21st century: The pursuit of an alternative to Portland cement, Cem. Concr. Res. 41 (2011) 750–763. doi:10.1016/j.cemconres.2011.03.016.

[6] M.C.G. Juenger, F. Winnefeld, J.L. Provis, J.H. Ideker, Advances in alternative cementitious binders, Cem. Concr. Res. 41 (2011) 1232–1243. doi:10.1016/j.cemconres.2010.11.012.

[7] E. Gartner, T. Sui, Alternative cement clinkers, Cem. Concr. Res. 114 (2018) 27–39. doi:10.1016/j.cemconres.2017.02.002.

[8] N. Li, C. Shi, Z. Zhang, Understanding the roles of activators towards setting and hardening control of alkali-activated slag cement, Compos. Part B Eng. 171 (2019) 34–45. doi:10.1016/j.compositesb.2019.04.024.

[9] Y.H.M. Amran, N. Farzadnia, A.A.A. Ali, Properties and applications of foamed concrete; A review, Constr. Build. Mater. 101 (2015) 990–1005. doi:10.1016/j.conbuildmat.2015.10.112.

[10] M. Nabiyouni, T. Brückner, H. Zhou, U. Gbureck, S.B. Bhaduri, Magnesium-based bioceramics in orthopedic applications, Acta Biomater. 66 (2018) 23–43. doi:10.1016/j.actbio.2017.11.033.

[11] S. Luo, M. Liu, L. Yang, J. Chang, W. Yang, X. Yan, H. Yu, Y. Shen, Utilization of waste from alumina industry to produce sustainable cement-based materials, Constr. Build. Mater. 229 (2019) 116795. doi:10.1016/j.conbuildmat.2019.116795.

[12] G. Mestres, M.P. Ginebra, Novel magnesium phosphate cements with high early strength and antibacterial properties, Acta Biomater. 7 (2011) 1853–1861. doi:10.1016/j.actbio.2010.12.008.

[13] F. Qiao, C.K. Chau, Z. Li, Property evaluation of magnesium phosphate cement mortar as patch repair material, Constr. Build. Mater. 24 (2010) 695–700. doi:10.1016/j.conbuildmat.2009.10.039.

[14] A.S. Wagh, S.Y. Jeong, Chemically Bonded Phosphate Ceramics: I, A Dissolution Model of Formation, J. Am. Ceram. Soc. 86 (2003) 1838–1844. doi:10.1111/j.1151-2916.2003.tb03569.x.

[15] H. Lahalle, C.C.D. Coumes, A. Mesbah, D. Lambertin, C. Cannes, S. Delpech, S. Gauffinet, Investigation of magnesium phosphate cement hydration in diluted suspension and its retardation by boric acid, Cem. Concr. Res. 87 (2016) 77–86. doi:10.1016/j.cemconres.2016.04.010.

[16] A.S. Wagh, S.Y. Sayenko, A.N. Dovbnya, V.A. Shkuropatenko, R. V. Tarasov, A. V. Rybka, A.A. Zakharchenko, Durability and shielding performance of borated Ceramicrete coatings in beta and gamma radiation fields, J. Nucl. Mater. 462 (2015) 165–172. doi:10.1016/j.jnucmat.2015.03.049.

[17] A.S. Wagh, Chemically Bonded Phosphate Ceramics, First edit, Elsevier Science, Oxford, UK, 2004. doi:10.1016/B978-0-08-044505-2.X5000-5.

[18] N. Roghanian, N. Banthia, Development of a sustainable coating and repair material to prevent bio-corrosion in concrete sewer and waste-water pipes, Cem. Concr. Compos. 100 (2019) 99–107. doi:10.1016/j.cemconcomp.2019.03.026.

[19] X. Jia, J. Li, P. Wang, J. Qian, M. Tang, Preparation and mechanical properties of magnesium phosphate cement for rapid construction repair in ice and snow, Constr. Build. Mater. 229 (2019) 116927. doi:10.1016/j.conbuildmat.2019.116927.

[20] W. Montague, L. Vandeperre, M. Hayes, Processing Characteristics and Strength of Magnesium Phosphate Cement Formulations Compatible with UK Nuclear Waste Treatment Plants, MRS Proc. 1475 (2012) imrc11-1475-nw35-p03. doi:10.1557/opl.2012.588.

[21] Y. Tao, L. Zhenyu, R. Chunrong, W. Yuanyuan, H. Zhichao, H. Xin, W. Jie, L. Mengliang, D. Qiubai, K. Khan, L. Zhongyuan, L. Shuzhen, Study on solidification properties of chemically bonded phosphate ceramics for cesium radionuclides, Ceram. Int. 46 (2020) 14964–14971. doi:10.1016/j.ceramint.2020.03.025.

[22] A. Viani, A.F. Gualtieri, Preparation of magnesium phosphate cement by recycling the product of thermal transformation of asbestos containing wastes, Cem. Concr. Res. 58 (2014) 56–66. doi:10.1016/j.cemconres.2013.11.016.

[23] A.S. Wagh, Chapter 14: Chemically Bonded Phosphate Ceramic Matrix Compsites, in: Chem. Bond. Phosphate Ceram. Twenty-First Century Mater. With Divers. Appplications, First edit, Elsevier Ltd, Argonne, USA, 2004: pp. 157–176. doi:10.1016/B978-008044505-2/50018-1.

[24] M. Niubó, J. Formosa, A. Maldonado-Alameda, R. del Valle-Zermeño, J.M. Chimenos, Magnesium phosphate cement formulated with low grade magnesium oxide with controlled porosity and low thermal conductivity as a function of admixture, Ceram. Int. 42 (2016) 15049–15056. doi:10.1016/j.ceramint.2016.06.159.

[25] J. Formosa, A.M. Lacasta, A. Navarro, R. Del Valle-Zermeño, M. Niubó, J.R. Rosell, J.M. Chimenos, Magnesium Phosphate Cements formulated with a low-grade MgO by-product: Physico-mechanical and durability aspects, Constr. Build. Mater. 91 (2015) 150–157. doi:10.1016/j.conbuildmat.2015.05.071.

[26] M. Morales, J. Formosa, E. Xuriguera, M. Niubó, M. Segarra, J.M. Chimenos, Elastic modulus of a chemically bonded phosphate ceramic formulated with low-grade magnesium oxide determined by Nanoindentation, Ceram. Int. 41 (2015) 12137–12146. doi:10.1016/j.ceramint.2015.06.031.

[27] B. Xu, H. Ma, H. Shao, Z. Li, B. Lothenbach, Influence of fly ash on the compressive strength and micro-characteristics of magnesium potassium phosphate cement mortars, Cem. Concr. Res. 99 (2017) 86–94. doi:10.1016/j.cemconres.2017.05.008.

[28] J. Giro-Paloma, C. Barreneche, A. Maldonado-Alameda, M. Royo, J. Formosa, A.I. Fernández, J.M. Chimenos, Alkali-activated cements for TES materials in buildings' envelops formulated with glass cullet recyclingwaste and microencapsulated phase change materials, Materials (Basel). 12 (2019) 1–11. doi:10.3390/ma12132144.

[29] M. Ruth, P. Dell'Anno, An industrial ecology of the US glass industry, Resour. Policy. 23 (1997) 109–124. doi:10.1016/s0301-4207(97)00020-2.

[30] N. Dias, I. Garrinhas, A. Maximo, N. Belo, P. Roque, M.T. Carvalho, Recovery of glass from the inert fraction refused by MBT plants in a pilot plant, Waste Manag. 46 (2015) 201–211.

doi:10.1016/j.wasman.2015.07.052.

[31] E.R. Vieitez, P. Eder, A. Villanueva, H. Saveyn, End-of-waste criteria for glass cullet: Technical proposals, 2011. doi:10.2791/7150.

[32] J. Formosa, M.A. Aranda, J.M. Chimenos, J.R. Rosell, A.I. Fernández, O. Ginés, Cementos químicos formulados con subproductos de óxido de magnesio, Boletín La Soc. Española Cerámica y Vidr. 47 (2008) 293–297. doi:10.3989/cyv.2008.v47.i5.169.

[33] A. Maldonado-Alameda, A.M. Lacasta, J. Giro-Paloma, J.M. Chimenos, L. Haurie, J. Formosa, Magnesium phosphate cements formulated with low grade magnesium oxide incorporating phase change materials for thermal energy storage, Constr. Build. Mater. 155 (2017) 209–216. doi:10.1016/j.conbuildmat.2017.07.227.

[34] J. Formosa, J.M. Chimenos, A.M. Lacasta, M. Niubó, Interaction between low-grade magnesium oxide and boric acid in chemically bonded phosphate ceramics formulation, Ceram. Int. 38 (2012) 2483–2493. doi:10.1016/j.ceramint.2011.11.017.

[35] C.A. Strydom, E.M. Van Der Merwe, M.E. Aphane, The effect of calcining conditions on the rehydration of dead burnt magnesium oxide using magnesium acetate as a hydrating agent, J. Therm. Anal. Calorim. 80 (2005) 659–662. doi:10.1007/s10973-005-0710-x.

[36] D.C. Montgomery, Design and Analysis of Experiments, Sixth edit, John Wiley & Sons, Ltd, New York, USA, 2004.

[37] M. Niubó, A.I. Fernández, L. Haurie, X.G. Capdevila, J.M. Chimenos, J.I. Velasco, Influence of the Electric Arc Furnace Dust in the physical and mechanical properties of EVA–polyethylene–butene blends, Mater. Sci. Eng. A. 528 (2011) 4437–4444. doi:10.1016/j.msea.2011.02.006.

[38] J.R. Rosell, I.R. Cantalapiedra, Simple method of dynamic Young's modulus determination in lime and cement mortars, Mater. Constr. 61 (2011) 39–48. doi:10.3989/mc.2010.53509.

[39] L.J. Gardner, S.A. Bernal, S.A. Walling, C.L. Corkhill, J.L. Provis, N.C. Hyatt, Characterisation of magnesium potassium phosphate cements blended with fly ash and ground granulated blast furnace slag, Cem. Concr. Res. 74 (2015) 78–87. doi:10.1016/j.cemconres.2015.01.015.

[40] Y. Xie, X. Lin, X. Pan, T. Ji, Preliminary investigation of the hydration mechanism of MgO-SiO_2-

K_2HPO_4 cement, Constr. Build. Mater. 235 (2020) 117471. doi:10.1016/j.conbuildmat.2019.117471.

[41] J. Formosa, J.M. Chimenos, A.M. Lacasta, L. Haurie, Thermal study of low-grade magnesium hydroxide used as fire retardant and in passive fire protection, Thermochim. Acta. 515 (2011) 43–50. doi:10.1016/j.tca.2010.12.018.

[42] H. Lahalle, C. Patapy, M. Glid, G. Renaudin, M. Cyr, Microstructural evolution/durability of magnesium phosphate cement paste over time in neutral and basic environments, Cem. Concr. Res. 122 (2019) 42–58. doi:10.1016/j.cemconres.2019.04.011.

[43] R. del Valle-Zermeño, J. Giro-Paloma, J. Formosa, J.M. Chimenos, Low-grade magnesium oxide by-products for environmental solutions: Characterization and geochemical performance, J. Geochemical Explor. 152 (2015) 134–144. doi:10.1016/j.gexplo.2015.02.007.

[44] D. V. Ribeiro, G.R. Paula, M.R. Morelli, Use of microwave oven in the calcination of MgO and effect on the properties of magnesium phosphate cement, Constr. Build. Mater. 198 (2019) 619–628. doi:10.1016/j.conbuildmat.2018.11.289.

[45] S.A. Emamian, H. Eskandari-Naddaf, Effect of porosity on predicting compressive and flexural strength of cement mortar containing micro and nano-silica by ANN and GEP, Constr. Build. Mater. 218 (2019) 8–27. doi:10.1016/j.conbuildmat.2019.05.092.

[46] B. Xu, B. Lothenbach, A. Leemann, F. Winnefeld, Reaction mechanism of magnesium potassium phosphate cement with high magnesium-to-phosphate ratio, Cem. Concr. Res. 108 (2018) 140–151. doi:10.1016/j.cemconres.2018.03.013.

[47] C. Yu, Q. Wu, J. Yang, Effect of seawater for mixing on properties of potassium magnesium phosphate cement paste, Constr. Build. Mater. 155 (2017) 217–227. doi:10.1016/j.conbuildmat.2017.08.050.

[48] D.A. Hall, R. Stevens, B. El-Jazairi, The effect of retarders on the microstructure and mechanical properties of magnesia-phosphate cement mortar, Cem. Concr. Res. 31 (2001) 455–465. doi:10.1016/S0008-8846(00)00501-9.

[49] M.R. Ahmad, B. Chen, Effect of silica fume and basalt fiber on the mechanical properties and

microstructure of magnesium phosphate cement (MPC) mortar, Constr. Build. Mater. 190 (2018) 466–478. doi:10.1016/j.conbuildmat.2018.09.143.

[50] S. Graeser, W. Postl, H.-P. Bojar, P. Berlepsch, T. Armbruster, T. Raber, K. Ettinger, F. Walter, Struvite-(K), $KMgPO_4 \cdot 6H_2O$, the potassium equivalent of struvite – a new mineral, Eur. J. Miner. 20 (2008) 629–633. doi:10.7868/s002347611506020x.

[51] I. Kansal, A. Reddy, F. Muñoz, S.J. Choi, H.W. Kim, D.U. Tulyaganov, J.M.F. Ferreira, Structure, biodegradation behavior and cytotoxicity of alkali-containing alkaline-earth phosphosilicate glasses, Mater. Sci. Eng. C. 44 (2014) 159–165. doi:10.1016/j.msec.2014.08.016.

[52] B. Lothenbach, B. Xu, F. Winnefeld, Thermodynamic data for magnesium (potassium) phosphates, Appl. Geochemistry. 111 (2019) 104450. doi:10.1016/j.apgeochem.2019.104450.

[53] P. Mácová, A. Viani, Investigation of setting reaction in magnesium potassium phosphate ceramics with time resolved infrared spectroscopy, Mater. Lett. 205 (2017) 62–66. doi:10.1016/j.matlet.2017.06.063.

[54] D. Leng, X. Li, Y. Lv, H. Tan, N. Li, Z. Liu, W. Jiang, D. Jiang, Cesium immobilization by K-struvite crystal in aqueous solution: Ab initio calculations and experiments, J. Hazard. Mater. 387 (2020) 121872. doi:10.1016/j.jhazmat.2019.121872.

[55] Z. Zhang, H. Wang, J.L. Provis, F. Bullen, A. Reid, Y. Zhu, Quantitative kinetic and structural analysis of geopolymers. Part 1. the activation of metakaolin with sodium hydroxide, Thermochim. Acta. 539 (2012) 23–33. doi:10.1016/j.tca.2012.03.021.

[56] C.Z. Tan, J. Arndt, Interaction of longitudinal and transverse optic modes in silica glass, J. Chem. Phys. 112 (2000) 5970–5974. doi:10.1063/1.481169.

[57] P. Padmaja, G.M. Anilkumar, P. Mukundan, G. Aruldhas, K.G.K. Warrier, Characterisation of stoichiometric sol-gel mullite by fourier transform infrared spectroscopy, Int. J. Inorg. Mater. 3 (2001) 693–698. doi:10.1016/S1466-6049(01)00189-1.

[58] P. Makreski, G. Jovanovski, MINERALS FROM MACEDONIA IX . DISTINCTION BETWEEN SOME, (2003).

[59] A. Viani, P. Mácová, Polyamorphism and frustrated crystallization in the acid-base reaction of

magnesium potassium phosphate cements, CrystEngComm. 20 (2018) 4600–4613. doi:10.1039/c8ce00670a.

[60] S. Jähnigen, E. Brendler, U. Böhme, G. Heide, E. Kroke, Silicophosphates containing SiO_6 octahedra-anhydrous synthesis under ambient conditions, New J. Chem. 38 (2014) 744–751. doi:10.1039/c3nj00721a.

[61] A. Udduttula, J. Li, P.Y. Zhao, G.C. Wang, J. V. Zhang, P.G. Ren, Sol-gel derived nanosized $Sr_5(PO_4)_2SiO_4$ powder with enhanced in vitro osteogenesis and angiogenesis for bone regeneration applications, Ceram. Int. 45 (2019) 3148–3158. doi:10.1016/j.ceramint.2018.10.215.

Table Captions

Table 1. Summary of DoE formulations, factors, range of study, and responses results.

Table 2. XRF results of the by-products as raw materials.

Table 3. XRD-TG-XRF raw materials analysis results.

Table 4. Optimization criteria and optimal formulation.

Table 1

Run	Factors		Responses									
			Apparent density 7 d (kg·m^{-3})		MOE 7 d (GPa)		FS 7 d (MPa)		CS 7 d (MPa)		CS 28 d (MPa)	
	CSP (%)	W/C	Experimental value	Predicted value	Experimental value	Predicted value	Experimental value	Predicted value	Experimental value	Predicted value	Experimental value	Predicted value
1	**0.00**	**0.38**	1772.36	1778.83	10.61	9.89	2.67	2.44	11.58	11.32	13.40	13.06
2	0.00	0.38	1770.90	1778.83	10.20	9.89	2.70	2.44	11.30	11.32	13.10	13.06
3	4.86	**0.34**	1818.67	1812.52	12.76	13.06	3.79	3.63	14.07	14.05	17.70	18.19
4	0.47	0.34	1785.53	1792.49	12.83	12.58	3.43	3.48	15.75	15.34	18.90	18.30
5	8.57	0.36	1813.99	1809.59	11.90	11.98	3.17	3.18	12.75	12.80	15.80	15.38
6	**15.00**	0.38	1801.61	1805.45	11.89	11.52	3.02	2.94	11.89	11.63	16.30	15.99
7	15.00	0.34	1860.03	1858.80	14.37	14.16	4.09	3.96	18.03	18.09	25.80	24.87
8	15.00	0.36	1830.59	1832.13	13.57	12.84	3.79	3.45	14.20	13.44	19.40	20.43
9	7.50	0.38	1799.54	1792.14	10.37	10.70	2.67	2.69	10.30	10.49	13.50	11.88
10	9.38	0.35	1813.23	1825.24	12.66	12.99	3.13	3.56	15.00	15.27	17.20	18.39
11	0.00	0.35	1793.72	1787.09	11.78	11.78	3.27	3.18	13.80	13.82	17.30	16.90
12	15.00	0.38	1812.35	1805.45	10.70	11.52	2.75	2.94	10.80	11.63	15.60	15.99
13	0.47	0.34	1784.30	1792.49	12.60	12.58	3.40	3.48	15.20	15.34	18.70	18.30
14	0.70	0.37	1809.85	1784.90	10.10	10.91	2.58	2.83	9.76	10.36	12.80	14.70
15	15.00	0.34	1861.23	1858.80	14.20	14.16	4.00	3.96	18.00	18.09	25.10	24.87
16	7.50	0.38	1779.00	1792.14	10.70	10.70	2.40	2.69	11.08	10.49	11.60	11.88

Compounds	LG-MgO (wt.%)	CSP (wt.%)
MgO	61.70	1.61
SiO_2	2.70	70.78
CaO	9.32	9.37
Al_2O_3	0.55	4.81
Fe_2O_3	2.43	0.35
K_2O	-	0.94
Na_2O	-	11.15
SO_3	6.55	-
Loss of ignition (LOI)	16.75	0.99

Table 3

Compounds (wt.%)	LG-MgO	CSP
MgO	43.58 ± 0.71	1.61 ± 0.05
$Mg(OH)_2$	3.77 ± 0.12	-
$MgCO_3$	23.83 ± 0.23	-
$MgCa(CO_3)_2$	4.96 ± 0.15	-
CaO	0.00	9.37 ± 0.11
$CaCO_3$	13.46 ± 0.30	-
$MgSO_4$	2.12 ± 0.15	-
$CaSO_4$	2.68 ± 0.09	-
SiO_2	2.31 ± 0.06	70.78 ± 0.50
Fe_2O_3	2.08 ± 0.12	0.35 ± 0.03
Al_2O_3	0.47 ± 0.11	4.81 ± 0.51
K_2O	-	0.94 ± 0.07
Na_2O	-	11.15 ± 0.48
H_2O	0.74 ± 0.11	-
Others	-	0.99 ± 0.13

Table 4

Constraints	Goal	Limits		Importance	Optimal formulation
		Lower	Upper		Value (predicted range)
W/C ratio	is in range	0.34	0.38	3	0.34
CSP (%)	is in range	0.00	15.00	3	15.00
ρ ($kg \cdot m^{-3}$)	is in range	1770.90	1861.23	3	1858.80 (1844.09-1873.51)
MOE (GPa)	is in range	10.10	14.35	3	14.16 (13.63-14.69)
FS (MPa)	is in range	2.40	4.09	3	3.96 (3.71-4.21)
CS-7d (MPa)	maximize	9.76	18.03	3	18.09 (17.18-18.99)
CS-28d (MPa)	maximize	11.60	25.80	3	24.87 (23.45-27.00)
				Desirability	0.9668

Figure Captions

Fig. 1. XRD of (a) CSP and (b) LG-MgO raw materials.

Fig. 2. TGA-SDT thermal decomposition of LG-MgO.

Fig. 1**.** Surface plot of (a) apparent density at 7 d, (b) modulus of elasticity (MOE) at 7 d, (c) flexural strength (FS) at 7 d, (d) compressive strength (CS) at 7 d, and (e) at 28 d as a function of W/C ratio and CSP.

Fig. 4. XRD patterns of R11 and R15 samples at 365 d.

Fig. 5. TG/DTG Thermal decomposition of R11-365d and R15-365d (a) TG signals (b) DTG signals.

Fig. 6. BSEM-EDS of R15-365d embedded in epoxy resin (a) general elemental mapping and (b) elemental mapping of the red zone indicated in (a).

Fig. 7. FTIR-ATR spectra of CSP, R11-365d and R15-365d.

Fig. 8. FTIR-ATR spectra: (a) in the range of interest of CSP, R11-365d, and R15-365d; (b) deconvolution of the experimental R15-365d; (c) deconvolution of the experimental CSP; (d) deconvolution of the experimental R11-365d, and their corresponding fit sum (discontinuous red lines).

Figure 1

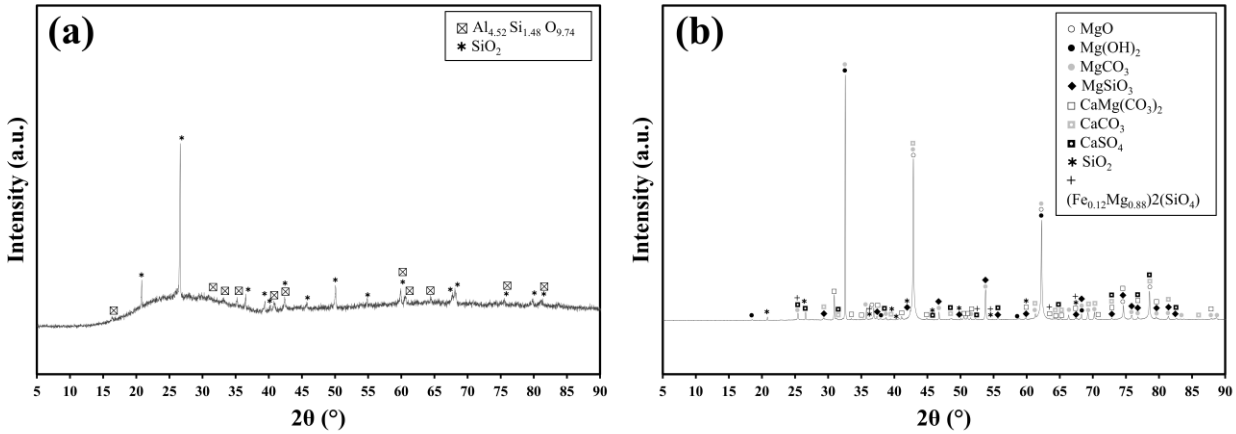

Figure 2

Click here to access/download;Figure;Figure 2.docx

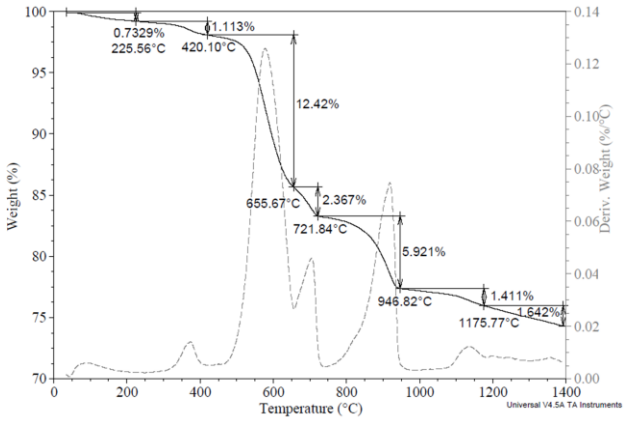

Figure 3

Click here to access/download;Figure;Figure 3.docx

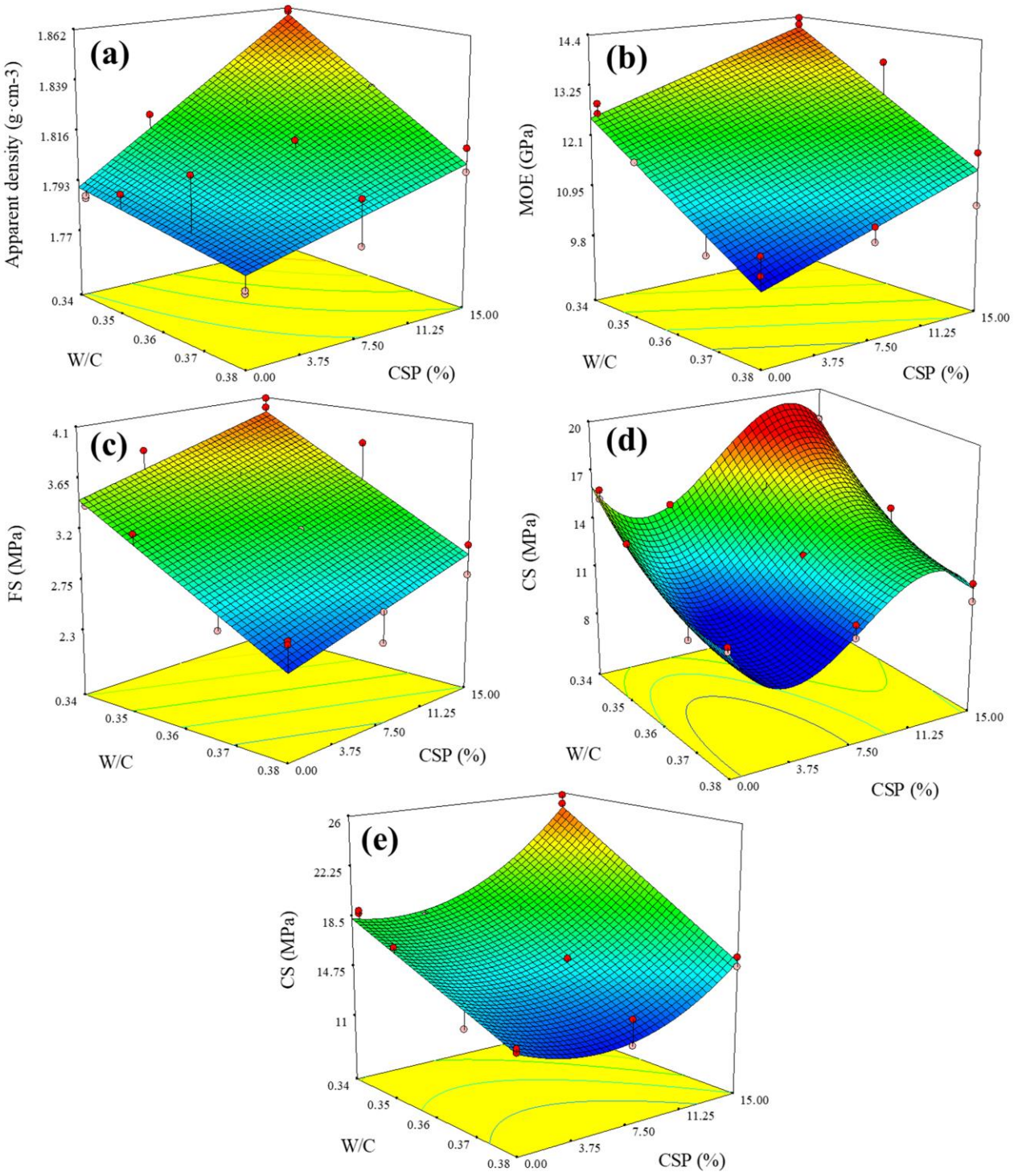

Figure 4

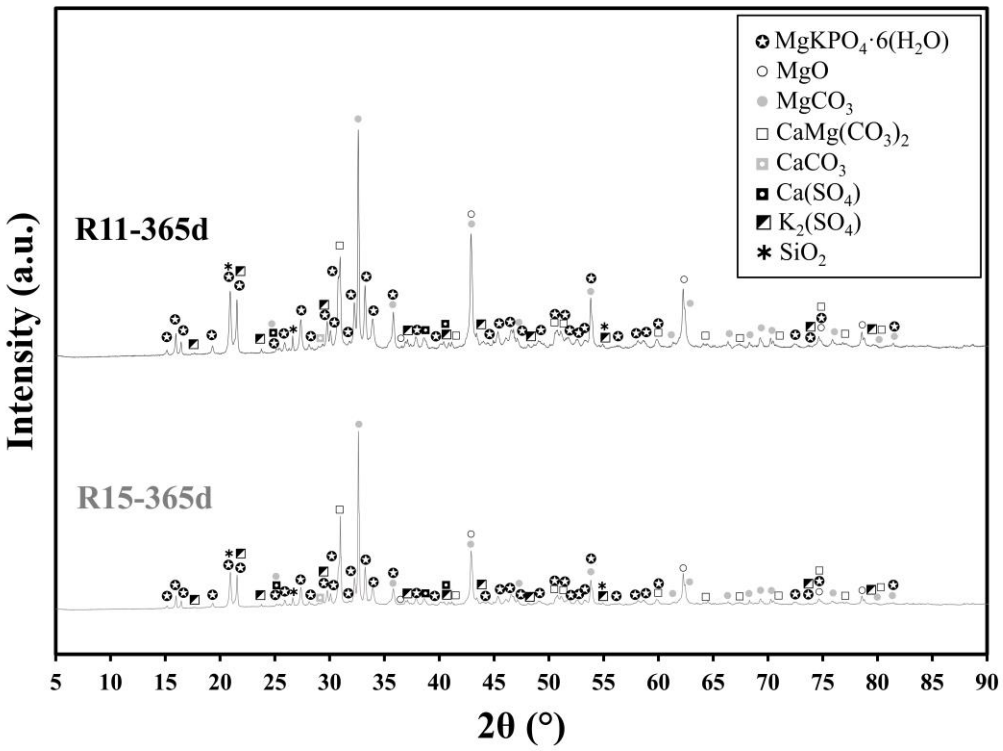

Figure 5

Click here to access/download;Figure;Figure 5.docx

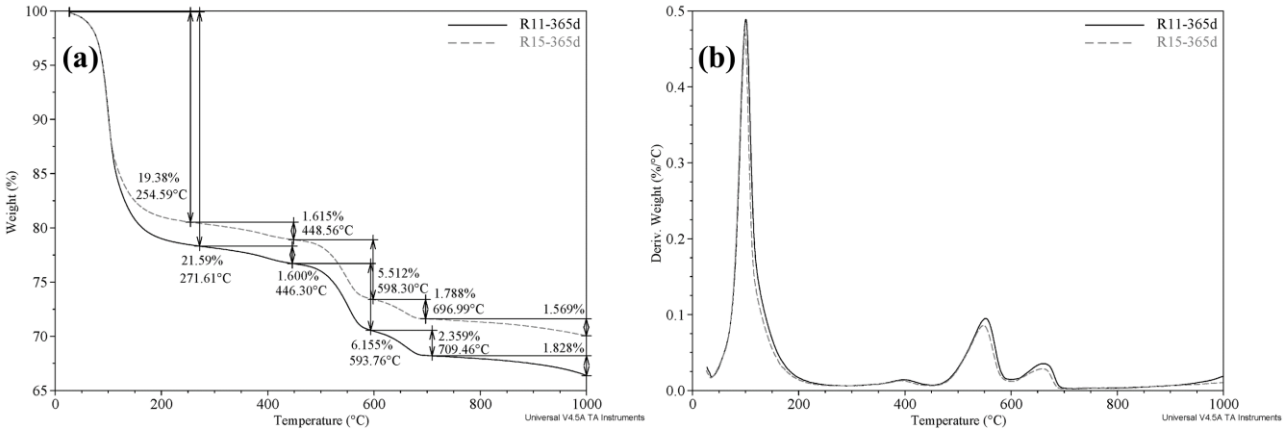

Figure 6

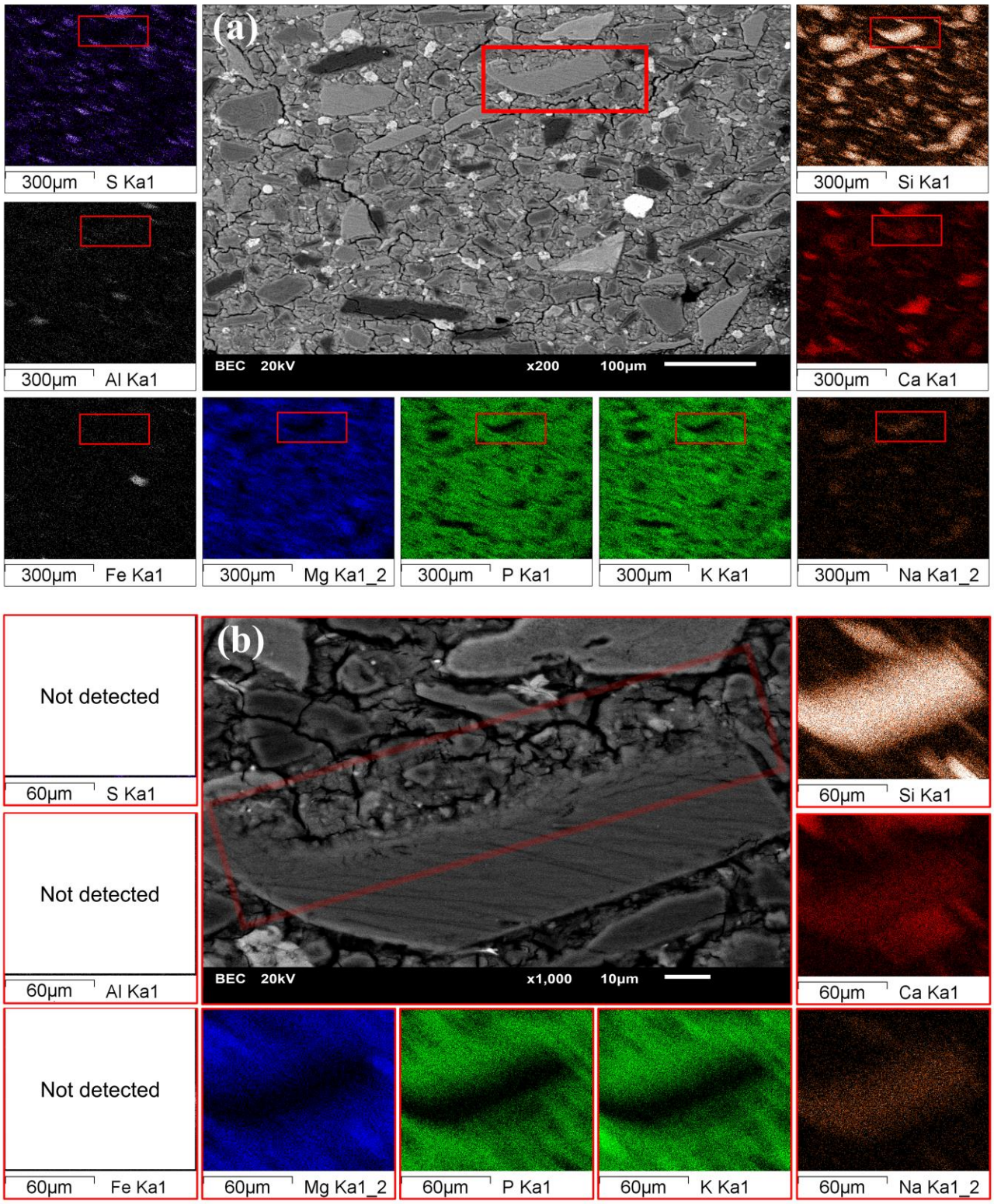

Figure 7

Click here to access/download;Figure;Figure 7.docx

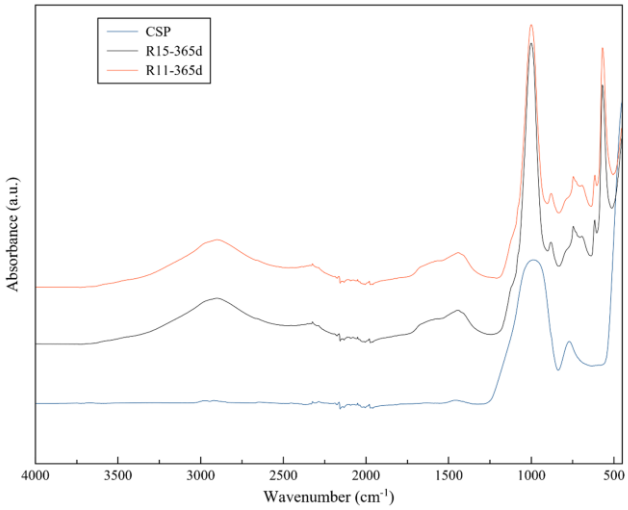

Figure 8

Click here to access/download;Figure;Figure 8.docx